An approximate method for nonlinear diffusion applied to enzyme inactivation during drying

Promotor: dr.ir.S. Bruin, oud-hoogleraar in de proceskunde
Co-promotor: dr.ir.H.A.C. Thijssen, hoogleraar in de fysische technologie aan de Technische Hogeschool Eindhoven

Jun Kong Liou

An approximate method for nonlinear diffusion applied to enzyme inactivation during drying

Proefschrift

ter verkrijging van de graad van

doctor in de landbouwwetenschappen,

op gezag van de rector magnificus,

dr. C. C. Oosterlee,

hoogleraar in de veeteeltwetenschap,

in het openbaar te verdedigen

op woensdag 24 maart 1982 des namiddags te vier uur

in de aula van de Landbouwhogeschool te Wageningen.

ISBN = 157404-03

A B S T R A C T

Liou, J.K.(1982) An approximate method for nonlinear diffusion applied to enzyme inactivation during drying. Doctoral thesis, Agricultural University Wageningen, (14 + 137 pp., 40 figs, 11 tables, 57 refs, 2 app., English and Dutch summaries).

An approximate model was developed for nonlinear diffusion with a power-function variation of the diffusion coefficient with concentration. This model may serve for the computation of desorption times and concentration profiles in non-shrinking or shrinking slabs, cylinders or spheres, under isothermal as well as non-isothermal conditions.

For the kinetics for thermal enzyme inactivation, a relation was postulated, which includes a possible moisture dependence of the inactivation rate, which was tested by experiments with soy bean lipoxygenase, entrapped in a glucose-calciumalginate gel.

The model was applied to the simulation of enzyme inactivation during drying and tested by drying experiments with soy bean lipoxygenase in the above-mentioned model material.

Good agreement was observed between the results, obtained with the approximate model, the numerical solution of the complete model and the experimental results.

STELLINGEN

1. Voor niet lineaire diffusie in vlakke lagen, cylinders en bollen met een diffusiecoëfficiënt, die een machtsfunctie is van de concentratie (macht $a \geq 0$), is onder een Dirichlet randvoorwaarde, het Sherwood kengetal in het regulier regime, een pseudo-lineaire functie van $a/(a+2)$.

   Dit proefschrift: p51,52.

2. Het door Schoeber gedefinieerde overgangspunt tussen penetratie periode en regulier regime voldoet voor diffusie in vlakke lagen en cylinders, maar leidt voor het geval van diffusie in een bol met een constante diffusiecoëfficiënt tot een theoretisch onmogelijke waarde van de centrum-concentratie.

   Schoeber, W,J.A.H. Regular regimes in sorption processes. Proefschrift, Technische Hogeschool Eindhoven (1976) p96-98.

   Dit proefschrift: p55-59.

3. Aangezien Chen's benaderende oplossing van de diffusievergelijking voor een krimpende bol volkomen verschilt van de numerieke oplossing, is de waarde van de door Chen bepaalde diffusiecoëfficiënt voor vochtdiffusie in druiven, twijfelachtig.

   Chen, C.S. Simultaneous heat and mass transfer in convective drying of biological materials. In: Comptes rendus du Symposium International sur la conservation des grains récoltés humides. Paris (1973) p165-173.

4. De door Eriksson voorgeschreven pH voor de activiteitsbepaling van lipoxygenase is te laag.

   Eriksson, C.E., Svensson, S.G. Activation energy of reaction catalyzed by alcohol dehydrogenase, lipoxygenase, denatured peroxidase and hematin. Lebensm. Wiss. Technol., 7(1974) p38-41.

   Dit proefschrift: p102-104.

5. De vaak verkondigde bewering, dat de thermostabiliteit van enzymen toeneemt bij afnemend vochtgehalte, is aanvechtbaar.

   Tumerman, L. Thermal inactivation of enzymes. In: Encyclopedia of food technology (Ed. A.H. Johnson & M.S. Peterson). Avi Publishing Company, Westport (1974) p292-306.

   Dit proefschrift: p107.

6. In een één-fase modelbeschrijving van warmtediffusie in poreuze hygroscopische materialen, is het gebruik van zowel een effectieve thermische diffusiecoëfficiënt, gecorrigeerd voor het aanwezige vochtgehalte, als een sorptie/desorptieterm in de diffusievergelijking, onjuist.

   Liou, J.K., Bruin,S. A model for watermigration in porous hygroscopic materials caused by temperature gradients. Lebensm. Wiss. technol., 14(1981) p206-212.

7. Terecht merkt Viollaz op, dat rekenmodellen voor praktische doeleinden eenvoudig dienen te zijn. Het door Viollaz voorgestelde rekenmodel voor een droogproces, bevat echter dermate sterke vereenvoudigingen, dat de praktische betekenis ervan te betwijfelen valt.

   Viollaz, P.E., Suarez, C., Alzamora, S. Temperature prediction in air drying of food materials: a simple model.
   J. Food Technol., 15(1980) p361-367.

8. Fast en Popper stellen terecht, dat het gelijkstellen van selectieve informatie aan negentropie door Brillouin, voor niet fysische systemen (bijvoorbeeld een taal) absurd is. Het gebruik van entropie als grootheid in de informatietheorie, dient derhalve afgeschaft te worden.

   Fast, J.D. Entropy. MacMillan London (1970) Appendix 5.
   Popper, K. Unended quest. Fontana/Collins, Glasgow (1976) p162-167.

9. Feyerabend's kritiek op de waarde van empirische toetsing van wetenschappelijke theorieën is terecht, aangezien "empirische resultaten" niet altijd "theorievrij" zijn.

   Feyerabend, P. Against Method, Minnesota studies in the philosophy of Science 4(1970) chapter 5.

10. Het stabiliteitsconcept van Rutledge et al., toegepast op energievoorzieningssystemen, houdt in, dat een grotere diversiteit aan energiebronnen en energieroutes tot een hogere stabiliteit van het systeem leidt. Dit pleit voor de ontwikkeling van alternatieve vormen van energie.

    Rutledge, R., Basore, W., Mulholland, R.J. Ecological stability:
    An information theory viewpoint. J. Theor. Biol., 57(1976) p365-373.

11. De verzilting van de Rijn is tegen te gaan, door zout weer als betaalmiddel in te voeren. Zwitserland kan dan als veilige opslagplaats dienen.

12. Een zoutloos dieet alleen, maakt de Rijn nog niet gezond.

13. Wit begint en geeft mat in drie zetten.

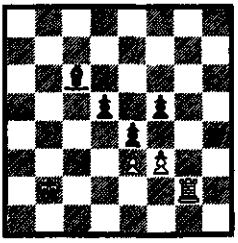

Proefschrift van J.K. Liou
An approximate method for nonlinear diffusion applied to enzyme inactivation during drying
Wageningen, 24 maart 1982

E R R A T A in:

"An approximate method for nonlinear diffusion applied to enzyme inactivation during drying." J.K. Liou (1982).

Page	Line	Text	Correction
3	18	facilitate	facilitates
12	7	inflection point	asymptote
20	20	obtainded	obtained
27	6	$[0,R_d)$	$[0,R_d]$
29	14	$[0,R_d)$	$[0,R_d]$
79	20	sytems	systems
92	9	yield	yields
119	24	facilitate	facilitates
122	27	vergemakkelijken	vergemakkelijkt
122	28	kunnen	kan
130	10	0.50 - 0.60	0.05 - 0.06
131	21	Neth. Milk Dairy J., to be published.	The destruction of enzymes and bacteria during the spray-drying of milk and whey. 1. The thermoresistance of some enzymes and bacteria in milk and whey with various total solids contents. Neth. Milk Dairy J., 35(1981)133-144.

V O O R W O O R D

In dit voorwoord, zou ik mijn dank willen uitspreken aan al degenen, die op welke wijze dan ook hebben bijgedragen aan de totstandkoming van dit proefschrift. Mijn promotor, dr.ir. S. Bruin, voor zijn kritische begeleiding, mijn co-promotor, prof.dr.ir.H.A.C. Thijssen, vanwege zijn enthousiaste belangstelling, mijn collega's van de sectie proceskunde, voor de plezierige werksfeer, André Stam en Jan Jakob Bleeker voor het uitvoeren van een groot deel van de experimenten gedurende hun doctoraal onderzoek, de leden van de Centrale Dienst Biotechnion en in het bijzonder de heer A. van Wijk voor het vervaardigen van de droogcel, de heer A. van Baaren voor de fotografische verzorging, *et surtout toi, Véronique, pour ta patience!*

Curriculum vitae

De auteur, geboren op 19 october 1949 te Rotterdam, bezocht aldaar van 1962-1968 de Van Oldenbarnevelt HBS. Na het behalen van het diploma HBS-B, ging hij in hetzelfde jaar scheikunde studeren aan de Technische Hogeschool te Delft. Zijn doctoraalstudie, met als keuzevakken systeemtechniek, procesdynamica en regeling en wetenschapsfilosofie, werd verricht bij de sectie Biochemische Reactoren, onder leiding van prof.dr.ir. N.W.F. Kossen en ir.G.C. van Eybergen, en werd afgerond in juni 1978 met het behalen van het ingenieursdiploma (met lof). In september 1978 trad hij als wetenschappelijk medewerker met gedeeltelijke onderwijstaak in dienst bij de Sectie Proceskunde van de Landbouwhogeschool te Wageningen en startte daar een promotie-onderzoek op het gebied van drogen onder leiding van prof.dr.ir.S. Bruin. Dit onderzoek werd eind 1981 afgerond. Zijn contract bij de Landbouwhogeschool loopt in september 1982 af.

C O N T E N T S

LIST OF SYMBOLS

a = power dependence in diffusion coefficient

a_w = water activity

b = parameter in eqn.(4.101)

B = beta function

c_p = heat capacity (J/kgK)

d = density (kg/m^3)

D = diffusion coefficient (m^2/s)

E = efficiency

E_a = activation energy (J/Mole)

f = time dependent part of the large time solution

F = flux parameter

g = space dependent part of the large time solution

G = flux function

h = Planck's constant (J.s)

H = shrinkage factor

j = mass flux (kg/m^2s)

J = Bessel function

k = Boltzmann's constant (J/MoleK)

k_e = specific inactivation rate (s^-)

k_g = gas phase mass transfer coefficient (m/s)

K = function defined in eqn.(2.10)

$K_{\frac{1}{4}}$ = modified Bessel function of order $\frac{1}{4}$

m = dimensionless moisture content

M = molecular weight (kg/Mole)

n = mass flux (kg/m^2s)

p = parameter in eqn.(2.7)

P = pressure (Pa)

q = parameter in eqn.(2.8)

r = space coordinate (m)

R = gas law constant (J/MoleK)

R_d = radius or half-thickness (m)

R_s = dry solids radius (m)

Sh_d = Sherwood number dispersed phase

$\overline{Sh}_d$ = Sherwood number in critical point

Sh_g = Sherwood number gas phase

t = time (s)

T = temperature (K)

v = mass velocity (m/s)

X = geometry variable

y = variable, defined in eqn.(4.78)

z = auxiliary variable in appendix A

α_g = heat transfer coefficient gas phase (W/m^2K)

γ = parameter in eqn.(3.69)

ΔH = enthalpy change (J/Mole)

ΔS = entropy change (J/MoleK)

λ = separation parameter in eqns.(4.5) and (4.6)

$\lambda_{a,g}$ = thermal conductivity of air (W/mK)

μ_n = n-th eigenvalue

ν = geometry parameter

ρ = mass concentration (kg/m^3)

τ = dimensionless time

ϕ = dimensionless space coordinate

ω = mass fraction on total basis (kg/kg total)

ω' = mass fraction on solids basis (kg/kg solids)

∇ = nabla operator

Subscripts:

b = bulk of gas phase
c = centre
d = dispersed phase
e = enzyme
g = gas phase
i = interface
m = moisture
o = initial
r = reduced
s = solid component

Superscripts:

^{eff} = effective
$^{(n)}$ = n-th derivative
^{ref} = reference value
^{s} = relative to solids velocity
^{sat} = saturated value
^{v} = relative to volume average velocity
$^{-}$ = average value
$^{\sim}$ = in inflection point
* = referring to shrinking systems
$^{'}$ = short time solution
$^{''}$ = large time solution
$^{\wedge}$ = optimum

C H A P T E R 1

General introduction.

One of the main reasons for drying in food processing is the wish to improve the keepability of the end product. As high moisture contents enhance deterioration of foods through microbial and enzyme action, foods are dried to moisture contents of 10% or lower. At these moisture levels, microbial growth is usually prevented. However, food degrading reactions, catalyzed by enzymes, may still proceed, even at very low moisture contents and subzero temperatures. Eventually, this will lead to the development of off-flavours, changes in colour and texture and loss of nutritional value. In *table 1.1* some of the important food degrading enzymes together with their specific activity are given [1].
Moreover, a varying storage temperature may cause moisture migration inside the dried product, resulting in increased local moisture contents and consequently improved conditions for microbial and enzymatic action [2].
It is therefore of great importance to choose drying conditions in such a way, that food deteriorating micro organisms and enzymes are destroyed during processing. At the same time, however, food quality has to be preserved, which requires careful adjustment of drying rate and temperature. The necessity of process control during drying operations is illustrated by the fact that the food product may suffer severe losses of flavour, colour, texture and nutritional value by heat treatment, evolving from thermally induced chemical, microbial and enzymatic degradation reactions. In view of this, it

Enzyme	Catalyzed reaction	Quality defect
Lipase	Hydrolysis of lipids.	Rancidity (soapy flavour)
Lipoxygenase	Oxidation of poly unsaturated fatty acids and carotenoids.	Rancidity (green flavour) Loss in vitamin A content
Protease	Hydrolysis of proteins.	Bitterness
Polyphenol oxidase	Oxidation of phenols.	Dark colour
Amylase	Hydrolysis of starch.	Softness/loss in viscosity
Pectin methyl-esterase	Hydrolysis of pectin.	Softness/loss in viscosity
Polygalacturonase	Hydrolysis of α-1,4 glycosidic bonds.	Softness/loss in viscosity
Ascorbic acid oxidase	Oxidation of L-ascorbic acid.	Loss in vitamin C content
Thiaminase	Hydrolysis of thiamin.	Loss in vitamin B_1 content

Table 1.1 Enzymes related to food quality (from Svensson [1]).

is worthwhile mentioning, that particularly at the initial stage of the drying process, the conditions prevailing may be favourable for microbial growth and enzymatic reactions, due to high moisture contents and moderate temperatures.

Similar problems, although of opposite character, are encountered in the production of enzyme granulates (marumes) for application in detergent powders, immobilized enzymes for biotechnological applications, enzyme powders for pharmaceutical purposes and dried micro organisms, of which spray dried yeast is a prominent example. Evidently, thermal destruction of enzymes or micro organisms is not wanted here and process conditions have to be adjusted corresponding to the requirement of minimizing losses of enzyme or microbial activity.

A prerequisite for optimum control, is a fundamental knowledge of the process. In particular, a quantitative approach is indispensable in studying processes of high complexity. The application of mathematical models and simulation techniques facilitate the interpretation of process data and may lead to a better understanding of the process dynamics. Unfortunately, the description of complex processes usually results in mathematical models of equivalent complexity, cumbersome for practical applications. In most cases it is however possible, to deduce a simplified model based on regularities found in the behaviour of the original model.

The scope of this thesis is the development of such a simplified model for drying with simultaneous enzyme inactivation. In chapter 2, a model is proposed for thermal inactivation of enzymes, where special attention is paid to the influence of moisture content. In chapter 3, a physical description of the drying process together with the kinetics of enzyme

inactivation is presented. Chapter 4, representing the main part of this thesis, deals with the construction of approximate methods for the computation of drying times and moisture profiles and their application to enzyme inactivation during drying. Chapter 5 treats the experimental part and contains kinetic experiments on the thermal inactivation of soy bean lipoxygenase immobilized in a glucose-calciumalginate gel-matrix together with the drying experiments. In chapter 6, the results from both drying experiments and corresponding computer simulations are compared and discussed.

C H A P T E R 2

Thermal inactivation of enzymes.

2.1 Introduction

Thermal inactivation of enzymes is a process, involving structural changes of the enzyme molecule, leading to a loss of its catalytic properties. In this process, the three-dimensional structure of the enzyme, maintained by noncovalent bonds like hydrogen bonds and salt bridges, is disrupted. The immensely complex nature of the inactivation process makes it virtually impossible to give a complete reaction mechanism. This is the reason why one usually considers only the overall reaction, but even then, a multitude of secondary factors including influences of pH, ion strength and interactions between the enzyme and other compounds, may lead to complex descriptions. Furthermore, these secondary factors complicate the comparison between experimental data from different sources.

Although thermal inactivation of enzymes has been a research topic for many years, only little attention has been paid to inactivation in systems at low or intermediate moisture contents. The majority of the studies in this field concerns inactivation experiments in diluted aqueous systems. Still, the knowledge of the thermostability of enzymes at varying moisture contents is essential for drying enzyme containing materials as foods for instance. In spite of the importance of the role of enzymes in relation to food quality, there is still a clear lack of physical or physico-chemical

models, describing the moisture dependence of thermal enzyme inactivation. Our major concern will therefore be the formulation of a model of acceptable accuracy for engineering applications.

2.2 *Thermodynamics of enzyme inactivation.*

The thermodynamics of enzyme inactivation is usually described according to either Eyring's or Arrhenius' theory, both providing a relation for the temperature dependence of the inactivation rate. These relations are satisfactory as far as the description of enzyme inactivation in highly diluted solutions is concerned. At lower moisture contents however, an extension might be necessary in order to account for the effect of moisture content on the inactivation rate. In this section we will treat concisely the theories of Eyring and Arrhenius. Next we will introduce the moisture dependence of the inactivation rate, for which an appropriate relation will be postulated. Finally, this relation will be analyzed in order to describe its functional behaviour in terms of enzyme stability.

2.2.1 *Eyring's theory of rate processes.*

According to Eyring's theory of rate processes, applied to thermal denaturation of proteins and the inactivation of enzymes, the specific inactivation rate k_e may be expressed by:

$$k_e = \frac{kT}{h} \exp\left(\frac{-\Delta G}{RT}\right) \qquad (2.1)$$

where $k = 1.38\ 10^{-23}$ (Boltzmann's constant) and $h = 6.62\ 10^{-34}$ (Planck's constant). The change in free enthalpy ΔG satisfies the thermodynamic relation:

$$\Delta G = \Delta H - T\Delta S \tag{2.2}$$

which, substituted in eqn.(2.1) yields:

$$ln(\frac{k_e h}{kT}) = - \frac{\Delta H}{RT} + \frac{\Delta S}{R} \tag{2.3}$$

The change in enthalpy ΔH or heat of activation and the change in entropy ΔS can be derived from the plot of the left hand term of eqn.(2.3) against $1/T$, which for inactivation of enzymes usually results in high values of ΔH, indicating a strongly endothermic reaction. This high heat of activation is however compensated to a great extent by a simultaneous increase of entropy, resulting in moderate values for the free enthalpy [3]. An attempt to explain these high entropies of activation is the concept of salt bridges being broken as a result of heating, causing a loosening of the protein structure [3].

2.2.2 Arrhenius' theory.

Arrhenius' theory of reaction rates may be considered as the ancestor of Eyring's theory and was originally proposed in order to describe the temperature dependence of the rate of inversion of sucrose. Applied to enzyme inactivation, the familiar Arrhenius equation reads:

$$\ln k_e = -\frac{E_a}{RT} + \ln k_{e,\infty} \qquad (2.4)$$

where E_a represents the energy of activation and $k_{e,\infty}$ is usually designated as the "frequency factor". If the temperature range is not too large, E_a and $k_{e,\infty}$ are approximately constant, but by combining the Arrhenius and Eyring equations it appears that both E_a and $k_{e,\infty}$ are in fact temperature dependent:

$$E_a = \Delta H + RT \qquad (2.5)$$

and:

$$\ln k_{e,\infty} = \ln(\frac{kT}{h}) + \frac{\Delta S}{R} - 1 \qquad (2.6)$$

Both theories have been succesfully applied in fitting experimental data on enzyme inactivation, but in view of the above-mentioned temperature dependence of activation energy and frequency factor, it would be more correct to apply Eyring's theory rather than Arrhenius' theory. Another advantage of Eyring's theory is avoiding the concept of the frequency factor, which merely has a mathematical significance. On the other hand, Eyring's theory does not provide any information about the inactivation process on a molecular level as the thermodynamic quantities are referring to the overall process. Consequently, the interpretation of these quantities must be done with reservation.

2.2.3 Moisture dependence of the specific inactivation rate.

In addition to Eyring's theory we introduce the concept of a moisture dependent inactivation rate by assuming enthalpy and entropy changes to be functions of moisture content:

$$\Delta H = \Delta H_1 + (\Delta H_0 - \Delta H_1) exp(\frac{-p\omega_m}{1-\omega_m}) \qquad (2.7)$$

and:

$$\Delta S = \Delta S_1 + (\Delta S_0 - \Delta S_1) exp(\frac{-q\omega_m}{1-\omega_m}) \qquad (2.8)$$

with ω_m representing the moisture content on total basis. The indices $_0$ and $_1$ are referring to the limiting cases of $\omega_m=0$ (complete dryness) and $\omega_m=1$ (pure water), whereas p and q are positive constants. It may be easily verified that these functional relationships satisfy the conditions for the above-mentioned limiting cases. If in addition we assume that for enzyme inactivation, $\Delta H_0 < \Delta H_1$ and $\Delta S_0 < \Delta S_1$, ΔH and ΔS will be monotonously increasing functions of moisture content, showing an asymptotic behaviour in the limit $\omega_m=1$. As for the plausibility of the above-mentioned assumption regarding the behaviour of ΔH and ΔS, we may argue as follows. In a solution, breaking of the first salt bridges may be followed by spontaneous breaking of many other bonds, which will finally be the major contribution to the heat of activation and increase of entropy. At increasing moisture contents it may also be expected that finally the influence of moisture content will disappear and ΔH and ΔS will approach their limiting values asymptotically. At lower moisture contents however,

we may expect that this "chain effect" of spontaneous breaking of bonds will be considerably less than in a solution, due to a more restricted configuration of the enzyme and consequently both heat of activation and increase of entropy will be less.
Substitution of eqns.(2.7) and (2.8) in eqn.(2.3) leads to:

$$ln(\frac{k_e h}{kT}) = -\frac{\Delta H_1}{RT} + \frac{\Delta S_1}{R} - \frac{\Delta H_0 - \Delta H_1}{RT} exp(\frac{-p\omega_m}{1-\omega_m}) + \frac{\Delta S_0 - \Delta S_1}{R} exp(\frac{-q\omega_m}{1-\omega_m}) \quad (2.9)$$

Eqn.(2.9) was applied in fitting experimental data on thermal inactivation of soy bean lipoxygenase, immobilized in a glucose calciumalginate gelmatrix (this thesis). A similar approach, based on Arrhenius' theory has been adopted by Saguy et al.[4] for ascorbic acid degradation and by Luyben and Liou [5] for fitting experimental data on inactivation of catalase, lipase and alkaline phosphatase.

In order to comprehend the functional behaviour of the postulated relation for the moisture dependence of the inactivation rate, we shall start by analyzing its properties. For ease of notation we first write:

$$K = ln(\frac{k_e h}{kT}) \quad (2.10)$$

The moisture dependence of K and $ln\ k_e$ at a given temperature are similar, differing only a constant factor $ln(h/kT)$.
Therefore, the analysis on the functional behaviour of K will also apply to $ln\ k_e$.
If the first derivative of K with respect to ω_m equals zero, the function K, depending on the sign of the second deriva-

tive, possesses a minimum (positive sign) or a maximum (negative sign), whereas in case of a zero second derivative, the function K has a point of inflection. The first and second derivatives of K with respect to ω_m are:

$$\frac{\partial K}{\partial \omega_m} = \frac{1}{(1-\omega_m)^2}\left[p\,\frac{\Delta H_0-\Delta H_1}{RT}\exp\left(\frac{-p\omega_m}{1-\omega_m}\right) - q\,\frac{\Delta S_0-\Delta S_1}{R}\exp\left(\frac{-q\omega_m}{1-\omega_m}\right)\right] \quad (2.11)$$

and:

$$\frac{\partial^2 K}{\partial \omega_m^2} = \frac{1}{(1-\omega_m)^4}\left[p^2\,\frac{\Delta H_1-\Delta H_0}{RT}\exp\left(\frac{-p\omega_m}{1-\omega_m}\right) - q^2\,\frac{\Delta S_1-\Delta S_0}{R}\exp\left(\frac{-q\omega_m}{1-\omega_m}\right)\right] + \frac{2}{1-\omega_m}\,\frac{\partial K}{\partial \omega_m} \quad (2.12)$$

For the location of the extremum then follows:

$$\frac{\hat{\omega}_m}{1-\hat{\omega}_m} = \frac{1}{p-q}\,\ln\frac{p(\Delta H_1-\Delta H_0)}{qT(\Delta S_1-\Delta S_0)} \quad (2.13)$$

with the corresponding functional value:

$$\hat{K} = -\frac{\Delta H_1}{RT}+\frac{\Delta S_1}{R}+\left(\frac{1}{p}-\frac{1}{q}\right)\left[p\,\frac{\Delta H_1-\Delta H_0}{RT}\right]^{\frac{-q}{p-q}}\left[q\,\frac{\Delta S_1-\Delta S_0}{R}\right]^{\frac{p}{p-q}} \quad (2.14)$$

and the second derivative:

$$\frac{\partial^2 \hat{K}}{\partial \omega_m^2} = \frac{p-q}{(1-\hat{\omega}_m)^4}\left[p\,\frac{\Delta H_1-\Delta H_0}{RT}\right]^{\frac{-q}{p-q}}\left[q\,\frac{\Delta S_1-\Delta S_0}{R}\right]^{\frac{p}{p-q}} \quad (2.15)$$

As ΔH and ΔS are assumed to be monotonously increasing functions of moisture content, we may derive from eqn.(2.15) that:

$$\frac{\partial^2 \hat{K}}{\partial \omega_m^2} \gtrless 0 \quad \text{if} \quad p \gtrless q \quad \text{and} \quad \hat{\omega}_m \neq 1, \quad (2.16)$$

indicating, that a minimum will occur, if $p>q$ and a maximum if $p<q$.

The extremum may be located in the region $0 \leqq \omega_m < 1$. The particular case of an extremum at $\omega_m = 0$ occurs if:

$$T = \frac{p(\Delta H_1 - \Delta H_0)}{q(\Delta S_1 - \Delta S_0)} \quad (=T_2) \tag{2.17}$$

whereas at $\omega_m = 1$ both first and second derivatives are zero, implying a horizontal inflection point.

For the existence of an inflection point at an intermediate moisture content, a zero second derivative is required. According to eqns.(2.11) and (2.12), this condition leads to the implicit relation, determining the location of the inflection point:

$$\frac{2(1-\tilde{\omega}_m) - q}{2(1-\tilde{\omega}_m) - p} \exp\left[\frac{(p-q)\tilde{\omega}_m}{1-\tilde{\omega}_m}\right] = \frac{p(\Delta H_1 - \Delta H_0)}{qT(\Delta S_1 - \Delta S_0)} \tag{2.18}$$

In the foregoing analysis, we have already considered some of the properties at $\omega_m = 0$ and $\omega_m = 1$. In addition we may derive from eqn.(2.9), that:

$$K_1 \gtrless K_0 \quad if \quad T \gtrless \frac{\Delta H_1 - \Delta H_0}{\Delta S_1 - \Delta S_0} \quad (=T_1) \tag{2.19}$$

which indicates, that thermostability in the above-mentioned limiting cases, relative to each other depends on temperature, with a point of inversion at a specified temperature T_1.

We will conclude our analysis by investigating the specific case of $p=q$ for which the function K simplifies into a monotonously decreasing or increasing function:

$$K = -\frac{\Delta H_1}{RT} + \frac{\Delta S_1}{R} + \left[-\frac{\Delta H_0 - \Delta H_1}{RT} + \frac{\Delta S_0 - \Delta S_1}{R}\right] exp\left(\frac{-p\omega_m}{1-\omega_m}\right) \qquad (2.20)$$

and correspondingly, the first derivative becomes:

$$\frac{\partial K}{\partial \omega_m} = \frac{p}{(1-\omega_m)^2}\left[\frac{\Delta H_0 - \Delta H_1}{RT} - \frac{\Delta S_0 - \Delta S_1}{R}\right] exp\left(\frac{-p\omega_m}{1-\omega_m}\right) \qquad (2.21)$$

Hence, the function K will be monotonously decreasing with moisture content in case of a negative first derivative and monotonously increasing in case of a positive first derivative. Consequently, this leads to the condition:

$$\frac{\partial K}{\partial \omega_m} \gtrless 0 \quad if \quad T \gtrless \frac{\Delta H_1 - \Delta H_0}{\Delta S_1 - \Delta S_0} \quad (=T_1) \qquad (2.22)$$

which evidently is in agreement with our previous result of condition (2.19). The point of inversion, occurring at a temperature T_1 corresponds with the particular situation in which the function K is no longer dependent on moisture content:

$$K = -\frac{\Delta H_1}{RT} + \frac{\Delta S_1}{R} \qquad (2.23)$$

This analysis has shown, that in principle we may distinguish three categories of different behaviour, regarding thermostability of the enzyme:

1) $p<q$, showing a minimum stability at an intermediate moisture content and a maximum stability at either $\omega_m=0$ or at $\omega_m=1$, depending on temperature. In the specific case of $T=T_1$, the thermostability at $\omega_m=0$ and $\omega_m=1$ will be equal.

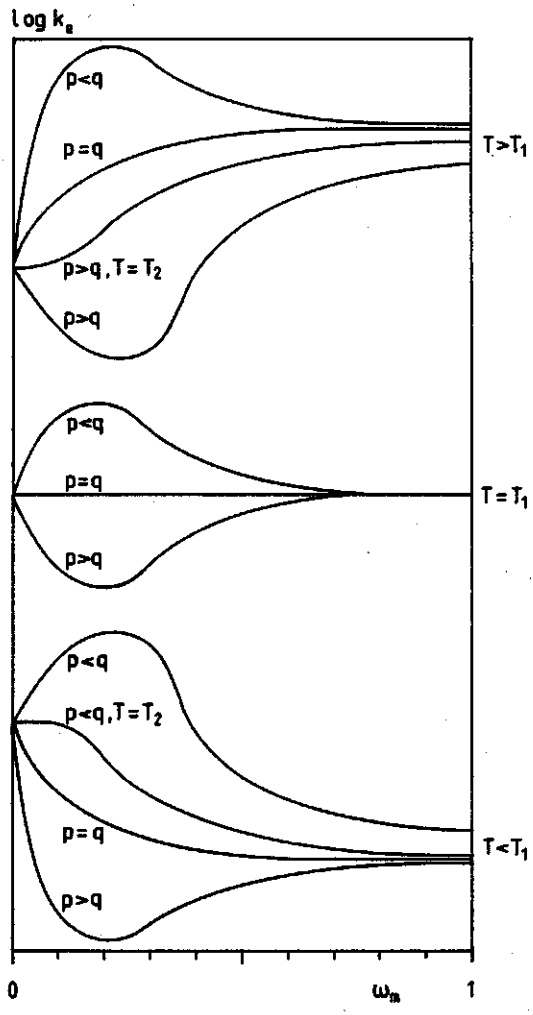

Fig. 2.1 Various possibilities for the moisture dependence of the specific inactivation rate k_e in different temperature regions.

2) $p>q$, showing a maximum stability at an intermediate moisture content and a minimum stability at either $\omega_m=0$ or at $\omega_m=1$ depending on temperature.

3) $p=q$, showing a monotonously decreasing, increasing or constant behaviour, depending on temperature.

In *fig. 2.1* the various possibilities of functional behaviour for the specific inactivation rate k_e are shown schematically. As indicated in the foregoing analysis, enzyme thermostability below a temperature T_1 is higher in solution than in the dry state, whereas above a temperature T_1 the reverse situation occurs.
An interesting consequence of this behaviour is, that drying an enzyme containing system below a temperature T_1 will exhibit an overall increasing inactivation rate, whereas above a temperature T_1 the reverse effect will occur. Furthermore, depending on the category, to which the enzyme belongs, the enzyme may pass through a point of optimum stability, which may be a minimum or a maximum, during the drying process.

The influence of moisture content on the inactivation rate also follows from more general considerations with regard to Arrhenius' or Eyring's theory. As is usually observed, Arrhenius or Eyring plots for different moisture contents, exhibit different slopes, corresponding to differences in activation energies or enthalpies. If we restrict ourselves to Eyring plots, this behaviour implies that the different K lines intersect. Evidently, the thermostability behaviour on both sides of an intersection point will be opposite, which is shown schematically in *fig. 2.2*, representing an

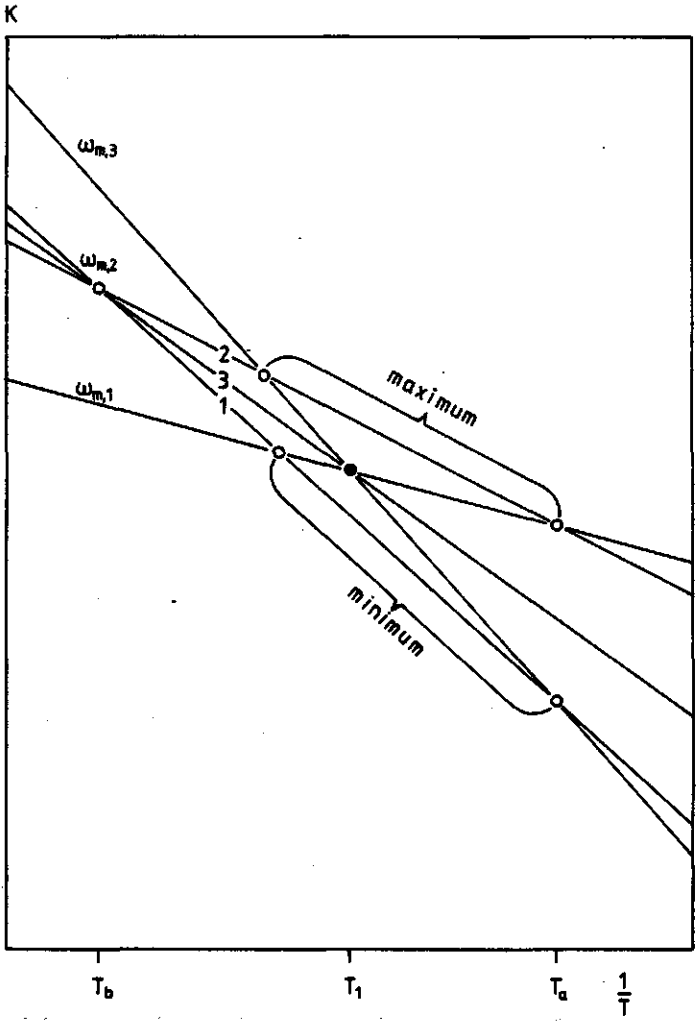

Fig. 2.2 Eyring plots for three different moisture contents.

Eyring plot for three different moisture contents: $\omega_{m,1} < \omega_{m,2} < \omega_{m,3}$, in case of increasing slopes with decreasing moisture contents. This phenomenon of increasing slopes with decreasing moisture contents is in agreement with experimental data on thermal inactivation of alkaline phosphatase in skim milk [6] and of soy bean lipoxygenase in a glucose calciumalginate gel (this thesis). Within the interval: $T_a < T < T_b$, the K line for $\omega_{m,2}$ may intersect the other two lines in three different ways, leading to a minimum in case 1, a maximum in case 2 and a monotonously decreasing, increasing or constant behaviour in case 3, if K is plotted as a function of moisture content. These are precisely the possibilities, which were already established in the foregoing analysis. It may be easily verified, that a similar behaviour will occur in case of decreasing slopes with decreasing moisture contents. This behaviour is apparently in contradiction to the widely spread opinion, that the thermostability of enzymes is increased at decreasing moisture contents.

Rothe [7- 9] investigated the thermal inactivation of the enzymes: lipase, acetylesterase, peroxydase and lipoxygenase from cereals and found a significantly increasing resistance to heat treatment at decreasing moisture contents.

Farkas and Goldblith [10] found in their studies on the kinetics of thermal inactivation of soy bean lipoxygenase, that the presence of 20% pea solids increased thermostability by a factor 6 to 10. Similar observations were reported by Svensson and Eriksson [11] with regard to thermal inactivation of pea lipoxygenase in pea press juice, containig 10% sucrose, 0.1% glucose, soluble starch and pectin and proteins in a concentration of 10 mg/ml. An increase in thermostability of cata-

lase in the presence of mono- and disaccharides was reported by Kiermeyer and Koberlein [12]. Also the data of Verhey [13] on the thermal inactivation of alkaline phosphatase in skim milk powder indicated that high solids concentrations have a protective influence on the enzyme against heat treatment. The above mentioned observations demonstrate that decreasing of moisture content or increasing of solids concentration, has undoubtedly an increasing effect on thermostability. However, when thermostability varies with moisture content, this implies that according to Eyring's theory, the corresponding K lines will intersect and necessarily, inversion in thermostability behaviour will occur. On the other hand, it will entirely depend on the temperature range of the inactivation experiments whether thermostability inversion will be observed or not. That increasing solids concentration does not always correspond with increased thermostability is demonstrated by the studies of Hillier et al.[14] on the influence of total solids on thermal denaturation of α-lactalbumin and β-lactoglobulin in cheese whey. Their results indicated that increasing total solids in the range 3.6-21.5% increased the thermostability of β-lactoglobulin, but decreased the thermostability of α-lactalbumin. Moreover, in storage experiments with peroxydase on high polymer carriers, Roozen and Pilnik [15] found minima as well as maxima in enzyme stability at intermediate moisture contents, depending on the enzyme-carrier combination. This tendency towards an optimum stability was also observed by Kulys et al.[16]. Their investigations on the thermostability of glucose oxydase, entrapped in high concentration 2-hydroxyethyl methacrylate (HEMA) gels, demonstrated a definite increase in thermostabi-

lity at gelconcentrations higher than 29%, arriving at a maximum thermostability at a gelconcentration of about 80%. With this brief survey we have tried to show that enzyme systems may indeed exhibit those characteristics with regard to thermostability as resulted from our previous analysis. It should however be mentioned that the postulated model does not involve the influence of secondary factors like pH, and therefore applies only to systems, which may differ in moisture content and temperature, but must have the same pH, ion strength etc.

Although this model for enzyme inactivation lacks a molecular basis, as far as the moisture dependence is concerned, it may be quite useful in setting up a catalogue of thermostability behaviour of different enzymes.

C H A P T E R 3

Mathematical description of the model for enzyme inactivation during drying.

3.1 Introduction.

In the vast literature on mathematical models for drying, only a few publications have dealt with the problem of simultaneous heat and mass transfer with variable physical properties in detail. A survey on different model concepts has been given recently by Fortes et al.[17], together with their own contributions in this field. Fortes et al.[17] proposed a general set of equations, incorporating most of the existing models, describing heat and mass transfer in porous media by combining the mechanistic approaches of liquid and vapour diffusion, liquid movement by capillarity and vaporization-condensation together with the concepts of irreversible thermodynamics. In their approach, flux relations for liquid, vapour and heat transfer are derived from irreversible thermodynamics by assuming local equilibrium and by considering the porous medium as a continuum and isotropic. The phenomenological coefficients in these relations are obtainded from flux relations, having their origin in mechanistic approaches. The authors have applied their model to describe non-isothermal drying of corn kernels [18] and found good agreement between predicted and experimental values. One may however question whether such an approach should be adopted, because of the large complexity of the resulting model, despite of important assumptions regarding the physical state of the

medium. Other authors [19-20] have applied the method of spatial averaging in order to derive a macroscopic form of Fick's law for unsteady diffusion. This approach however, also requires many assumptions in order to obtain the desired form. For liquid food systems, Kerkhof [21], Schoeber [22] and Van der Lijn [23] have developed a mathematical model, based on a macroscopic form of the diffusion equation, where all possible contributions to internal moisture transfer are lumped into an effective diffusion coefficient. This model, which also includes the effect of shrinkage, has been succesfully applied to the prediction of aroma retention during drying of carbohydrate solutions and the evaluation of concentration and temperature dependences of the effective diffusion coefficient [21-25]. Furthermore, the model has been applied in studies on enzyme inactivation during spray-drying [26-27].
The model for enzyme inactivation during drying is basically composed of the diffusion equation for binary systems, the heat balance and a part, describing enzyme inactivation kinetics. The thermodynamic equilibrium condition at the interface is given by the sorption isotherm, whereas variable physical properties of the medium like the moisture and temperature dependence of the diffusion coefficient are also included. In the following sections, the model equations for mass transfer, heat transfer and enzyme inactivation kinetics will be presented and transformed into appropriate coordinates in order to deal with the effect of shrinkage. At the end of this chapter, the complete model is given in a block diagram, interrelating the various model components.

3.2 *Mass balance of the dispersed phase.*

3.2.1 *The continuity equations for binary diffusion.*

Consider the binary system, consisting of a migrating component m and a solid component s. In case of binary diffusion, the mass fluxes relative to stationary coordinates are given by:

$$n_m = v_m \rho_m \tag{3.1}$$

and:

$$n_s = v_s \rho_s \tag{3.2}$$

where ρ_m and ρ_s are the mass concentrations and v_m and v_s the velocities of components m and s respectively. According to Fick's first law of binary diffusion, we may write [28]:

$$n_m = (n_m + n_s)\omega_m - D\rho\nabla\omega_m \tag{3.3}$$

where ω_m $(=\rho_m/\rho)$ represents the mass fraction of component m on total basis, ρ the total mass concentration and D the diffusion coefficient. The continuity equations for components m and s are expressed by:

$$\frac{\partial \rho_m}{\partial t} = -\nabla \cdot n_m \tag{3.4}$$

and:

$$\frac{\partial \rho_s}{\partial t} = - \nabla \cdot n_s \qquad (3.5)$$

Eqns.(3.1-3.5) are the basic equations, from which all other formulations of the diffusion equation with respect to different coordinate systems may be derived.
First we rewrite eqn.(3.3):

$$n_m = n_s \omega'_m - D\rho_s \nabla \omega'_m \qquad (3.6)$$

with ω'_m $(=\rho_m/\rho_s)$ representing the mass fraction of component m on component s basis. If we define the mass flux j^s_m relative to the velocity of component s, by:

$$j^s_m = \rho_m (v_m - v_s) = n_m - n_s \omega'_m \qquad (3.7)$$

then substitution in eqn.(3.6) gives:

$$j^s_m = -D\rho_s \nabla \omega'_m \qquad (3.8)$$

As for a binary system:

$$\frac{\rho_m}{d_m} + \frac{\rho_s}{d_s} = 1 \qquad (3.9)$$

where d_m and d_s denote the partial densities of components m and s, it follows that the mass concentration ρ_s is related to the mass fraction ω'_m by:

$$\frac{1}{\rho_s} = \frac{1}{d_s} + \frac{\omega'_m}{d_m} \qquad (3.10)$$

Substitution in eqn.(3.8) gives:

$$j_m^s = -D\left(\frac{d_m d_s}{d_m + d_s \omega'_m}\right)\nabla\omega'_m \qquad (3.11)$$

which expresses the mass flux j_m^s in terms of the mass fraction ω'_m only. Furtermore we may write:

$$\frac{\partial\omega'_m}{\partial t} = \frac{\partial}{\partial t}\left(\frac{\rho_m}{\rho_s}\right) = \frac{1}{\rho_s}\frac{\partial\rho_m}{\partial t} - \frac{\rho_m}{\rho_s^2}\frac{\partial\rho_s}{\partial t} \qquad (3.12)$$

which, after substitution of eqns.(3.4) and (3.5) turns into:

$$\rho_s \frac{\partial\omega'_m}{\partial t} = -\nabla\cdot n_m + \omega'_m \nabla\cdot n_s \qquad (3.13)$$

As, according to eqn.(3.7):

$$\nabla\cdot j_m^s = \nabla\cdot n_m - \omega'_m \nabla\cdot n_s - n_s\cdot\nabla\omega'_m \qquad (3.14)$$

eqn.(3.13) becomes:

$$\frac{\partial\omega'_m}{\partial t} + v_s\cdot\nabla\omega'_m = -\frac{1}{\rho_s}\nabla\cdot j_m^s = \frac{1}{\rho_s}\nabla\cdot(D\rho_s\nabla\omega'_m) \qquad (3.15)$$

where ρ_s may again be eliminated by applying eqn.(3.10). Eqn.(3.15) is a convenient formulation of the diffusion equation for shrinking systems, as will be shown later. For non-shrinking systems, a simpler formulation may however be obtained. Let the mass flux j_m^v relative to the volume averaged velocity v be defined as [28]:

$$j_m^v = \rho_m(v_m - v) = n_m - \rho_m v \qquad (3.16)$$

with:

$$v = v_m \frac{\rho_m}{d_m} + v_s \frac{\rho_s}{d_s} \tag{3.17}$$

resulting in:

$$j_m^v = n_m \frac{\rho_s}{d_s} - n_s \frac{\rho_m}{d_s} \tag{3.18}$$

From eqns.(3.7) and (3.18) then follows:

$$j_m^v = \frac{\rho_s}{d_s} j_m^s \tag{3.19}$$

or, according to eqn.(3.8):

$$j_m^v = -D \frac{\rho_s^2}{d_s} \nabla \omega'_m \tag{3.20}$$

Applying eqn.(3.10):

$$j_m^v = -D \nabla \rho_m \tag{3.21}$$

Since for non-shrinking systems the volume averaged velocity v is zero, according to eqn.(3.16) j_m^v will be equal to n_m, which turns eqn.(3.21) into:

$$n_m = -D \nabla \rho_m \tag{3.22}$$

and consequently, eqn.(3.4) becomes:

$$\frac{\partial \rho_m}{\partial t} = \nabla \cdot (D \nabla \rho_m) \tag{3.23}$$

which represents the simplified formulation of the diffusion equation for non-shrinking systems.

3.2.2 *Dimensionless forms of the diffusion equation.*

3.2.2.1 *Non-shrinking slabs, cylinders and spheres.*

For non-shrinking systems, the diffusion equation may be presented in fixed space coordinates. The one-dimensional diffusion equation for infinite slabs of finite thickness, infinitely long cylinders and spheres, according to eqn.(3.23) reads:

$$\frac{\partial \rho_m}{\partial t} = \frac{1}{r^\nu} \frac{\partial}{\partial r}(D\, r^\nu \frac{\partial \rho_m}{\partial r}) \tag{3.24}$$

which transforms into the dimensionless form:

$$\frac{\partial m}{\partial \tau} = \frac{\partial}{\partial \phi}(D_r X^2 \frac{\partial m}{\partial \phi}) \tag{3.25}$$

in which the dimensionless concentration m is defined as:

$$m = \frac{\rho_m}{\rho_{m,o}} \tag{3.26}$$

with $\rho_{m,o}$ the initial mass concentration of component m.
The dimensionless time τ is defined as:

$$\tau = \frac{D_o t}{R_d^2} \tag{3.27}$$

where D_o represents a reference value of the diffusion coefficient and R_d the radius or half-thickness of the system.
The dimensionless diffusion coefficient D_r is defined as:

$$D_r = \frac{D}{D_o} \tag{3.28}$$

The dimensionless space coordinate ϕ is defined as:

$$\phi = \left(\frac{r}{R_d}\right)^{\nu+1} \tag{3.29}$$

with r the fixed space coordinate and ν a geometry parameter, having the values $0,1$ and 2 for slab, cylinder and sphere respectively. In fact, the space coordinate ϕ represents the volume ratio of the regions $[0,r)$ and $[0,R_d)$. The dimensionless geometry variable X is defined as:

$$X = (\nu+1)\left(\frac{r}{R_d}\right)^{\nu} = (\nu+1)\phi^{\frac{\nu}{\nu+1}} \tag{3.30}$$

which represents the surface ratio of the above-mentioned regions times the factor $(\nu+1)$. The mass flux n_m for slab, cylinder and sphere becomes in case of one-dimensional diffusion, according to eqn.(3.22):

$$n_m = -D \frac{\partial \rho_m}{\partial r} \tag{3.31}$$

or, expressed in dimensionless variables:

$$F = \frac{R_d}{D_o \rho_{m,o}} n_m = -D_r X \frac{\partial m}{\partial \phi} \tag{3.32}$$

where F represents a dimensionless flux parameter, which is directly proportional to the mass flux n_m.

3.2.2.2 Shrinking slabs, cylinders and spheres.

When shrinkage occurs during desorption, the phase boundary will no longer remain at a fixed position in space.

This complication of a moving phase boundary is however avoided by transforming the diffusion equation into reference component mass centered coordinates [23], which may be considered as shrinking coordinates, following the movement of an arbitrary reference component. In case of one-dimensional diffusion, eqn.(3.15) becomes for slab, cylinder and sphere:

$$\frac{\partial \omega'_m}{\partial t} + v_s \frac{\partial \omega'_m}{\partial r} = \frac{1}{\rho_s r^\nu} \frac{\partial}{\partial r}\left(D \rho_s r^\nu \frac{\partial \omega'_m}{\partial r}\right) \tag{3.33}$$

which is converted into the dimensionless form, considering component s as the above-mentioned reference component:

$$\frac{\partial m}{\partial \tau} = \frac{\partial}{\partial \phi}\left(D_r X^{*2} \frac{\partial m}{\partial \phi}\right) \tag{3.34}$$

The dimensionless concentration m is now defined as:

$$m = \frac{\omega'_m}{\omega'_{m,o}} \tag{3.35}$$

where $\omega'_{m,o}$ represents the initial mass fraction of component m. The dimensionless time τ is defined as:

$$\tau = \frac{D_o \rho^2_{s,o}}{d_s^2 R_s^2} t \tag{3.36}$$

with $\rho_{s,o}$ the initial mass concentration of component s and R_s the radius or half-thickness of the system in case the mass concentration of component s equals its density. This so called "dry solids radius" is related to the initial radius R_o of the system by:

$$R_s = \left(\frac{\rho_{s,o}}{d_s}\right)^{\frac{1}{\nu+1}} R_o \tag{3.37}$$

which holds, if the total mass of component s is conserved within the system. The dimensionless diffusion coefficient D_r is defined as:

$$D_r = \frac{D\ \rho_s^2}{D_o \rho_{s,o}^2} \tag{3.38}$$

The dimensionless space coordinate ϕ reads:

$$\phi = \int_o^r \rho_s r^\nu\, dr \;/\; \int_o^{R_d} \rho_s r^\nu\, dr =$$

$$= \frac{\nu+1}{\rho_{s,o} R_o^{\nu+1}} \int_o^r \rho_s r^\nu\, dr \quad =$$

$$= \frac{\nu+1}{d_s R_s^{\nu+1}} \int_o^r \rho_s r^\nu\, dr \tag{3.39}$$

or, inversely:

$$r = (d_s R_s^{\nu+1} \int_o^\phi \frac{1}{\rho_s}\, d\phi)^{\frac{1}{\nu+1}} \tag{3.40}$$

and consequently:

$$R_d = R_s (1 + \frac{d_s \rho_{m,o}}{d_m \rho_{s,o}} \bar{m})^{\frac{1}{\nu+1}} \tag{3.41}$$

The dimensionless space coordinate ϕ represents the mass ratio of component s between the regions $[0,r)$ and $[0,R_d)$. If the partial densities d_m and d_s do not change upon mixing, the geometry variable X^* is given by:

$$X^* = (\nu+1)(\frac{r}{R_s})^\nu = (\nu+1)[\int_o^\phi \frac{d_s}{\rho_s}\, d\phi\ ]^{\frac{\nu}{\nu+1}} =$$

$$= (\nu+1)\left[\int_0^{\phi}\left(1 + \frac{d_s \rho_{m,o}}{d_m \rho_{s,o}}\, m\right) d\phi\right]^{\frac{\nu}{\nu+1}} \qquad (3.42)$$

which represents the surface ratio of the regions mentioned above times the factor $(\nu+1)$.

By means of this transformation from r-space to ϕ-space, the phase boundary is now fixed at the position $\phi=1$. Moreover, the velocity of component s in ϕ-space will be zero, as may be derived from eqns.(3.2) and (3.5). The mass flux j_m^s in case of one-dimensional diffusion becomes according to eqn.(3.8):

$$j_m^s = -D\rho_s \frac{\partial \omega_m'}{\partial r} \qquad (3.43)$$

or, expressed in dimensionless variables:

$$F^* = \frac{d_s R_s}{D_o \rho_{m,o} \rho_{s,o}}\, j_m^s = -D_r X^* \frac{\partial m}{\partial \phi} \qquad (3.44)$$

where F^* represents a dimensionless flux parameter, similar to the flux parameter F for non-shrinking systems, but is now directly proportional to the mass flux j_m^s.

3.2.3 Initial and boundary conditions.

In this subsection we will consider the initial and boundary conditions, which accompany the diffusion equation. The initial condition reads:

$$\rho_m = \rho_{m,o} \quad for\ t=0 \tag{3.45}$$

As for the boundary conditions we will restrict ourselves to three different kinds, i.e. the Dirichlet, Neumann and Robin boundary conditions, also known as boundary conditions of the first, second and third kind from potential theory. Furthermore we will only consider symmetrical solutions with respect to the centre, central axis or central plane of sphere, cylinder or slab. This symmetry condition may be expressed by:

$$\frac{\partial \rho_m}{\partial r} = 0 \quad for\ t>0\ and\ r=0 \tag{3.46}$$

The Dirichlet boundary condition specifies the concentration at the interface of the particle (dispersed phase) and the continuous gas phase:

$$\rho_m = \rho_{m,i} \quad for\ t>0\ and\ r=R_d \tag{3.47}$$

The Neumann and Robin boundary conditions on the contrary specify the normal derivative at the interface, which is given by the flux relations:

$$-D\,\frac{\partial \rho_m}{\partial r} = n_m = k_g^{eff}(\rho_{m,g,i} - \rho_{m,g,b}) \quad for\ t>0\ and\ r=R_d \tag{3.48}$$

in case of non-shrinking systems, and:

$$-D\rho_s \frac{\partial \omega'_m}{\partial r} = j_m^s = k_g^{eff}(\rho_{m,g,i} - \rho_{m,g,b}) \quad for\ t>0\ and\ r=R_d \qquad (3.49)$$

in case of shrinking systems, where the effective mass transfer coefficient k_g^{eff} represents the mass transfer coefficient corrected for Stefan diffusion [28], according to:

$$k_g^{eff} = \frac{k_g}{\omega_{m,g,i} - \omega_{m,g,b}} \ln \frac{1-\omega_{m,g,b}}{1-\omega_{m,g,i}} \qquad (3.50)$$

which in case the concentration difference between phase boundary and bulk of the gas phase is very small, turns into the limiting form:

$$k_g^{eff} = \frac{k_g}{1 - \omega_{m,g,i}} \qquad (3.51)$$

where the mass fractions of component m in the gas phase, $\omega_{m,g,i}$ (interface) and $\omega_{m,g,b}$ (bulk) are related to the corresponding mass concentrations $\rho_{m,g,i}$ and $\rho_{m,g,b}$ by:

$$\omega_{m,g} = \frac{\rho_{m,g}}{d_{a,g} + \rho_{m,g}(1-d_{a,g}/d_{m,g})} \qquad (3.52)$$

with $d_{a,g}$ and $d_{m,g}$ the partial densities of the gaseous component a (air) and component m (moisture) respectively. According to the ideal gas law, these densities may be related to pressure P and temperature T by:

$$d_{a,g} = M_a \frac{P}{RT} \qquad (3.53)$$

and:

$$d_{m,g} = M_m \frac{P}{RT} \tag{3.54}$$

with M the molecular weight.
In case of thermodynamic equilibrium at the phase boundary, the interfacial concentrations in both phases are related by the sorption isotherm, which is given by the general function:

$$a_w = a_w(\omega'_{m,i}, T_i) \tag{3.55}$$

where the wateractivity a_w is defined as:

$$a_w = \rho_{m,g,i} / \rho^{sat}_{m,g,i} \tag{3.56}$$

with $\rho^{sat}_{m,g,i}$ denoting the saturated water vapour concentration, which is a function of the interfacial temperature T_i (see also appendix B):

$$\rho^{sat}_{m,g,i} = \rho^{sat}_{m,g,i}(T_i) \tag{3.57}$$

It should be mentioned that the mass transfer coefficient may also be affected by shrinkage, but as Kerkhof [26] showed, this effect is only of minor importance. The mass transfer coefficient will however depend on the prevailing flow conditions around the system. In *table 3.1* some empirical correlations are presented for mass transfer in forced convection around submerged objects of different geometries [28-30].
The Neumann and Robin boundary conditions express the dependence of the internal mass flux on external mass transfer, which is absent in the Dirichlet boundary condition. The difference between the Neumann and Robin boundary conditions re-

Flow conditions		Gas phase mass transfer correlations. (Sc>0.6)
Flow parallel to slab over length L.		$Sh_g = \frac{k_g L}{D_g} = 0.332\, Re^{1/2} Sc^{1/3}$ ($Re < 3\times10^5$)
		$Sh_g = \frac{k_g L}{D_g} = 0.664\, Re^{1/2} Sc^{1/3}$ ($Re < 3\times10^5$)
Flow parallel to axis of long cylinder with radius R and length L.	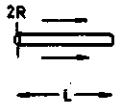	$Sh_g = \frac{k_g 2R}{D_g} = 1.86\, Re^{1/3} Sc^{1/3} (\frac{L}{2R})^{1/3} (\frac{\eta}{\eta_i})^{1/7}$ ($Re < 2300$)
		$Sh_g = \frac{k_g 2R}{D_g} = 0.027\, Re^{0.8} Sc^{1/3} (\frac{\eta}{\eta_i})^{1/7}$ ($2300 < Re < 10^5$)
Flow perpendicular to axis of long cylinder with radius R	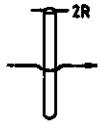	$Sh_g = \frac{k_g 2R}{D_g} = 0.42\, Sc^{0.2} + 0.57\, Re^{1/2} Sc^{1/3}$ ($1 < Re < 10^4$)
Flow past sphere with radius R.	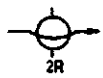	$Sh_g = \frac{k_g 2R}{D_g} = 2 + 0.552\, Re^{0.53} Sc^{1/3}$ ($1 < Re < 4.8\times10^4$)

Table 3.1

Empirical correlations for mass transfer in forced convection around submerged objects of different geometries.

gards the interfacial concentration $\rho_{m,g,i}$ which in case of a Neumann boundary condition remains constant, but varies in case of a Robin boundary condition. As the latter situation is less restrictive, the application of the Robin boundary condition throughout the desorption process is to be preferred. However, in the initial stage of the desorption process, in case internal diffusion is not yet rate limiting and the desorption rate is mainly controlled by external mass transfer, a constant wateractivity will be maintained at the phase boundary on the gas phase side. Under constant flow conditions and constant temperature, the Sherwood number for gas phase mass transfer at the interface, Sh_g will remain constant. If in addition the water vapour concentration in the bulk of the gas phase, $\rho_{m,g,b}$ remains constant, this will result in a constant flux for slabs, non-shrinking cylinders or spheres and a constant value of the product $j^s_{m,i} R_d$ for shrinking cylinders or spheres. These specific circumstances allow the application of the Neumann boundary condition. On the other hand, if the desorption rate is mainly controlled by internal diffusion, then the internal moisture content at the interface will be virtually constant and consequently the Dirichlet boundary condition applies. Finally, the initial and boundary conditions, expressed in dimensionless variables become:
The initial condition:

$$m = 1 \quad for\ \tau = 0 \tag{3.58}$$

The boundary condition at the centre (ϕ=0):

$$X \frac{\partial m}{\partial \phi} = 0 \tag{3.59}$$

for non-shrinking systems, or:

$$X^* \frac{\partial m}{\partial \phi} = 0 \qquad (3.60)$$

for shrinking systems.

The Dirichlet boundary condition at the interface (ϕ=1):

$$m = m_i \qquad (3.61)$$

The Neumann and Robin boundary conditions at the interface:

$$-(D_r X \frac{\partial m}{\partial \phi}) = F \qquad (3.62)$$

for non-shrinking systems, or:

$$-(D_r X^* \frac{\partial m}{\partial \phi}) = F^* \qquad (3.63)$$

for shrinking systems.

3.3 Heat balance of the dispersed phase.

In setting up the heat balance for the drying species (dispersed phase), we assume that heat is mainly supplied by air convection.

	Moisture diffusivity (m^2/s)	Thermal diffusivity (m^2/s)
Dispersed phase	$D_d < 10^{-9}$	$a_d \sim 10^{-7}$
Continuous phase	$D_g \sim 10^{-5}$	$a_g \sim 2 \times 10^{-5}$

Table 3.2
Typical values of thermal and moisture diffusivities.

A comparison between typical values of thermal and moisture diffusivities (*table 3.2*) referring to air drying of foods, shows that:

- Resistance to mass transfer is mainly situated in the dispersed phase.
- Resistance to heat transfer is mainly situated in the dispersed phase.
- Heat and mass diffusion in the gas phase are of the same order of magnitude.
- Heat diffusion in the dispersed phase is much faster than mass diffusion.

As on a time scale of mass diffusion, temperature gradients

will vanish relatively fast, we may therefore assume that the temperature profile in the dispersed phase is approximately uniform. Consequently the heat balance is expressed by:

$$\bar{\rho}_d \bar{c}_{p,d} \frac{dT_d}{dt} = \frac{\nu+1}{R_d}[\alpha_g^{eff}(T_b - T_d) - j_{m,i}^{s} \Delta H_{vap}] \qquad (3.64)$$

where $\bar{\rho}_d$, $\bar{c}_{p,d}$ and T_d represent the average density, heat capacity and temperature of the drying species; α_g^{eff} is the gas phase heat transfer coefficient, corrected for mass transfer; T_b is the temperature in the bulk of the gas phase and ΔH_{vap} the heat of vaporization. With the aid of eqns.(3.9) and (3.10), the average density $\bar{\rho}_d$ may be expressed in terms of the dimensionless concentration $\bar{m}$, yielding:

$$\bar{\rho}_d = \bar{\rho}_m + \bar{\rho}_s = d_s + \bar{\rho}_m(1 - \frac{d_s}{d_m}) = d_s + \rho_{m,o}\bar{m}(1 - \frac{d_s}{d_m}) \qquad (3.65)$$

for non-shrinking systems, or:

$$\bar{\rho}_d = \frac{1 + \bar{\omega}'_m}{1/d_s + \bar{\omega}'_m/d_m} = \frac{1 + \bar{\omega}'_{m,o}\bar{m}}{1/d_s + \bar{\omega}'_{m,o}\bar{m}/d_m} \qquad (3.66)$$

for shrinking systems.

If we assume, that the average heat capacity $\bar{c}_{p,d}$ is a function of the average moisture content and temperature (see also appendix B), we may write:

$$\bar{c}_{p,d} = \bar{c}_{p,d}(\bar{m}, T_d) \qquad (3.67)$$

According to Bird et al.[28], the heat transfer coefficient α_g^{eff} corrected for mass transfer reads:

$$\alpha_g^{eff} = \begin{cases} \alpha_g(1-\frac{\gamma}{2}) & \text{for } \gamma<0.1 \\ \alpha_g \frac{\gamma}{e^{\gamma}-1} \end{cases} \qquad (3.68)$$

where γ is defined as:

$$\gamma = \frac{j_{m,i}^{s} c_{p,m,g}}{\alpha_g} \qquad (3.69)$$

and $c_{p,m,g}$ is the heat capacity of water vapour. The uncorrected heat transfer coefficient α_g follows from the Chilton-Colburn analogy between heat and mass transfer:

$$\alpha_g = k_g(\bar{d}_{a,g}\bar{c}_{p,a,g})^{1/3} \left(\frac{\bar{\lambda}_{a,g}}{\bar{D}_g}\right)^{2/3} \qquad (3.70)$$

For the water vapour diffusivity D_g, the density $d_{a,g}$, the heat capacity $c_{p,a,g}$ and the thermal conductivity $\lambda_{a,g}$ of air, the average values between interface and bulk of the gas phase are taken. Moreover, water vapour diffusivity, thermal conductivity and heat of vaporization are assumed to be temperature dependent (see also appendix B):

$$D_g = D_g(T) \qquad (3.71)$$

and:

$$\lambda_{a,g} = \lambda_{a,g}(T) \qquad (3.72)$$

and:

$$\Delta H_{vap} = \Delta H_{vap}(T) \qquad (3.73)$$

3.4 Kinetics of enzyme inactivation.

Thermal inactivation of enzymes may in many cases be described by first order kinetics with a reaction rate proportional to the concentration of the active enzyme, ρ_e:

$$r_e = -k_e \rho_e \tag{3.74}$$

where the specific inactivation rate k_e is a function of moisture content and temperature (see chapter 2). The continuity equation for the enzyme reads:

$$\frac{\partial \rho_e}{\partial t} = -\nabla \cdot n_e + r_e \tag{3.75}$$

which is equivalent to:

$$\rho_s \frac{\partial \omega'_e}{\partial t} + v_s \cdot \nabla \omega'_e = -\nabla \cdot j_e^s + r_e \tag{3.76}$$

If we assume, that the velocities of enzyme and component s are equal, then the mass flux j_e^s relative to velocity v_s will be zero. Transforming eqn.(3.76) into reference component mass centered coordinates then leads to:

$$\rho_s \frac{\partial \omega'_e}{\partial t} = r_e \tag{3.77}$$

or:

$$\frac{\partial \omega'_e}{\partial t} = -k_e \omega'_e = r'_e \tag{3.78}$$

which yields after integration:

$$\frac{\omega'_e}{\omega'_{e,o}} = exp\ (-\int_o^t k_e dt) \tag{3.79}$$

or, in terms of the dimensionless time variable τ:

$$\frac{\omega'_e}{\omega'_{e,o}} = [exp\ (-\int_o^\tau k_e d\tau)]^{\frac{R_d^2}{D_o}} \tag{3.80}$$

for non-shrinking systems, or:

$$\frac{\omega'_e}{\omega'_{e,o}} = [exp\ (-\int_o^\tau k_e d\tau)]^{\frac{d_s^2 R_s^2}{D_o \rho_{s,o}^2}} \tag{3.81}$$

for shrinking systems.

A block diagram of the complete model for enzyme inactivation during drying is presented in *fig. 3.1*. It should be mentioned that the effective mass transfer coefficient is assumed to be known here. In case the mass transfer coefficient is unknown and for instance has to be evaluated from the Sherwood correlations as given in *table 3.1*, the diagram changes correspondingly. The model has been used for computer simulations of lipoxygenase inactivation during drying of which the results are given in chapter 6, where they are compared with experimental inactivation data. Furthermore, the model has been used for the development of an approximate method, involving a simplified computational procedure for the nonlinear diffusion equation, which will be treated in the next chapter.

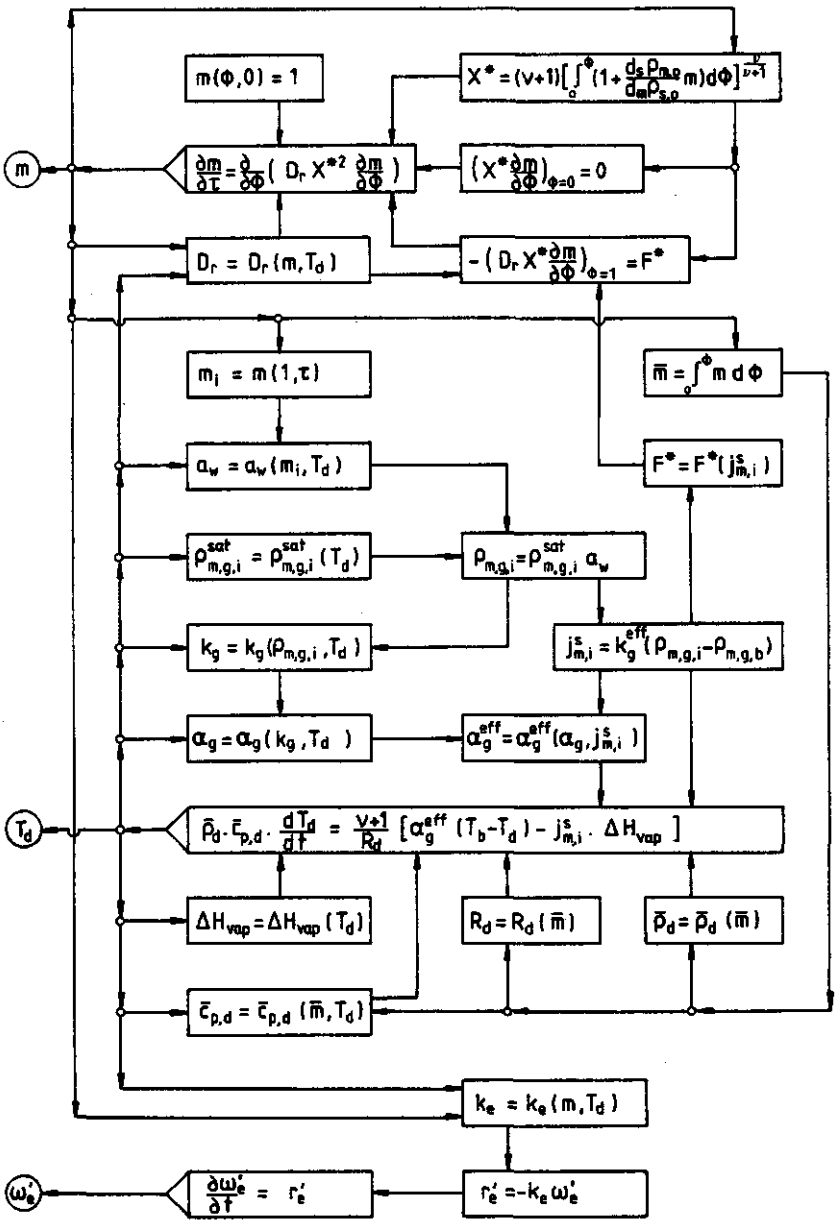

Fig. 3.1

Block diagram of the model for enzyme inactivation during drying.

C H A P T E R 4

An approximate method for the nonlinear diffusion problem.

4.1 Introduction.

The usual approach for solving nonlinear diffusion problems is the application of numerical techniques, which as a rule are only suitable for high-speed large-memory computers and require the necessary programming skill. In practice it would therefore be convenient when approximate methods, based on straightforward computational procedures are available for this class of problems in order to avoid time consuming programming and computing.
This chapter is concerned with the construction of such a computational procedure for desorption in non-shrinking or shrinking slabs, cylinders and spheres, which does not involve numerical techniques to solve the nonlinear partial differential equation, describing the diffusion process. Although the method developed here, is restricted to diffusion coefficients, which are power functions of concentration, this specific case is one of considerable interest for nonlinear diffusion in porous media, a topic, which has received much of attention in mathematical analysis in the last two decades, due to its importance in oil engineering and hydrology [31-37]. Other fields of possible applications are diffusion of vapours in high-polymer substances [38], drying of porous materials [39-41] and spray drying [21-27]. Furthermore, the approximate method is restricted to desorption with a uniform initial concentration profile and a constant surface concentration (Dirichlet boundary condition).

Other approximate methods were reported by Suzuki et al.[39], who developed a model for low-intensity drying of slabs, based on the assumption of a pseudo steady state, and by Schoeber [22,42], who introduced a general method for a short-cut calculation of the mass flux in nonlinear diffusion problems. The basic concept of Schoeber's method is the combination of the "short time solution", usually referred to as the penetration period, and the "large time solution", referred to as the regular regime. The same concept of combining these two limiting solutions served as a basis for this study, although the transition between the two solutions, as well as the effect of shrinkage were approached in a different way. An analysis of the numerical solution of the diffusion equation for the specific case mentioned above resulted in a simplified model based on approximate relations, which will be established in section 4.2. This model allows the computation of mass flux and desorption time by following a procedure, merely consisting of a sequence of straightforward calculations. However, this approximate method does not involve the computation of concentration profiles, which may be needed for specific applications as enzyme inactivation during drying, where the reaction rate is dependent on the local concentration. In case of a concentration dependent diffusion coefficient of the type: $D_r = m^a$, it was found that accurate approximations for the concentration profiles could be constructed by applying existing analytical solutions for the limiting cases: a=0 (constant diffusion coefficient) and $a \to \infty$. These approximations, again involve short and large time behaviour of the solutions and are treated in section 4.3. In addition an

appropriate transition criterion is formulated in order to link both limits. It has already been mentioned that the present method is only valid in case of a Dirichlet boundary condition, corresponding to the situation in which external mass transfer is not rate limiting. This situation may occur in high-intensity drying when the surface concentration rapidly decreases to a constant value. For other drying conditions, however, when resistance to mass transfer is gradually shifting from external to internal, application of the Robin boundary condition is to be preferred (see section 3.2.3). Unfortunately, the Robin boundary condition is far less susceptive to analytical treatment than the Dirichlet or Neumann boundary conditions. For this reason, the Robin boundary condition is replaced by the Neumann boundary condition for the initial stage and the Dirichlet boundary condition for the final stage of the drying process, which corresponds to the usual subdivision into a constant activity period and a falling rate period. In section 4.4 this matter will be discussed in further detail. Another matter of concern is drying under non-isothermal conditions, which will be treated in section 4.5. Application of the approximate method to enzyme inactivation during drying is easily realized, as drying conditions influence enzyme inactivation, but not inversely.

The approximate method has been tested by solving the diffusion equation numerically according to Crank-Nicolson's method with variable implicitness [21-23]. In addition, another numerical technique, involving orthogonal collocation, was employed for obtaining the large time solution.

4.2 *An approximate method for the computation of mass flux and desorption time under Dirichlet boundary conditions.*

In this section, a method is proposed for approximate calculations, concerning concentration dependent diffusion with a power relation between diffusion coefficient and concentration ($D_r = m^a$). This method can be applied to a desorption process in non-shrinking as well as shrinking systems with slab, cylindrical or spherical geometry. The method is restricted to desorption, with a uniform initial concentration profile and a Dirichlet boundary condition, i.e. constant surface concentration, whereas symmetry is assumed with respect to centre, central axis or central plane of the system.

4.2.1 *Non-shrinking systems.*

For the nonlinear diffusion equation with $D_r = m^a$, no explicit general solution in terms of familiar analytical functions is known to exist. For a slab, however, a particular solution can be derived, which represents the "large time solution" or "regular regime solution", but is only applicable when the centre concentration starts to deviate appreciably from the initial centre concentration. This particular solution is found after separation of variables in the diffusion equation, followed by solution of the space and time dependent parts. For non-shrinking systems with $D_r = m^a$, the diffusion equation, according to eqn.(3.25) is:

$$\frac{\partial m}{\partial \tau} = \frac{\partial}{\partial \phi}\left[m^a (\nu+1)^2 . \phi^{\frac{2\nu}{\nu+1}} . \frac{\partial m}{\partial \phi}\right] \qquad (4.1)$$

subject to:

$$m = 1 \qquad for\ \tau = 0 \quad and \quad 0 \leq \phi \leq 1 \tag{4.2}$$

$$X.\ \frac{\partial m}{\partial \phi} = 0 \qquad for\ \tau > 0 \quad and \quad \phi = 0 \tag{4.3}$$

$$m = 0 \qquad for\ \tau > 0 \quad and \quad \phi = 1 \tag{4.4}$$

Separation of variables is achieved by substituting: $m(\phi,\tau) = f(\tau).g(\phi)$ in eqn.(4.1), resulting in two ordinary differential equations:

$$\frac{df}{d\tau} = \lambda.f^{a+1} \tag{4.5}$$

and:

$$\frac{d}{d\phi}[g^{a}(\nu+1)^{2}.\phi^{\frac{2\nu}{\nu+1}}.\frac{dg}{d\phi}] = \lambda.g \tag{4.6}$$

In terms of the reduced variable g_r, defined as:

$$g_r(\phi) = \frac{g(\phi)}{g(0)} = \frac{g(\phi)}{g_c} \tag{4.7}$$

eqn.(4.6) becomes:

$$\frac{d}{d\phi}[g_r^{a}.\phi^{\frac{2\nu}{\nu+1}}.\frac{dg_r}{d\phi}] = -P_{a,\nu}.g_r \tag{4.8}$$

with:

$$P_{a,\nu} = \frac{-\lambda}{(\nu+1)^{2}g_c^{a}} \tag{4.9}$$

Substitution of $\bar{m} = f.\bar{g}$ in eqn.(4.5) yields:

$$\lambda = \frac{1}{f^{a}.\bar{m}} \frac{d\bar{m}}{d\tau} \tag{4.10}$$

The overall mass balance follows from integration of eqn. (4.1) in the range $\phi = 0$ to $\phi = 1$, resulting in:

$$\frac{d\bar{m}}{d\tau} = -(\nu+1)F \tag{4.11}$$

Mass transfer in the dispersed phase may be characterized by means of an average Sherwood number. In accordance with Schoeber's definition [22] the average Sherwood number is given by:

$$Sh_{d} = \frac{2F}{(\bar{m} - m_{i})\bar{D}_{r}} \tag{4.12}$$

with $\bar{D}_{r}$ the concentration averaged reduced diffusion coefficient, defined as:

$$\bar{D}_{r} = \frac{1}{\bar{m} - m_{i}} \int_{m_{i}}^{\bar{m}} D_{r} d\bar{m} \tag{4.13}$$

For a zero surface concentration m_{i} and $D_{r}=m^{a}$, eqn.(4.12) yields:

$$F = \frac{Sh_{d,a,\nu}}{2(a+1)} \bar{m}^{a+1} \tag{4.14}$$

Substitution of eqn.(4.14) in eqn.(4.11) then leads to:

$$\frac{d\bar{m}}{d\tau} = \frac{-(\nu+1)Sh_{d,a,\nu}}{2(a+1)} \bar{m}^{a+1} \tag{4.15}$$

Substitution of eqn.(4.15) in eqn.(4.10) then gives:

$$\lambda = \frac{-(\nu+1)Sh_{d,a,\nu}}{2(a+1)f^{a}} \cdot \bar{m}^{a} = \frac{-(\nu+1)Sh_{d,a,\nu}}{2(a+1)} \cdot \bar{g}^{a} \qquad (4.16)$$

and consequently, the parameter $P_{a,\nu}$,according to eqn.(4.9) becomes:

$$P_{a,\nu} = \frac{Sh_{d,a,\nu} \cdot \bar{g}_r^{a}}{2(\nu+1)(a+1)} \qquad (4.17)$$

If we assume the large time solution to be valid at time τ_Q, when the average concentration has arrived at a value $\bar{m}_Q$, integration of eqn.(4.15) results in:

$$\bar{m} = [\bar{m}_Q^{-a} + \frac{(\nu+1)a.Sh_{d,a,\nu}}{2(a+1)} (\tau - \tau_Q)]^{-\frac{1}{a}} \quad for\ a \neq 0 \qquad (4.18)$$

The trivial case of $a=0$ will not be considered here. For the time dependent part of the particular solution we may write:

$$f(\tau) = \frac{m(\phi,\tau)}{g(\phi)} = \frac{\bar{m}}{\bar{g}} \qquad (4.19)$$

from which follows:

$$m(\phi,\tau) = \frac{g_r(\phi)}{\bar{g}_r}[\bar{m}_Q^{-a} + \frac{(\nu+1)a.Sh_{d,a,\nu}}{2(a+1)} (\tau - \tau_Q)]^{-\frac{1}{a}} \qquad (4.20)$$

As an alternative, this solution may be expressed in terms of the efficiency E, rather than in terms of the time variable τ, yielding:

$$m(\phi,E) = \frac{g_r(\phi)}{\bar{g}_r} (1-E) \qquad (4.21)$$

where the efficiency E is defined as:

$$E = 1 - \bar{m} \tag{4.22}$$

and $g_r(\phi)$ and $\bar{g}_r$ follow from eqn.(4.8), which is subject to the boundary conditions:

$$\phi^{\frac{\nu}{\nu+1}} \cdot \frac{dg_r}{d\phi} = 0 \quad and \quad g_r = 1 \quad at \ \phi = 0 \tag{4.23}$$

$$g_r = 0 \qquad at \ \phi = 1 \tag{4.24}$$

This nonlinear differential equation can be classified as a specific case of the Emden-Fowler equation, discussed extensively by Fowler [43] in relation to astrophysics and more recently has found a renewed interest in the context of diffusion with chemical reaction [44], where the steady state problem leads to a similar differential equation. An analytical solution for the case of slab geometry ($\nu=0$) is presented in appendix A, according to which the average value of g_r is expressed by:

$$\bar{g}_r = \frac{2}{B(\frac{a+1}{a+2}, \frac{1}{2})} \tag{4.25}$$

and the parameter $P_{a,0}$ by:

$$P_{a,0} = \frac{B^2(\frac{a+1}{a+2}, \frac{1}{2})}{2(a+2)} \tag{4.26}$$

Substitution of eqns.(4.25) and (4.26) in eqn.(4.17) yields:

$$Sh_{d,a,0} = 2^{-a}(\frac{a+1}{a+2}) \cdot B^{a+2}(\frac{a+1}{a+2}, \frac{1}{2}) \tag{4.27}$$

which gives explicitly the average Sherwood number for the case of slab geometry in terms of the beta function B. For cylinder and sphere, the Sherwood numbers were calculated numerically by Schoeber [22]. Surprisingly, almost straight lines are obtained, when Sh_d values are plotted against $\frac{a}{a+2}$, as is shown in *fig. 4.1*, suggesting an approximate linear relationship expressed by:

$$Sh_{d,a,\nu} = Sh_{d,0,\nu} + (Sh_{d,\infty,\nu} - Sh_{d,0,\nu})(\frac{a}{a+2}) \qquad (4.28)$$

where $Sh_{d,0,\nu}$ and $Sh_{d,\infty,\nu}$ represent the average Sherwood numbers for $a=0$ and $a \to \infty$ respectively of which the exact values are given in *table 4.1*. Introducing these values in eqn.(4.28), eventually results in the following expressions:

$$Sh_{d,a,0} = \frac{\pi^2 + e^2.a}{a+2} \qquad \textit{(slab)} \qquad (4.29)$$

$$Sh_{d,a,1} = \frac{11.566 + 4e.a}{a+2} \qquad \textit{(cylinder)} \qquad (4.30)$$

$$Sh_{d,a,2} = \frac{4\pi^2/3 + e^{8/3}.a}{a+2} \qquad \textit{(sphere)} \qquad (4.31)$$

After substitution of these Sherwood correlations in eqn. (4.14), simple expressions for the flux parameter F as a function of the power a and the average concentration are obtained. It should be observed, however, that these approximations are only valid after some arbitrary time τ_Q and are of no use for the initial stage of the desorption process. For this part of the process, an approximation, based on the short time solution for a slab, will be established later. First, an auxiliary variable G is introduced, which we shall

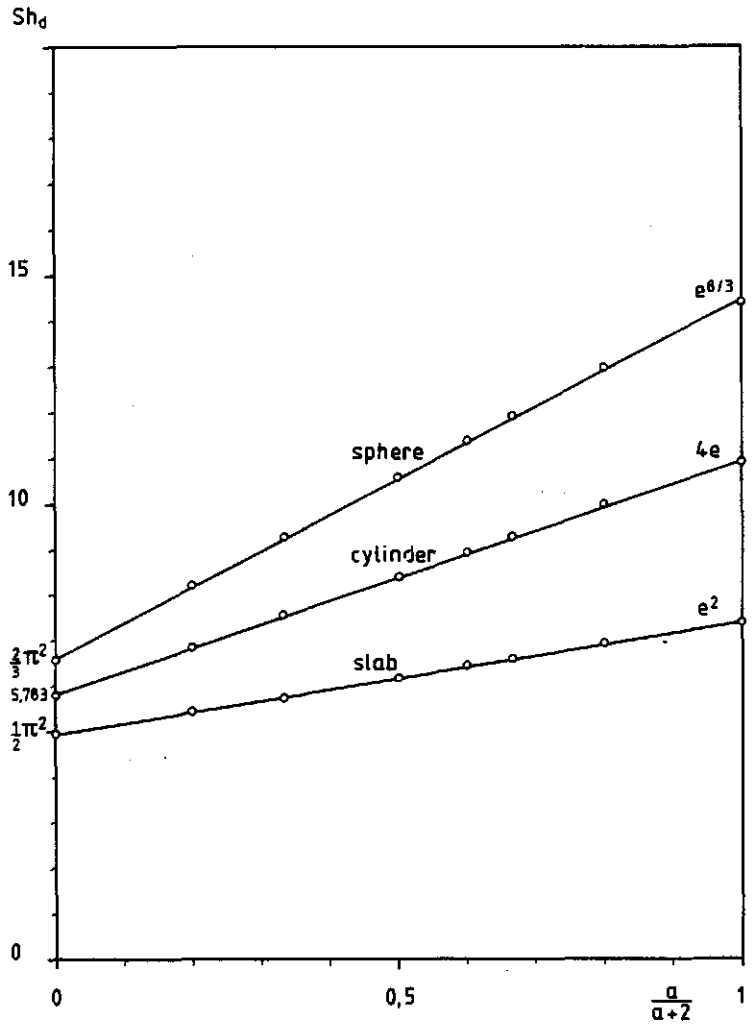

Fig. 4.1. The Sherwood number at different values of a.
(o): numerical, (−): linear approximation.

	Slab ν=0	Cylinder ν=1	Sphere ν=2
$Sh_{d,0,\nu}$	$\frac{1}{2}\pi^2$	5.783	$\frac{2}{3}\pi^2$
$Sh_{d,\infty,\nu}$	e^2	$4e$	$e^{8/3}$

Table 4.1
Limit values of the Sherwood number.

call the flux function:

$$G = \frac{E.F}{\nu+1} \tag{4.32}$$

which, expressed in terms of the efficiency E becomes:

$$G = \frac{Sh_{d,a,\nu}}{2(a+1)(\nu+1)} E(1-E)^{a+1} \tag{4.33}$$

For the derivatives of the flux function G with respect to E then follows:

$$G^{(1)} = \frac{1-(a+2)E}{E(1-E)} . G \tag{4.34}$$

$$G^{(n)} = \frac{n-(a+2)E}{E(1-E)^n} (-1)^{n+1} . \prod_{k=0}^{n-2} (a+1-k)G \tag{4.35}$$

The flux function G possesses a maximum S in case of a zero first derivative and negative second derivative. From eqn. (4.34) then follows:

$$E_S = \frac{1}{a+2} \tag{4.36}$$

and according to eqn. (4.35):

$$G_S^{(2)} = - \frac{(a+1)^4}{a^2} G_S < 0 \qquad (\forall\ a > 0) \tag{4.37}$$

indicating, that S is indeed a maximum. Moreover, the flux function possesses a point of inflection Q in case of a zero second derivative. Consequently, according to eqn.(4.35):

$$E_Q = \frac{2}{a+2} \tag{4.38}$$

Once again it is stressed that the relations given above do not hold for the initial stage of the desorption process. We continue our analysis by investigating the behaviour of the flux function G in the limit $E \to 0$. The value of G for very short times is equal for slab, cylinder and sphere, because the diffusion process at this stage takes place in an infinitesimally thin shell at the interface and consequently the influence of curvature is still negligible. Hence, we may write:

$$\lim_{E \to 0} G_{a,0} = \lim_{E \to 0} G_{a,1} = \lim_{E \to 0} G_{a,2} = G_o \tag{4.39}$$

For a constant diffusion coefficient ($a=0$), G_o can be derived analytically from the short time solution for a slab [45], according to which the average concentration is given by:

$$\bar{m} = m_o - 2(m_o - m_i)\left(\frac{\tau}{\pi}\right)^{\frac{1}{2}} = 1 - 2\left(\frac{\tau}{\pi}\right)^{\frac{1}{2}} \tag{4.40}$$

or, in terms of the efficiency E:

$$E = 2\left(\frac{\tau}{\pi}\right)^{\frac{1}{2}} \tag{4.41}$$

The flux parameter F follows from:

$$F = -\frac{d\bar{m}}{d\tau} = \frac{1}{\pi}\left(\frac{\tau}{\pi}\right)^{-\frac{1}{2}} \tag{4.42}$$

Substitution in eqn.(4.32) then results in:

$$G_o = \frac{2}{\pi} \tag{4.43}$$

For values of $a>0$, the limit G_o cannot be evaluated in a similar way. However, the following relation appeared to be of sufficient accuracy:

$$G_o = G_{a,\nu,S} + (G_{0,\nu,o} - G_{0,\nu,S})2^{-a} \qquad (4.44)$$

in which $G_{0,\nu,o}$ represents G_o for $a=0$ and $G_{a,\nu,S}$ the particular solution of G in point S, as given by eqn.(4.33). $G_{0,\nu,S}$ is also given by eqn.(4.33), which for $a=0$ results in:

$$G_{0,\nu,S} = \frac{\pi^2}{16} \qquad (4.45)$$

Eqn.(4.44) then turns into:

$$G_o = \frac{Sh_{d,a,0}}{2(a+1)(a+2)} \left(\frac{a+1}{a+2}\right)^{a+1} + \left(\frac{2}{\pi} - \frac{\pi^2}{16}\right)2^{-a} \qquad (4.46)$$

where $Sh_{d,a,0}$ has to be evaluated from eqn.(4.29). This approximate relation for the flux function is nevertheless only valid for very short times and a gap still remains between the short and large time limits. The problem is, how the flux function G, starting from its short time limit G_o, merges into its large time limit, the regular regime. In order to solve this transition problem, a transition point has to be defined, which belongs to the regular regime. It should be observed that the choice of such a point depends on the bounds of the regular regime, particularly the lower bound. According to the regular regime solution, the centre concentration may exceed the value one, which of course is impossible. The use of the regular regime solution is therefore restricted to the region $E \geq E_T$, in which $m_c \leq 1$.

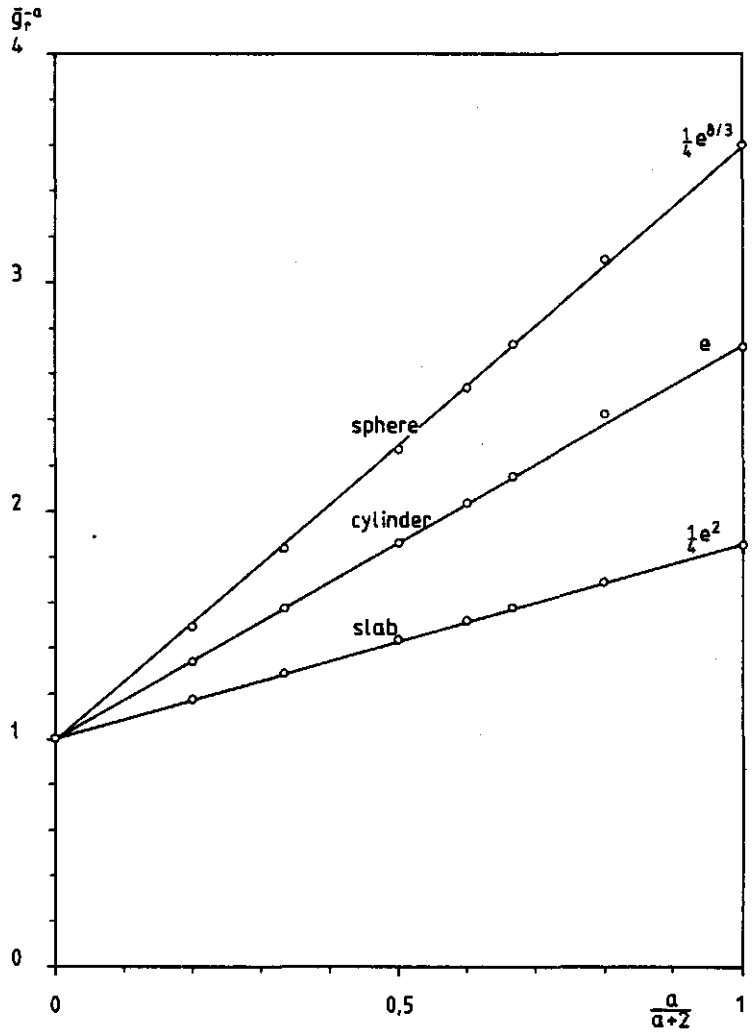

Fig. 4.2 The average reduced concentration $\bar{g}_r$ at different values of a.
(o): numerical, (−): linear approximation.

Since the efficiency E may be expressed as:

$$E = 1 - \bar{m} = 1 - \bar{g}_r . m_c \tag{4.47}$$

Hence, the lower bound of the regular regime, corresponding to $m_c=1$, reads:

$$E_T = 1 - \bar{g}_r \tag{4.48}$$

For a slab, $\bar{g}_r$ can again be evaluated analytically by applying eqn.(4.25), whereas for cylinder and sphere no relations are available. It appears, however, that a pseudo linear relationship exists between $\bar{g}_r^{-a}$ and the factor $\frac{a}{a+2}$, as is shown in *fig. 4.2*. This pseudo linearity is expressed by the following relations for slab, cylinder and sphere respectively:

$$\bar{g}_{r,a,0} = \left(\frac{a+2}{2 + \frac{1}{4}e^2 a}\right)^{\frac{1}{a}} \quad \text{for } a>0 \quad \left(\bar{g}_{r,0,0} = \frac{2}{\pi}\right) \tag{4.49}$$

$$\bar{g}_{r,a,1} = \left(\frac{a+2}{2 + e.a}\right)^{\frac{1}{a}} \quad \text{for } a>0 \quad (\bar{g}_{r,0,1} = 0.4318) \tag{4.50}$$

$$\bar{g}_{r,a,2} = \left(\frac{a+2}{2 + \frac{1}{4}e^{8/3}.a}\right)^{\frac{1}{a}} \quad \text{for } a>0 \quad \left(\bar{g}_{r,0,2} = \frac{3}{\pi^2}\right) \tag{4.51}$$

For the centre concentration m_c in the regular regime follows, according to eqn.(4.47):

$$m_c = \frac{1-E}{\bar{g}_r} \tag{4.52}$$

This relation is shown graphically in *figs. 4.3, 4.4* and *4.5*,

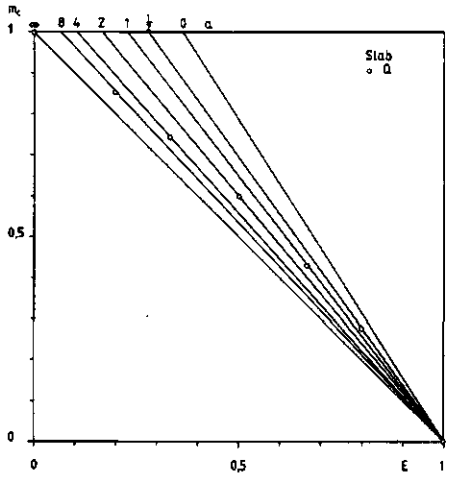

Fig. 4.3
Centre concentration m_c in the regular regime as a function of the efficiency E for a slab at different values of a.

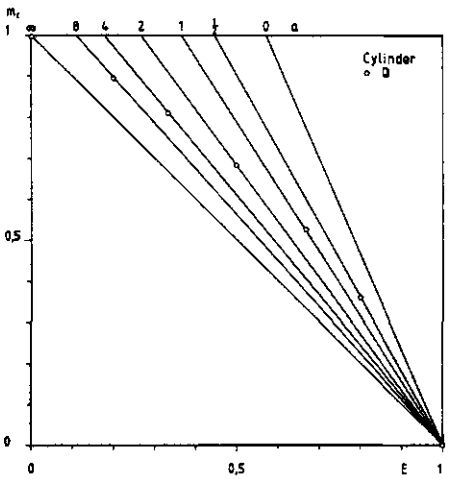

Fig. 4.4
Centre concentration m_c in the regular regime as a function of the efficiency E for a cylinder at different values of a.

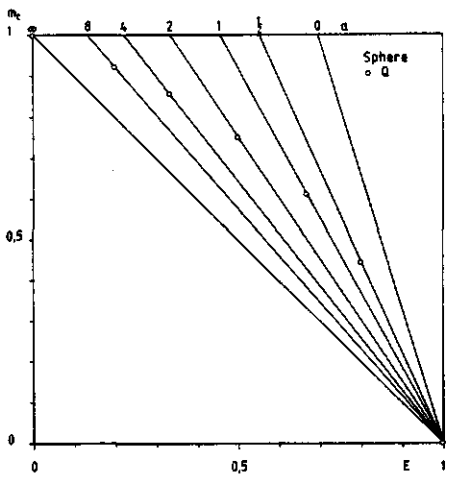

Fig. 4.5
Centre concentration m_c in the regular regime as a function of the efficiency E for a sphere at different values of a.

for slab, cylinder and sphere respectively. It may be observed that these lines intersect the line $m_c=1$, illustrating the bounds of the regular regime as discussed above. In these diagrams, also the location of the inflection point Q for different values of a is indicated. It may be shown graphically, that the condition $E_Q \geq E_T$ holds for $\nu = 0,1,2$ and for all values of $a \geq 0$, which means that point Q stays within the bounds of the regular regime and may therefore be chosen as a transition point. Moreover, as follows from eqn. (4.38), the location of point Q in terms of the efficiency E, is independent of the geometry parameter ν and a function of a only. For the transition region $0 < E \leq E_Q$ the flux function G is approximated by an appropriate Taylor series expansion, starting in point $(0,G_o)$ and merging into the large time solution. For a smooth transition in point Q, the Taylor series approximation must at least satisfy the conditions: $G = G_Q$ and $G^{(1)} = G_Q^{(1)}$. If these are the only conditions imposed on the transition, appropriate Taylor series approximations for the flux function in the transition region are:

a) Slab:

$$G = G_o + \frac{E^5}{5!} G_o^{(5)} + \frac{E^6}{6!} G_o^{(6)} \tag{4.53}$$

The two unknown derivatives $G_o^{(5)}$ and $G_o^{(6)}$ are evaluated with the aid of the two conditions in point Q, leading to:

$$G_o^{(5)} = \frac{6!}{E_Q^5} \left[G_Q - G_o - \frac{E_Q}{6} G_Q^{(1)} \right] \tag{4.54}$$

$$G_o^{(6)} = \frac{5!}{E_Q^5} \left[G_Q^{(1)} - \frac{E_Q^4}{4!} G_o^{(5)} \right] \tag{4.55}$$

where G_Q and $G_Q^{(1)}$ have to be evaluated from eqns.(4.33), (4.34) and (4.38).

b) Cylinder, sphere:

$$G = G_o + E.G_o^{(1)} + \frac{E^2}{2} G_o^{(2)} \tag{4.56}$$

with:

$$G_o^{(1)} = \frac{2}{E_Q}\left[G_Q - G_o + \frac{E_Q}{2} G_Q^{(1)}\right] \tag{4.57}$$

$$G_o^{(2)} = \frac{1}{E_Q}\left[G_Q^{(1)} - G_o^{(1)}\right] \tag{4.58}$$

It should be mentioned that, although the choice of the Taylor series is arbitrary, the resulting approximation is valid for all values of $a \geq 0$. The value of the flux parameter in the transition region follows from eqn.(4.32) together with either eqn.(4.53) or eqn.(4.56). Integration of the mass balance, represented by eqn.(4.11) then leads to the desorption time τ:

$$\tau = \frac{1}{\nu+1} \int_o^E \frac{1}{F}\, dE \qquad \text{for } 0 \leq E \leq E_Q \tag{4.59}$$

$$\tau = \tau_Q + \frac{1}{\nu+1} \int_{E_Q}^E \frac{1}{F}\, dE \qquad \text{for } E > E_Q \tag{4.60}$$

We shall first consider the interval $0 \leq E \leq E_Q$ and elaborate eqn.(4.59) for slab, cylinder and sphere by substitution of F.

a) Slab:

$$\tau = \int_0^E \frac{E}{G_o + \frac{E^5}{5!}G_o^{(5)} + \frac{E^6}{6!}G_o^{(6)}}\, dE \qquad (4.61)$$

Unfortunately this integral cannot be transformed into a simple algebraic expression. However, a simple numerical evaluation of the integral by applying the trapezium rule for instance, already gives satisfactory results.

b) Cylinder, sphere:

$$\tau = \frac{1}{(\nu+1)^2} \int_0^E \frac{E}{G_o + E.G_o^{(1)} + \frac{E^2}{2}G_o^{(2)}}\, dE =$$

$$= \frac{1}{(\nu+1)^2}\left[\frac{1}{G_o^{(2)}} ln\left(\frac{G}{G_o}\right) - \frac{G_o^{(1)}}{G_o^{(2)}\sqrt{q}} ln\left\{\frac{(G_o^{(2)}.E+G_o^{(1)}-\sqrt{q})(G_o^{(1)}+\sqrt{q})}{(G_o^{(2)}.E+G_o^{(1)}+\sqrt{q})(G_o^{(1)}-\sqrt{q})}\right\}\right]$$

with: $q = [G_o^{(1)}]^2 - 2G_o.G_o^{(2)}$ (4.62)

If $E=E_Q$ eqns.(4.61) and (4.62) can be used for the calculation of τ_Q, which value must be known for the determination of the desorption time in the region $E>E_Q$. Substitution of F according to eqn.(4.14) in eqn.(4.60) then results in:

$$\tau = \tau_Q + \frac{2(a+1)}{(\nu+1)a.Sh_{d,a,\nu}} [(1-E)^{-a} - (1-E_Q)^{-a}] \qquad (4.63)$$

A complete outline for the computation of the desorption time τ is presented in *fig. 4.6*, which applies to desorption in slabs, non-shrinking cylinders and spheres with a diffusion coefficient of the type $D_r = m^a$, a uniform initial concentration profile and a constant zero surface concentration.

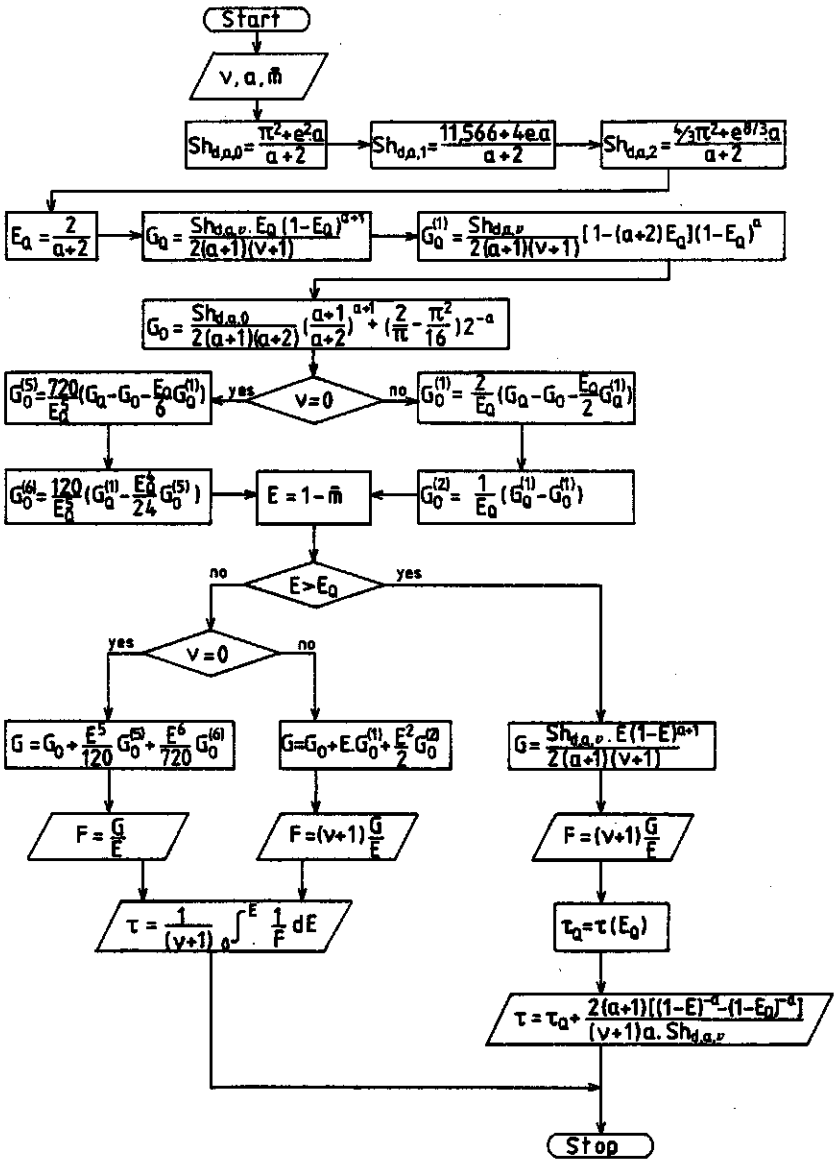

Fig. 4.6 Computational procedure for a desorption process in slabs, non-shrinking cylinders or spheres.

4.2.2 Shrinking systems.

When shrinkage of the system occurs during the desorption process, the mass flux has to be corrected for this phenomenon. Because the mass flux $j^{s}_{m,i}$ in a reference component mass centered coordinate system is directly proportional to the flux parameter F^* (see chapter 3), the correction for shrinkage can be applied directly to F^*. The mass balance for shrinking systems reads:

$$\frac{d\bar{m}}{d\tau} = -X^*_i . F^* \tag{4.64}$$

in which:

$$X^*_i = (\nu+1)(1 + \frac{d_s \cdot \rho_{m,o}}{d_m \cdot \rho_{s,o}} - \bar{m})^{\frac{\nu}{\nu+1}} \tag{4.65}$$

and:

$$F^* = -X^*_i . D_r (\frac{\partial m}{\partial \phi})_{\phi=1} \tag{4.66}$$

In the limit $\tau \to 0$, the concentration profile approaches the rectangular shape of the initial concentration profile for all values of $a \geq 0$, whereas the influence of shrinkage is still negligible, implying the following relation:

$$\lim_{\tau \to 0} \frac{F^*}{X^*_i} = \lim_{\tau \to 0} \frac{F}{X_i} \tag{4.67}$$

or:

$$\lim_{\tau \to 0} F^* = \lim_{\tau \to 0} \frac{X^*_i}{X_i} F = (1 + \frac{d_s \cdot \rho_{m,o}}{d_m \cdot \rho_{s,o}})^{\frac{\nu}{\nu+1}} . \lim_{\tau \to 0} F \tag{4.68}$$

We define the shrinkage factor H by:

$$H = \frac{F^*}{F} \tag{4.69}$$

From eqn.(4.68) then follows:

$$H_o = \lim_{\tau \to 0} H = (1 + \frac{d_s \cdot \rho_{m,o}}{d_m \cdot \rho_{s,o}})^{\frac{\nu}{\nu+1}} \tag{4.70}$$

which represents the short time limit of the shrinkage factor H. It was found by Schoeber, that the correction for shrinkage in the regular regime can be described accurately by:

$$H = 1 + \frac{\Delta Sh_{d,\nu}}{Sh_{d,a,\nu}} \qquad for\ E > E_Q \tag{4.71}$$

where:

$$\Delta Sh_{d,\nu} = Sh_{d,\infty,\nu}[(1 + \frac{d_s \cdot \rho_{m,o}}{d_m \cdot \rho_{s,o}} \cdot \bar{m})^{\frac{\nu}{\nu+1}} - 1] \tag{4.72}$$

and $Sh_{d,a,\nu}$ representing the average Sherwood number in case shrinkage is absent. The transition between the short and large time limits may be approached in a similar way as for the flux function. Starting from the short time limit H_o the shrinkage factor H is expanded in a Taylor series, containing the appropriate terms:

$$H = H_o + \frac{E^2}{2} H_o^{(2)} + \frac{E^3}{6} H_o^{(3)} \qquad for\ 0 \leq E \leq E_Q \tag{4.73}$$

with:

$$H_o^{(2)} = \frac{6}{E_Q^2}\left[H_Q - H_o - \frac{E_Q}{3} H_Q^{(1)}\right] \qquad (4.74)$$

$$H_o^{(3)} = \frac{2}{E_Q^2}\left[H_Q^{(1)} - E_Q . H_o^{(2)}\right] \qquad (4.75)$$

Integration of the mass balance leads to the following expressions for the desorption time τ:

$$\tau = \int_o^E \frac{1}{X_i^* . H . F}\, dE \qquad \text{for } 0 \leq E \leq E_Q \qquad (4.76)$$

and:

$$\tau = \tau_Q + \int_{E_Q}^E \frac{1}{X_i^* . H . F}\, dE \qquad \text{for } E > E_Q \qquad (4.77)$$

where F is the flux parameter if no shrinkage would have occurred and is an explicit function of the efficiency E, given by the relations from the preceding subsection. Moreover, X_i^* and H are explicit functions of E too. Hence, the evaluation of the integrals in eqns.(4.76) or (4.77) is straightforward. The computational procedure for a desorption process in a shrinking cylinder or sphere is presented in the flow diagram of *fig. 4.7.*

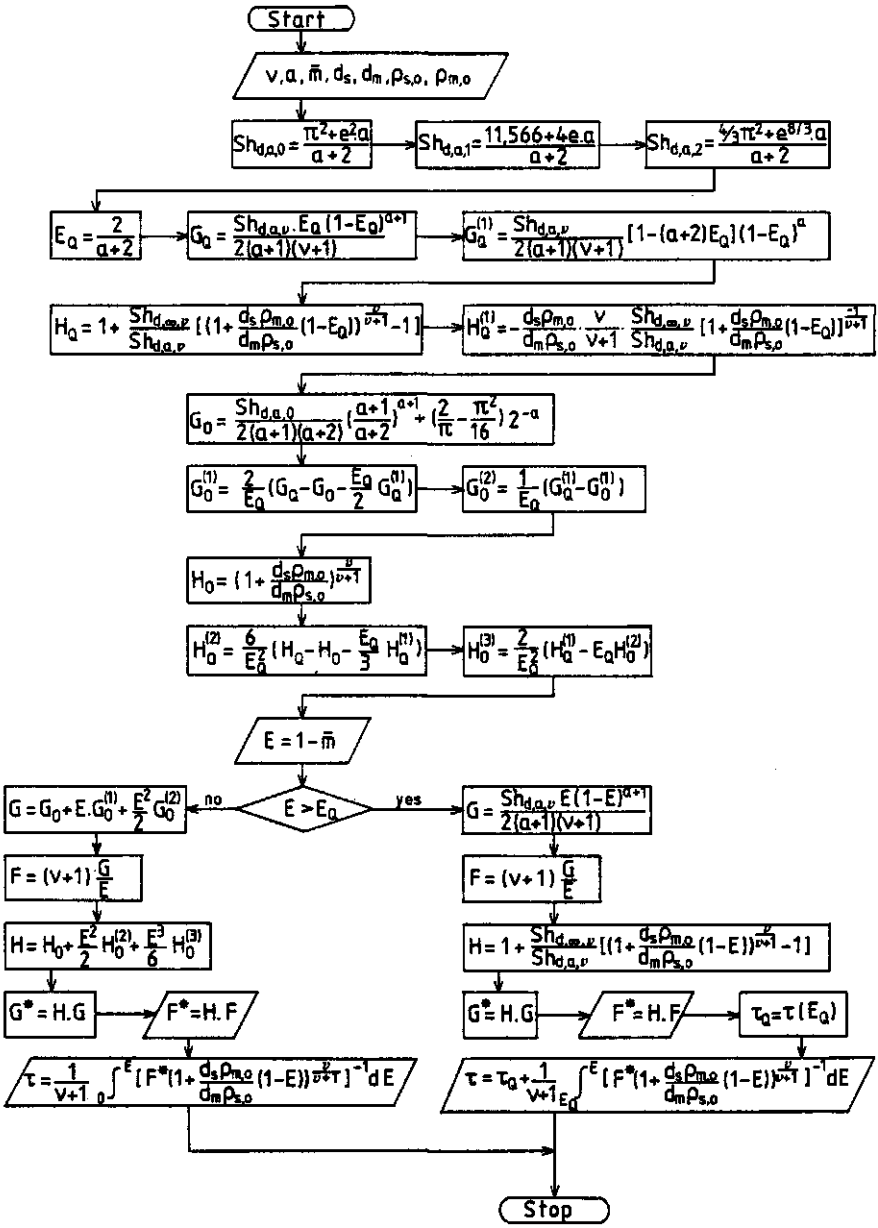

Fig. 4.7 Computational procedure for a desorption process in shrinking cylinders or spheres.

4.2.3 A comparison between approximate and numerical methods

The approximate solutions, generated by following the procedures as indicated in the flow diagrams of *figs. 4.6* and *4.7*, are shown in *figs. 4.8*, *4.9* and *4.10*, where the flux function G for non-shrinking slabs, cylinders and spheres is plotted against the efficiency E at different values of α; and in *figs. 4.11* and *4.12*, where the flux function G^* for shrinking cylinders and spheres is plotted against the efficiency E at different values of α. The drawn lines in these figures represent the exact (numerical) solution, obtained by solving the diffusion equation with Crank-Nicolson's method. As can be observed, hardly any differences occur between approximate and numerical solutions. For shrinking cylinders and spheres, also the desorption time τ was computed and plotted against the efficiency E as shown in *figs. 4.13* and *4.14*. A comparison between approximate and numerical solutions once more shows an excellent agreement over several decades of the desorption time τ. Eventually, an improvement in computational speed with a factor 1000 was obtained by applying the approximate method instead of the numerical method.

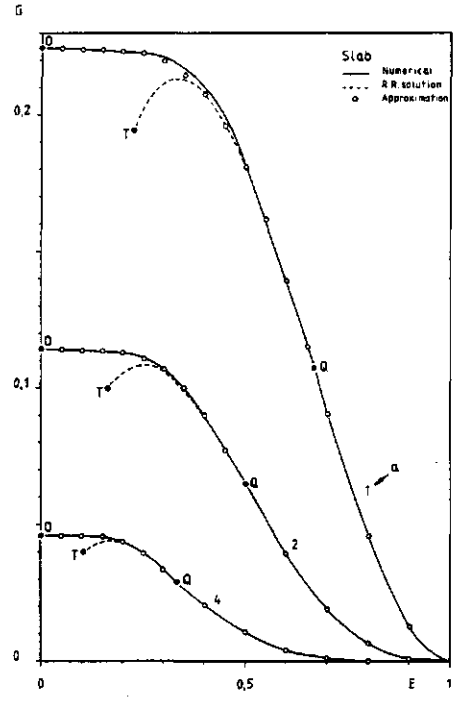

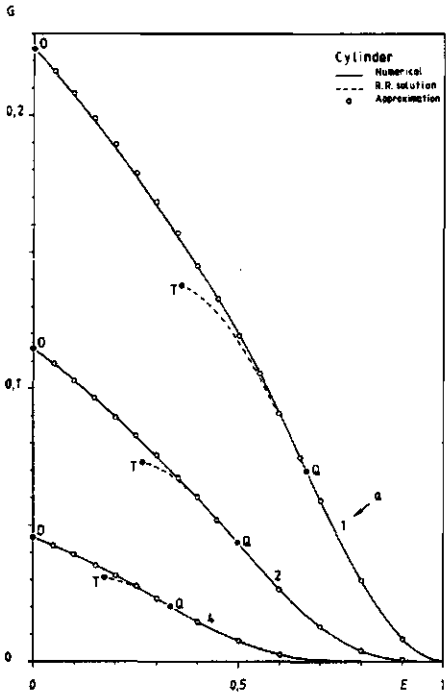

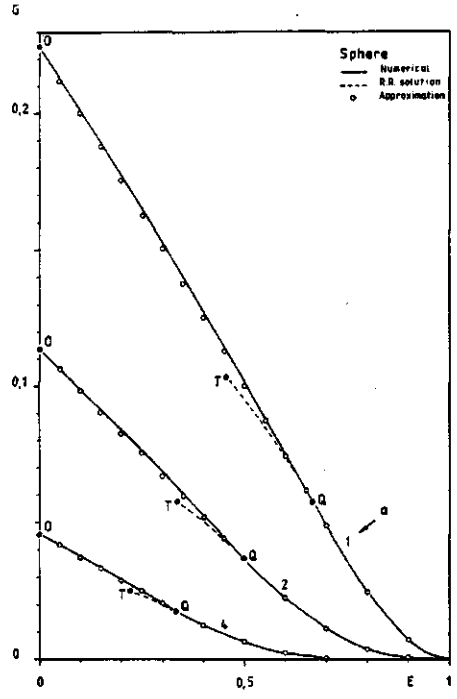

Fig. 4.8
The flux function G versus the efficiency E for a slab at different values of a.

Fig. 4.9
The flux function G versus the efficiency E for a cylinder at different values of a.

Fig. 4.10
The flux function G versus the efficiency E for a sphere at different values of a.

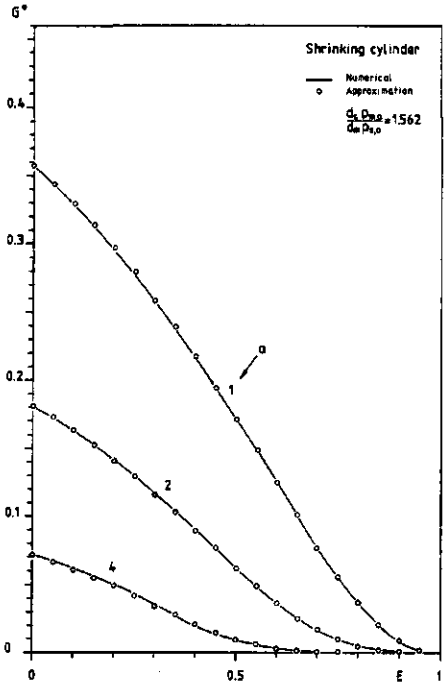

Fig. 4.11
The flux function G^* versus the efficiency E for an shrinking cylinder at different values of a.

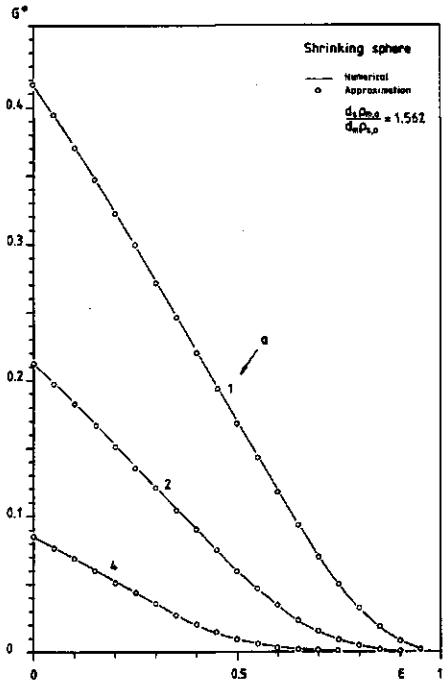

Fig. 4.12
The flux function G^* versus the efficiency E for a shrinking sphere at different values of a.

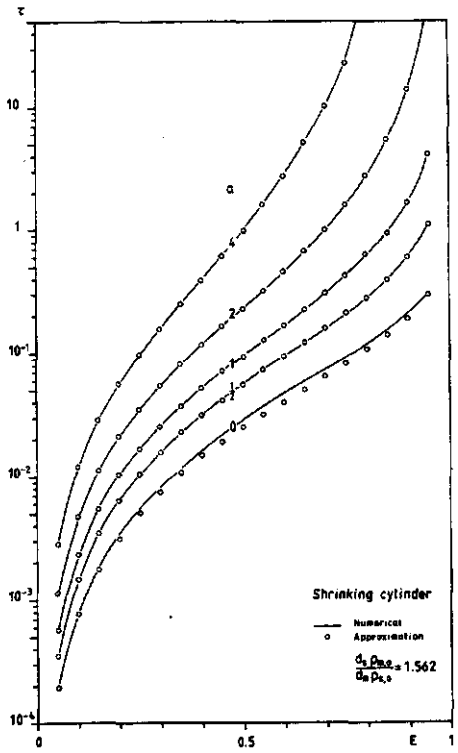

Fig. 4.13
Desorption time τ as a function of the efficiency E for a shrinking cylinder at different values of a.

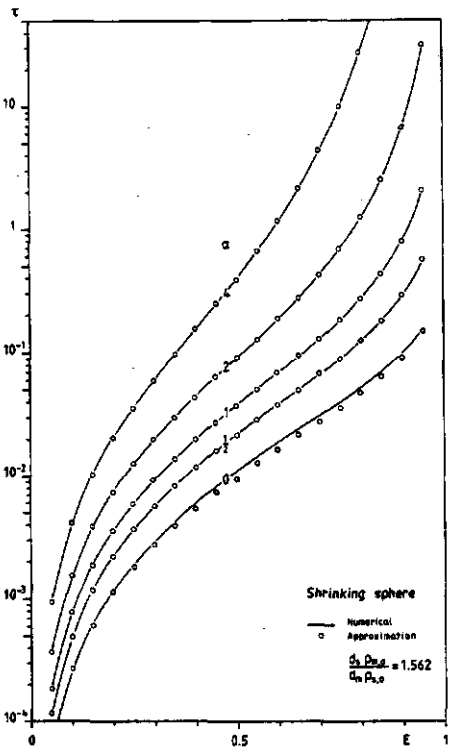

Fig. 4.14
Desorption time τ as a function of the efficiency E for a shrinking sphere at different values of a.

4.3.1 Approximate relations for concentration profiles.

In section 4.2.1, we presented the analytical solution for large times, in case of slab geometry. The concentration profile may in principle be evaluated from eqns.(4.20) or (4.21). This solution, however, still contains the function $g_r(\phi)$, which cannot be evaluated directly from its inverse function $\phi(g_r)$.

In order to examine the possibility of constructing approximate relations for the still unsolved cases of cylinder and sphere, a numerical solution of eqn.(4.8) was produced by means of an orthogonal collocation method [46]. An analysis of the numerical solution showed that the concentration profile may be approximated by the simple relation:

$$y_{a,\nu} = y_{0,\nu} + (y_{\infty,\nu} - y_{0,\nu})\left(\frac{a}{a+1}\right) \quad with \; y_{a,\nu} = g_{r,a,\nu}^{a+1} \tag{4.78}$$

Since the limiting solutions $y_{0,\nu}$ and $y_{\infty,\nu}$ are known analytical functions, the evaluation of $g_{r,a,\nu}$ from eqn.(4.78) is straightforward. *Figs. 4.15, 4.16* and *4.17* show the approximations for $g_{r,a,\nu}$ together with the numerical solution of eqn.(4.8), obtained with the orthogonal collocation method, mentioned above. The limiting solution for a constant diffusion coefficient $y_{0,\nu}$, is obtained from the first eigenfunction of the well known series solution [45]:

$$y_{0,0} = g_{r,0,0} = \cos(\tfrac{1}{2}\pi\phi) \qquad (slab) \tag{4.79}$$

$$y_{0,1} = g_{r,0,1} = J_0(\mu_1 \phi^{1/2}) \qquad (cylinder) \tag{4.80}$$

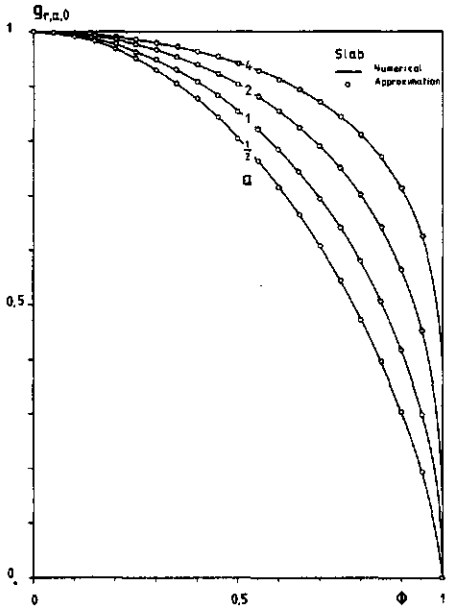

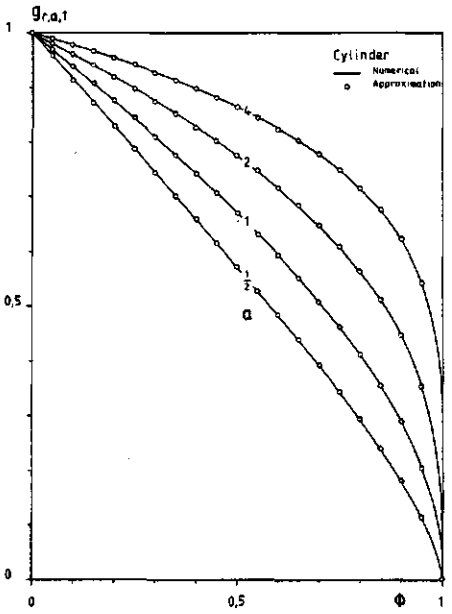

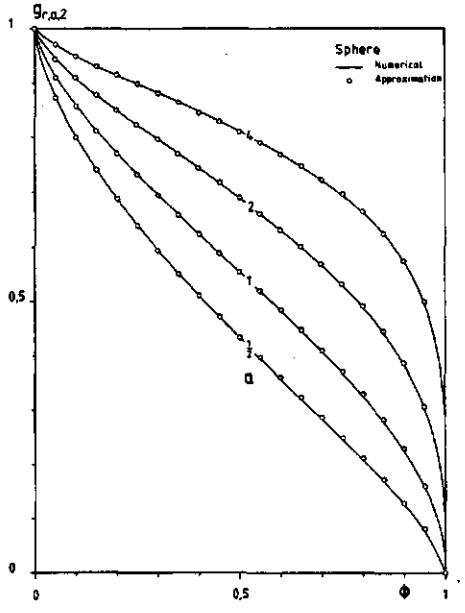

Fig. 4.15
The reduced concentration profiles for a slab in the regular regime.

Fig. 4.16
The reduced concentration profiles for a cylinder in the regular regime.

Fig. 4.17
The reduced concentration profiles for a sphere in the regular regime.

in which $\mu_1=2.40483$ is the first positive root of $J_0(\mu_n)=0$, with J_0 representing the zero order Bessel function. In appendix A, a polynomial approximation of the Bessel function: $J_0(\mu_1\phi^{1/2})$ is given for computational purposes [47].

$$y_{0,2} = g_{r,0,2} = \frac{sin(\pi\phi^{1/3})}{\pi\phi^{1/3}} \qquad (sphere) \qquad (4.81)$$

The limiting solution $y_{\infty,\nu}$ may be obtained by expressing eqn. (4.8) in terms of the variable y:

$$\frac{d}{d\phi}(\phi^{\frac{2\nu}{\nu+1}}.\frac{dy}{d\phi}) = -P_{\infty,\nu}(a+1)y^{\frac{1}{a+1}} \qquad (4.82)$$

The limiting form of this equation for $a\to\infty$ becomes:

$$\frac{d}{d\phi}(\phi^{\frac{2\nu}{\nu+1}}.\frac{dy}{d\phi}) = -P_{\infty,\nu}(a+1) \qquad (4.83)$$

which was solved by Schoeber [22], resulting in:

$$y_{\infty,\nu} = 1 - \phi^{\frac{2}{\nu+1}} \qquad (4.84)$$

Substitution of eqn.(4.79), (4.80), (4.81) and (4.84) in eqn. (4.78) yields the following expressions for slab, cylinder and sphere:

$$g_{r,a,0} = [cos(\tfrac{1}{2}\pi\phi) + \{1-\phi^2-cos(\tfrac{1}{2}\pi\phi)\}\{\frac{a}{a+1}\}]^{\frac{1}{a+1}} \qquad (4.85)$$

$$g_{r,a,1} = [J_0(\mu_1\phi^{1/2}) + \{1-\phi-J_0(\mu_1\phi^{1/2})\}(\frac{a}{a+1})]^{\frac{1}{a+1}} \qquad (4.86)$$

$$g_{r,a,2} = \left[\frac{\sin(\pi\phi^{1/3})}{\pi\phi^{1/3}} + \left\{1-\phi^{2/3} - \frac{\sin(\pi\phi^{1/3})}{\pi\phi^{1/3}}\right\}\left(\frac{a}{a+1}\right)\right]^{\frac{1}{a+1}} \qquad (4.87)$$

Together with the approximate relations for the average values of $g_{r,a,\nu}$, substitution in eqn.(4.21), finally results in the desired expressions for the concentration $m_{a,\nu}$:

$$m_{0,0} = \frac{\pi}{2}\cos(\tfrac{1}{2}\pi\phi)(1-E) \qquad (4.88)$$

$$m_{a,0} = \left(\frac{2+\frac{1}{4}e^2 a}{a+2}\right)^{\frac{1}{a}}\left[\frac{\cos(\frac{1}{2}\pi\phi)}{a+1} + \frac{a(1-\phi^2)}{a+1}\right]^{\frac{1}{a+1}}(1-E) \qquad (4.89)$$

for a slab and:

$$m_{0,1} = \frac{\mu_1}{2J_1(\mu_1)} J_0(\mu_1\phi^{1/2})(1-E) \qquad (4.90)$$

$$m_{a,1} = \left(\frac{2+e.a}{a+2}\right)^{\frac{1}{a}}\left[\frac{J_0(\mu_1\phi^{1/2})}{a+1} + \frac{a(1-\phi)}{a+1}\right]^{\frac{1}{a+1}}(1-E) \qquad (4.91)$$

for a cylinder, with $J_1(\mu_1)=0.51915$ and J_1 denoting the Bessel function of order 1.

$$m_{0,2} = \frac{\pi^2}{3}\,\frac{\sin(\pi\phi^{1/3})}{\pi\phi^{1/3}}(1-E) \qquad (4.92)$$

$$m_{c,0,2} = \frac{\pi^2}{3}(1-E) \quad at\ \phi=0 \qquad (4.93)$$

$$m_{a,2} = \left(\frac{2+\frac{1}{4}e^{8/3}a}{a+2}\right)^{\frac{1}{a}}\left[\frac{\sin(\pi\phi^{1/3})}{(a+1)\pi\phi^{1/3}} + \frac{a(1-\phi^{2/3})}{a+1}\right]^{\frac{1}{a+1}}(1-E) \qquad (4.94)$$

$$m_{c,a,2} = \left(\frac{2+\frac{1}{4}e^{8/3}a}{a+2}\right)^{\frac{1}{a}}(1-E) \quad at\ \phi=0 \qquad (4.95)$$

for a sphere. These approximations give explicitly the concentration profiles for large times. For short times, however, application of the relations given above leads to erroneous results, which has already been discussed at length in section 4.2.1. In the following, it will be demonstrated that simple approximations can also be constructed for the initial stage of the desorption process by modifying the analytical short time solutions for a constant diffusion coefficient.

For a constant diffusion coefficient, the short time solutions for slab, cylinder and sphere can be expressed by the first order approximation of an error function series [45]:

$$m_{0,0} = 1 - erfc\left(\frac{1-\phi}{2\sqrt{\tau}}\right) - erfc\left(\frac{1+\phi}{2\sqrt{\tau}}\right) \qquad (4.96)$$

for a slab, and:

$$m_{0,1} = 1 - \phi^{-1/4} erfc\left(\frac{1-\phi^{1/2}}{2\sqrt{\tau}}\right) \qquad (4.97)$$

$$m_{c,0,1} = 1 - \frac{exp(-1/8\tau)}{(\pi\tau)^{1/2}} K_{\frac{1}{4}}(1/8\tau) \quad at\ \phi=0 \qquad (4.98)$$

for a cylinder, with $K_{\frac{1}{4}}$ representing the modified Bessel function of order $\frac{1}{4}$. A computational formula of this function for large values of the argument is given in appendix A.

$$m_{0,2} = 1 - \phi^{-1/3} \left[erfc\left(\frac{1-\phi^{1/3}}{2\sqrt{\tau}}\right) - erfc\left(\frac{1+\phi^{1/3}}{2\sqrt{\tau}}\right)\right] \qquad (4.99)$$

$$m_{c,0,2} = 1 - \frac{2exp(-1/4\tau)}{(\pi\tau)^{1/2}} \quad at\ \phi=0 \qquad (4.100)$$

for a sphere. For nonzero values of the power a, Friedmann [48] solved the diffusion equation by considering a semi-infinite medium. In case of small fractional values of a, either positive or negative, a second order approximation appeared to be of sufficient accuracy. For larger values of a, however, this approximation fails and higher order terms have to be employed, leading to expressions of increasing complexity. As we are not only interested in weak dependences, another approach is necessary in order to arrive at more feasible relations, which in addition apply to the cases of cylinder and sphere as well. A particularly simple relation appeared to be of substantial value in approximating the initial stage of the diffusion process:

$$m_{a,\nu} = m_{0,\nu}^{b} \quad with\ b = \frac{1}{a+1} - \frac{a(\nu+1)}{2(\nu+2)(a+1)(a+2)} \tag{4.101}$$

in which $m_{0,\nu}$ represents the short time solution for a constant diffusion coefficient, given by eqns.(4.96)-(4.100). As long as the centre concentration remains unaltered, eqn. (4.101) provides a satisfactory approximation.

In order to effectuate a gradual transition between the short and large time approximations, a region is defined, in which a complete transition from short time to large time solution is established. In section 4.2.1 it was derived that the regular regime possesses a lower bound T, satisfying eqn. (4.48). Moreover, point Q was defined as a transition point belonging to the regular regime. The concentration profile, however, will exhibit much resemblance to the regular regime profile, long before point Q is reached. By examining the flux function G for a slab (section 4.2.1), it may be observed

that in point S, corresponding to the occurring maximum in the regular regime solution for the flux function G, the difference between the actual G curve and the regular regime curve (*fig. 4.8*) has already become small. Consequently, the concentration profile in point S is expected not to differ very much from the regular regime profile. Hence, point S, as far as the concentration profile is concerned, may serve as an upper bound of the transition region. Unfortunately, for cylinder and sphere, the maximum in the regular regime solution for G is located in the region $E<E_T$ and is therefore useless as an upper bound. For that reason we define the upper bound of the transition region for cylinder and sphere as the value of the efficiency E at which the centre concentration is equal to the centre concentration in point S for a slab. According to eqns.(4.36) and (4.47), the value of the efficiency in this point R, is then determined by:

$$E_R = 1 - \frac{\bar{g}_{r,a,\nu}}{\bar{g}_{r,a,0}} \left(\frac{a+1}{a+2}\right) \tag{4.102}$$

Together with point T as the lower bound of the transition region, the location of the transition is now established. A linear combination between the two limiting approximations appeared to provide an effective transition. The concentration profile during the transition is then determined by:

$$m_{a,\nu} = \frac{(E_R-E)m'_{a,\nu} + (E-E_T)m''_{a,\nu}}{E_R-E_T} \tag{4.103}$$

where $m'_{a,\nu}$ and $m''_{a,\nu}$ are the short and large time approximations for the concentration profile. In *table 4.2* a summary

SLAB (ν=0)	CYLINDER (ν=1)	SPHERE (ν=2)
Short time approximations with: $b = \frac{1}{\alpha+1} - \frac{\alpha(\nu+1)}{2(\nu+2)(\alpha+1)(\alpha+2)}$ (penetration period: $E < E_T$)		
$m'_{\alpha,0} = [1-\mathrm{erfc}(\frac{1-\Phi}{2\sqrt{\tau}}) - \mathrm{erfc}(\frac{1+\Phi}{2\sqrt{\tau}})]^b$	$m'_{\alpha,1} = [1-\Phi^{-1/2}\cdot\mathrm{erfc}(\frac{1-\Phi}{2\sqrt{\tau}})]^b$ $m'_{\epsilon,\alpha,1} = [1-(\pi.\tau)^{-1/2} e^{-1/8\tau}.K_{1/4}(\frac{1}{8\tau})]^b$	$m'_{\alpha,2} = [1-\Phi^{-1/3}(\mathrm{erfc}(\frac{1-\Phi^{1/3}}{2\sqrt{\tau}}) - \mathrm{erfc}(\frac{1+\Phi^{1/3}}{2\sqrt{\tau}}))]^b$ $m'_{\epsilon,\alpha,2} = [1-2(\pi.\tau)^{-1/2} e^{-1/4\tau}]^b$
Large time approximations (regular regime: $E > E_R$)		
$m''_{0,0} = \frac{\Pi}{2}\cos(\frac{1}{2}\pi\Phi)[1-E]$ $m''_{\epsilon,0} = [\frac{2+\frac{1}{2}e^2\alpha}{\alpha+2}]^{1/\alpha}[\frac{\cos(\frac{1}{2}\pi\Phi)}{\alpha+1} + \frac{\alpha(1-\Phi^2}{\alpha+1}]^{\frac{1}{\alpha+1}} \times [1-E]$	$m''_{0,1} = \frac{\mu_1}{2J_1(\mu_1)} J_0(\mu_1\Phi^{1/2})[1-E]$ $m''_{\epsilon,1} = [\frac{2+e.\alpha}{\alpha+2}]^{1/\alpha}[\frac{J_0(\mu_1\Phi^{1/2})}{\alpha+1} + \frac{\alpha(1-\Phi}{\alpha+1}]^{\frac{1}{\alpha+1}} \times [1-E]$	$m''_{0,2} = \frac{\pi^2}{3}\frac{\sin(\pi\Phi^{1/3})}{\pi\Phi^{1/3}}$ $m''_{\epsilon,2} = [\frac{2+\frac{1}{2}e^{\alpha/3}\alpha}{\alpha+2}]^{1/\alpha}[\frac{\sin(\pi\Phi^{1/3})}{(\alpha+1)(\pi\Phi^{1/3})} + \frac{\alpha(1-\Phi^{2/3}}{\alpha+1}]^{\frac{1}{\alpha+1}} \times [1-E]$
Transition region with: $m_{\alpha,\nu} = \frac{(E_R-E)m'_{\alpha,\nu} + (E-E_T)m''_{\alpha,\nu}}{E_R-E_T}$ ($E_T \leq E \leq E_R$)		
$E_T = \begin{cases} 1-\frac{2}{\pi} & (\alpha=0) \\ 1-(\frac{2+\frac{1}{2}e^2\alpha}{\alpha+2})^{-1/\alpha} \end{cases}$ $E_R = \frac{1}{\alpha+2}$	$E_T = \begin{cases} 1-\frac{2J_1(\mu_1)}{\mu_1} & (\alpha=0) \\ 1-(\frac{2+e.\alpha}{\alpha+2})^{-1/\alpha} \end{cases}$ $E_R = \begin{cases} 1-\frac{J_1(\mu_1)}{\pi\mu_1} & (\alpha=0) \\ 1-(\frac{2+\frac{1}{2}e^2\alpha}{2+e.\alpha})^{1/\alpha}(\frac{\alpha+1}{\alpha+2}) \end{cases}$	$E_T = \begin{cases} 1-\frac{3}{\pi^2} & (\alpha=0) \\ 1-(\frac{2+\frac{1}{2}e^{\alpha/3}\alpha}{\alpha+2})^{-1/\alpha} \end{cases}$ $E_R = \begin{cases} 1-\frac{3}{4\pi} & (\alpha=0) \\ 1-(\frac{2+\frac{1}{2}e^2\alpha}{2+\frac{1}{2}e^{\alpha/3}\alpha})^{1/\alpha}(\frac{\alpha+1}{\alpha+2}) \end{cases}$

Table 4.2

Approximate relations for the computation of concentration profiles in case of a concentration dependent diffusion coefficient of the type: $D_r = m^{\alpha}$.

is presented of the formulas, needed for the computation of the concentration profiles in the different regions of interest.

4.3.2 A comparison between approximate and numerical methods.

In *fig. 4.18* the results of approximate and numerical methods are shown for slab, cylinder and sphere at increasing values of a. It may be observed that the deviations are mainly located in the transition region, but vanish rapidly as soon as the regular regime is entered. In *fig.4.19* the concentration profiles for a shrinking cylinder and sphere are shown, together with the concentration profiles for a non-shrinking cylinder and sphere (open dots) at the same values of the efficiency E. As may be observed, the concentration profiles in case of shrinkage, tend to a slightly more rectangular shape compared to the profiles in case shrinkage is absent. These small differences are evidently inherent in the application of the shrinking coordinate system, as defined in section 3. Moreover, as the value of a increases, the differences gradually vanish. From these observations it may be concluded that also for shrinking sytems the approximate relations, given in *table 4.2* can be applied directly. Incidentally, it should be pointed out that, although the concentration profiles for shrinking and non-shrinking systems show an apparent similarity, the time scale of the diffusion process in both systems is entirely different.

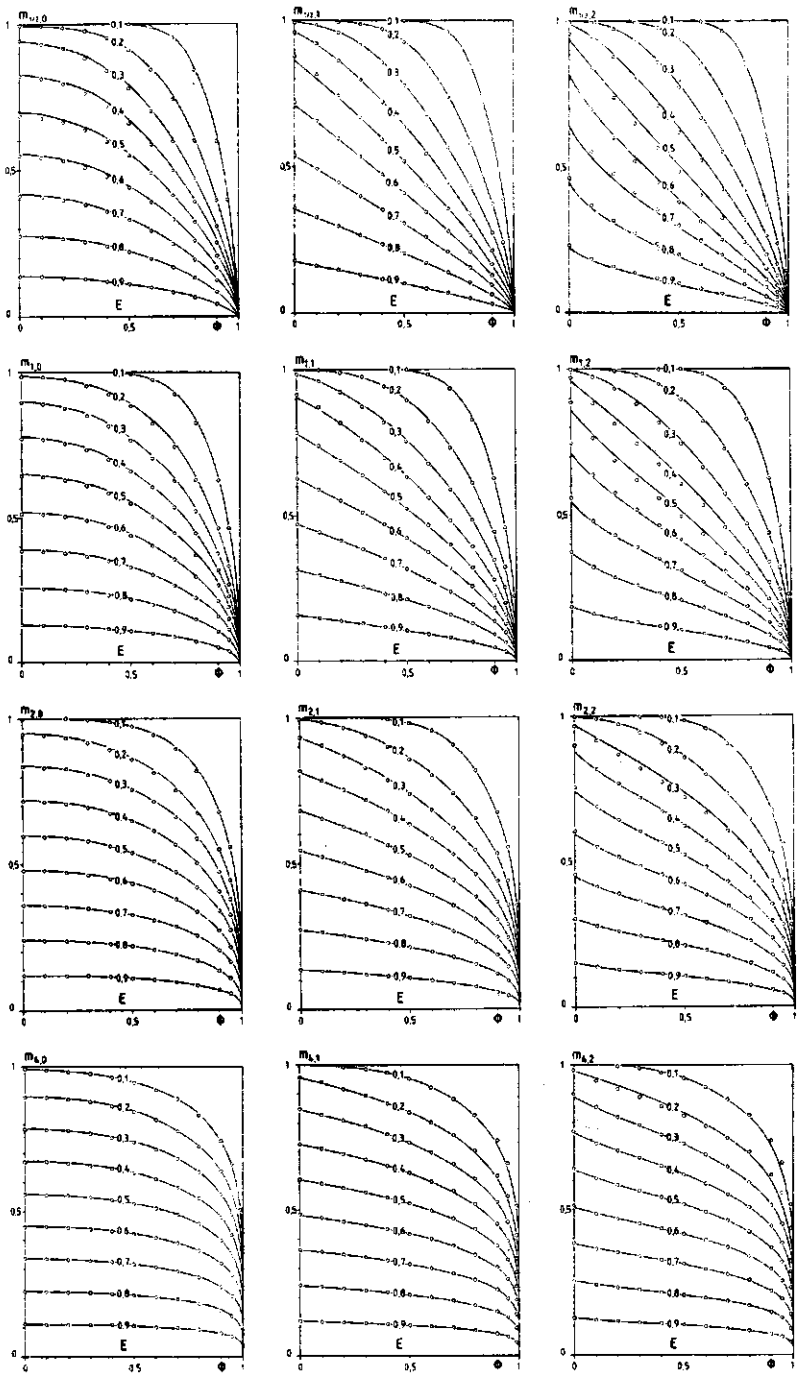

Fig. 4.18 Concentration profiles for non-shrinking slabs, cylinders and spheres. (–): numerical, (o): approximation.

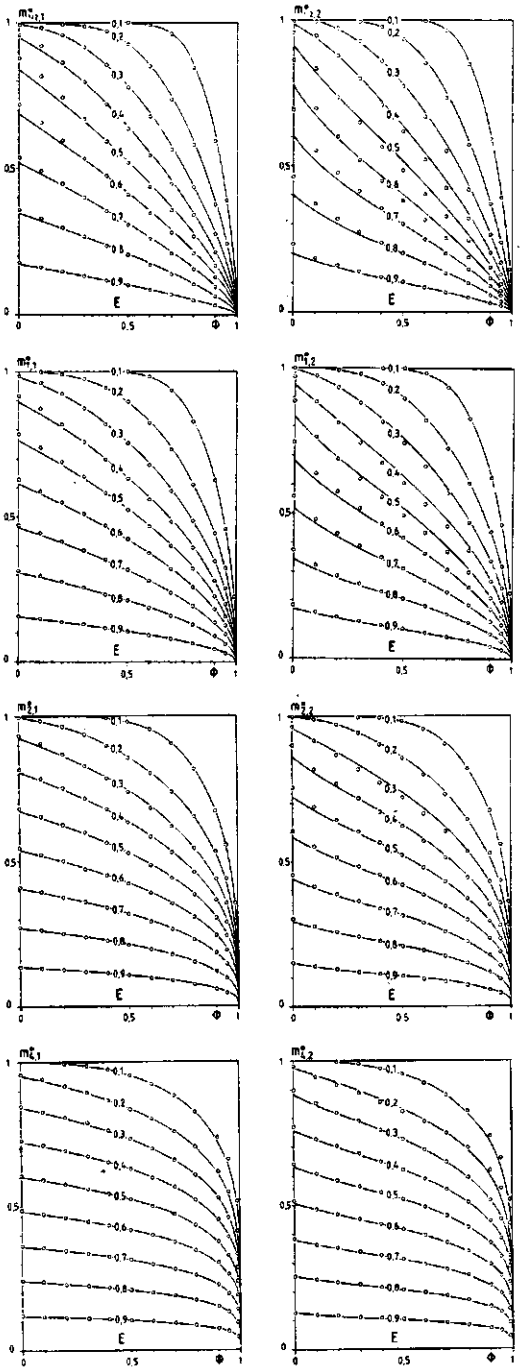

Fig. 4.19 Concentration profiles for shrinking cylinders and spheres. (—): numerical, (o): approximation.

4.4 *An approximate method for the computation of mass flux and desorption time under Neumann boundary conditions.*

In the previous sections, we considered the desorption process subject to Dirichlet boundary conditions, corresponding to an infinitely high initial flux. It has been mentioned in chapter 3 that the initial stage of the desorption process, if controlled by external mass transfer, may be described by means of a Neumann boundary condition, i.e. a constant flux $n_{m,i}$ for non-shrinking systems or a constant value of the product $j^{s}_{m,i}.R_d$ for shrinking systems. This stage of the desorption process is usually referred to as the constant rate or constant activity period.

4.4.1 *Non-shrinking systems.*

According to eqn.(3.32), the flux parameter in the constant activity period for non-shrinking systems is given by:

$$\overline{F} = \frac{n_{m,i}.R_d}{\rho_{m,o}.D_o} = \overline{F}_o = \frac{n_{m,i,o}.R_o}{\rho_{m,o}.D_o} \qquad (4.104)$$

The end of the constant activity period may be represented by a critical point P. In this point P, the surface concentration has reached a value at which a constant flux can no longer be maintained [21]. For a power function variation of the diffusion coefficient with concentration, Schoeber [22] computed the critical average concentration for different values of the initial flux by solving the diffusion equation numerically. He observed that in the critical point, the ratio between the Sherwood number, computed with a constant flux boun-

dary condition and the Sherwood number, computed with a constant surface concentration equal to the surface concentration in the critical point, was virtually independent of the value of the initial flux. According to eqn.(4.12), the Sherwood number ratio $\Lambda_{a,\nu}$ is equal to the corresponding flux ratio:

$$\Lambda_{a,\nu} = \frac{\overline{Sh}_{d,a,\nu}}{\overline{Sh}_{d,a,\nu}} = \frac{\overline{F}}{\overline{F}_P} \tag{4.105}$$

where F_P is a known function of the critical average concentration $\bar{m}_P$, given by the relations of *fig. 4.6*, in case of a zero critical surface concentration. For nonzero values of the critical surface concentration, the flux parameter follows from:

$$F_P(\bar{m}_P, m_{i,P}) = \frac{Sh_d}{2}(\bar{m}_P - m_{i,P})\bar{D}_r =$$

$$= \frac{Sh_d}{2} \int_{m_{i,P}}^{\bar{m}_P} D_r(m)dm =$$

$$= \frac{Sh_d}{2} \left[\int_0^{\bar{m}_P} D_r(m)dm - \int_0^{m_{i,P}} D_r(m)dm \right] =$$

$$= F_P(\bar{m}_P, 0) - F(m_{i,P}, 0) \tag{4.106}$$

which holds, if P belongs to the regular regime and if Sh_d is constant. The right-hand side of eqn.(4.106) may be evaluated by the relations for a constant zero surface concentration. In principle, the critical average concentration $\bar{m}_P$ may now

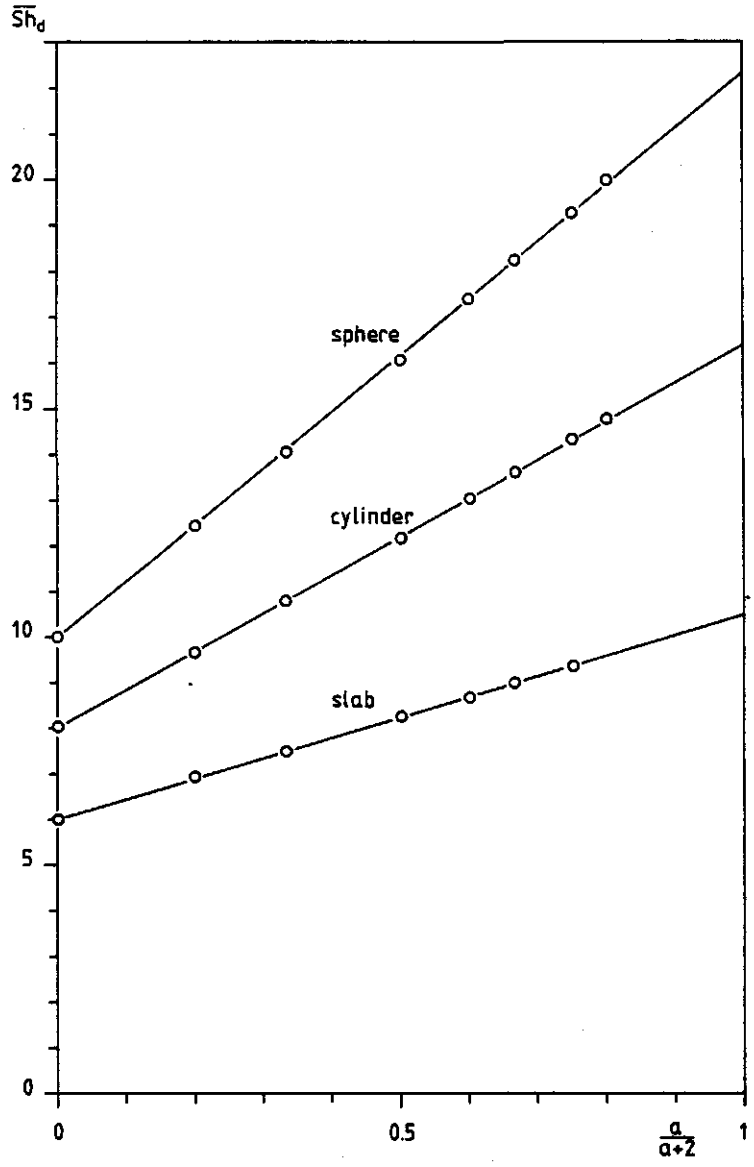

Fig. 4.20 The constant activity Sherwood number in the critical point P at different values of a.
(o): numerical, (−): linear approximation.

be determined from eqn.(4.105) by employing the numerically computed value of the Sherwood number ratio. As, according to eqn.(4.28) the constant surface concentration Sherwood number $Sh_{d,a,\nu}$ is constant in the regular regime, a similar relation may be expected for the constant activity Sherwood number $\overline{Sh}_{d,a,\nu}$. Indeed, a pseudo linear relationship was found by plotting the numerically computed values of the constant activity Sherwood number against the factor $\frac{a}{a+2}$, as shown in *fig. 4.20*. The linear correlation is given by:

$$\overline{Sh}_{d,a,\nu} = 6 + 2\nu + (4.4429 + 3.9348\nu)\left(\frac{a}{a+2}\right) \qquad (4.107)$$

The Sherwood number ratio $\Lambda_{a,\nu}$ then follows from eqns.(4.29)-(4.31) and eqn.(4.107):

$$\Lambda_{a,0} = \frac{12+10.4429a}{\pi^2+e^2.a} \qquad \textit{(slab)} \qquad (4.108)$$

$$\Lambda_{a,1} = \frac{16+16.3777a}{11.566+4e.a} \qquad \textit{(cylinder)} \qquad (4.109)$$

$$\Lambda_{a,2} = \frac{20+22.3125a}{4/3\pi^2 + e^{8/3}.a} \qquad \textit{(sphere)} \qquad (4.110)$$

The location of the critical point P, represented by the so called critical point curve $\overline{F}(\bar{m}_P)$, is shown in *figs. 4.21, 4.22* and *4.23*, for slab, cylinder and sphere respectively. The drawn lines in these figures correspond to the numerical solution of the diffusion equation, subject to a constant flux boundary condition, whereas the open dots correspond to the approximation, given by eqns.(4.105) and (4.108)-(4.110).

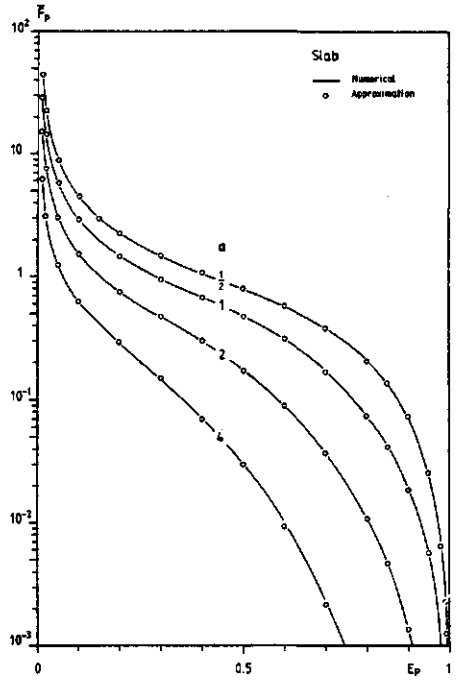

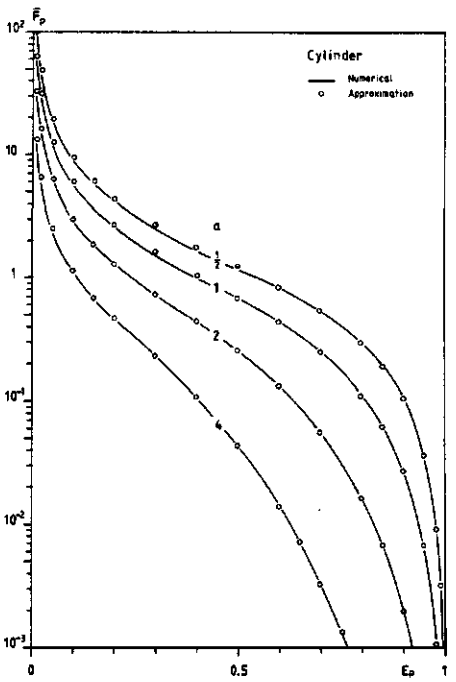

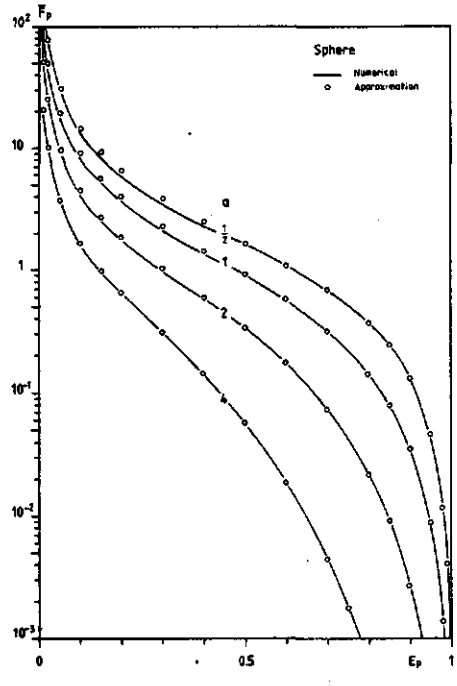

Fig. 4.21 The critical point curve for a slab at different values of a.

Fig. 4.22 The critical point curve for a cylinder at different values of a.

Fig. 4.23 The critical point curve for a sphere at different values of a.

The desorption time τ_p, denoting the length of the constant activity period follows from integration of the mass balance, given by eqn.(4.11):

$$\tau_p = \frac{1 - \bar{m}_p}{(\nu+1)\bar{F}} \tag{4.111}$$

4.4.2 Shrinking systems.

According to eqns.(3.41) and (3.44), the flux parameter in the constant activity period for shrinking systems is given by:

$$\bar{F}^*(1+\frac{d_s\rho_{m,o}}{d_m\rho_{s,o}}\bar{m})^{\frac{1}{\nu+1}} = \frac{d_s}{\rho_{m,o}\rho_{s,o}D_o}(j^s_{m,i}R_d) =$$

$$\bar{F}^*_o(1+\frac{d_s\rho_{m,o}}{d_m\rho_{s,o}})^{\frac{1}{\nu+1}} = \frac{d_s}{\rho_{m,o}\rho_{s,o}D_o}(j^s_{m,i,o}R_o) \tag{4.112}$$

The critical average concentration $\bar{m}_p$ follows from eqn. (4.105) and (4.112) together with the necessary correction for shrinkage as given in *fig. 4.7*. Integration of the mass balance, given by eqn.(4.64) finally yields the length of the constant activity period for shrinking systems:

$$\tau_p = \frac{d_m\rho_{s,o}}{2d_s\rho_{m,o}\bar{F}^*_o}(1+\frac{d_s\rho_{m,o}}{d_m\rho_{s,o}})^{\frac{-1}{\nu+1}}[(1+\frac{d_s\rho_{m,o}}{d_m\rho_{s,o}})^{\frac{2}{\nu+1}} - (1+\frac{d_s\rho_{m,o}}{d_m\rho_{s,o}}\bar{m}_p)^{\frac{2}{\nu+1}}] \tag{4.113}$$

4.5 Non-isothermal conditions.

In case of transient behaviour of the average particle temperature, internal mass transfer will also be affected, as heat and mass balances of the dispersed phase are coupled, due to the temperature dependence of the diffusion coefficient (see *fig. 3.1*, Chapter 3). This temperature dependence of the diffusion coefficient is usually given in the form of an Arrhenius relation [22]:

$$D = D^{ref} exp[- \frac{E_{a,d}}{R}(\frac{1}{T} - \frac{1}{T_{ref}})] \qquad (4.114)$$

where D^{ref} represents the diffusion coefficient at an arbitrary reference temperature T_{ref} and $E_{a,d}$ is the activation energy for diffusion.
If the activation energy does not depend on concentration, we may write:

$$D(\omega_m', T) = \Omega(\omega_m') . \Theta(T) \qquad (4.115)$$

In this form, the temperature dependent part $\Theta(T)$, which is independent of the space coordinate ϕ, may be incorporated in the time variable τ, as will be shown in the following.
According to eqn.(3.28), the diffusion coefficient for non-shrinking systems reads:

$$D = D_o D_r \qquad (4.116)$$

whereas, for shrinking systems, according to eqn.(3.38), the diffusion coefficient is given by:

$$D = D_o \frac{\rho_{s,o}^2}{\rho_s^2} D_r \qquad (4.117)$$

Consequently, the diffusion coefficient D assumes the separable form of eqn.(4.115), if D_o is a function of temperature only, i.e.:

$$D_o = D_o^{ref} exp[-\frac{E_{a,d}}{R}(\frac{1}{T}-\frac{1}{T_{ref}})] \qquad (4.118)$$

where D_o^{ref} represents the diffusion coefficient at temperature T_{ref} and moisture content $\omega'_{m,o}$.

The important advantage of writing the diffusion coefficient in the separable form of eqn.(4.115) is, that the approximate solutions, established in the preceding sections, apply without modifications. The only difference between the isothermal and non-isothermal case is expressed by the difference in real desorption times. For non-shrinking systems, the real desorption time t, under non-isothermal conditions is expressed by:

$$t = \int_o^\tau \frac{R_o^2}{D_o} d\tau = \int_o^E \frac{R_o^2}{D_o X_i^* F^*} dE \qquad (4.119)$$

whereas for shrinking systems:

$$t = \int_o^\tau \frac{d_s^2 R_s^2}{D_o \rho_{s,o}^2} d\tau = \int_o^E \frac{d_s^2 R_s^2}{D_o \rho_{s,o}^2 X_i^* F^*} dE \qquad (4.120)$$

In the non-isothermal case, D_o is a function of the average particle temperature T_d and consequently a function of τ or E as follows from the heat balance, given by eqn.(3.64). If the efficiency E is chosen as a time parameter, the heat balance becomes:

$$\bar{\rho}_d \bar{c}_{p,d} \frac{dT_d}{dE} = \frac{R_o}{D_o F}[\alpha_g^{eff}(T_b - T_d) - \frac{D_o \rho_{m,o}}{R_o} F \Delta H_{vap}] \qquad (4.121)$$

for non-shrinking systems, and:

$$\bar{\rho}_d \bar{c}_{p,d} \frac{dT_d}{dE} = \frac{\nu+1}{R_d X_i^* F^*}(\frac{d_s^2 R_s^2}{D_o \rho_{s,o}^2})[\alpha_g^{eff}(T_b - T_d) - \frac{D_o \rho_{m,o} \rho_{s,o}}{d_s R_s} F^* \Delta H_{vap}] \qquad (4.122)$$

for shrinking systems.

From eqn.(4.121) or (4.122), the average particle temperature T_d may be evaluated as a function of the efficiency E, which consequently gives D_o as a function of E, whereas the real desorption time t may now be determined by straightforward integration of eqn.(4.119) or (4.120).

A further complication may arise, if the activation energy $E_{a,d}$ depends on moisture content. As was found by Schoeber [22] from drying experiments with glucose-agar gels, the activation energy of the diffusion coefficient varies with the average moisture content. Although this implies an additional dependence on the efficiency E, the diffusion coefficient retains the separable form of eqn.(4.115) and consequently no further modifications of the approximate model are required.

4.6 *Application of the approximate method to enzyme inactivation during drying.*

In the preceding sections, approximate methods were constructed for the computation of a complete desorption process. The problem of a Robin boundary condition is replaced by the separate problems of a Neumann boundary condition at the initial stage of the desorption process (period of constant activity) and a Dirichlet boundary condition during the falling rate period. This replacement allows the computation of the desorption time as a function of the efficiency E by applying the approximate methods, given in sections 4.2 and 4.4, whereas the moisture profile in case of a Dirichlet boundary condition follows from the relations given in *table 4.2.* The moisture profile during the period of constant activity will lie between a uniform profile and the profile, corresponding to the Dirichlet case. Both extreme situations will be considered in chapter 6.

Enzyme inactivation, according to eqn.(2.9), is directly related to the moisture profiles. Concentration profiles of active enzyme may therefore be computed from the approximate relations of *table 4.2.*
The balance equation for enzyme inactivation, given by eqn. (3.78), becomes in terms of the efficiency E:

$$\frac{\partial \omega'_e}{\partial E} = \frac{R_o^2}{D_o X_i F} k_e \omega'_e \qquad (4.123)$$

for non-shrinking systems, and:

$$\frac{\partial \omega'_e}{\partial E} = \frac{d_s^2 R_s^2}{D_o \rho_{s,o}^2 X_i^* F^*} k_e \omega'_e \qquad (4.124)$$

for shrinking systems.

Integration yields:

$$\frac{\omega'_e}{\omega'_{e,o}} = exp[-\int_o^E \frac{R_o^2 k_e}{D_o X_i F} dE] \qquad (4.125)$$

for non-shrinking systems, and:

$$\frac{\omega'_e}{\omega'_{e,o}} = exp[-\int_o^E \frac{d_s^2 R_s^2 k_e}{D_o \rho_{s,o}^2 X_i^* F} dE] \qquad (4.126)$$

for shrinking systems.

The integrand in eqns.(4.125) and (4.126) is a function of the space coordinate ϕ and the efficiency E. Evaluation of the integral yield the concentration profile of the active enzyme as a function of the efficiency E.

C H A P T E R 5

Experiments on thermal enzyme inactivation.

5.1 Introduction.

A prerequisite for obtaining reproducable results from enzyme inactivation experiments is the application of a reproducable medium. In real food systems, factors like composition, pH etc. are hardly constant, which complicates comparison between different sets of experiments. For this reason food simulating systems of exactly known composition are to be preferred for fundamental studies. Only if the kinetics of enzyme inactivation in such model systems are better comprehended, research may be shifted towards real food systems. In this study, use was made of a glucose-calciumalginate combination with an enzyme entrapped in the gelmatrix. Glucose served as a dissolved solid component, which amount could be varied in order to adjust the moisture content of the gel to the desired value. An important advantage of using calciumalginate as an enzyme carrier, is the fact that the gel dissolves in a phosphate medium at an appropriate pH with an almost complete recovery of the enzyme. In this way a separation step, which may cause loss of enzyme activity, is avoided. It should be mentioned that similar gels have been used in simulating fruits [49]. The usual way of preparing alginate gels, consists of adding an alginate solution to a solution containing calcium or other appropriate ions and allow crosslinking by slow diffusion of the calcium ions into the alginate. This method fails however, if a gel of definite

shape and composition is desired. It is however possible to delay crosslinking by means of adding a sequestering agens, which forms slightly soluble calcium salts and in this way controls the concentration of free calcium ions. The addition of small amounts of sodium pyrophosphate for instance, keeps the gel in a liquid state for about 10 minutes, which is enhanced, if the gel is kept at a low temperature. This way of preparing, allows the gel to be injected in moulds of any desired shape with high reproducability, whereas the composition of the gel remains unchanged.

In view of the nature of this thesis, the choice of the enzyme is not very relevant. From the numerous enzymes, occurring in food systems, soy bean lipoxygenase was chosen for two reasons. In the first place, for its importance in a large variety of foods. Some important raw materials, containing lipoxygenase are given in *table 5.1*. Lipoxygenase activity causes degradation of several compounds of nutritional value like vitamin A and poly unsaturated fatty acids (linolic acid, oleic acid), resulting in off-flavour development (rancidity), which for instance is a severe problem in pasta manufacture.

Apple	*Cauliflower*	*Peas*	*Sunflower*
Alfalfa	*Egg plant*	*Peanut*	*Tomato*
Barley	*Maize*	*Potatoes*	*Wheat*
Beans	*Olive*	*Soy bean*	

Table 5.1 Some plants containing lipoxygenase [50].

In the second place, the availability of a rapid and accurate enzyme assay for the determination of enzyme activity.

5.2 *Thermal inactivation kinetics of soy bean lipoxygenase entrapped in a glucose-calciumalginate gel at different moisture content-temperature combinations.*

5.2.1 *Introduction*

The moisture and temperature dependence of soy bean lipoxygenase inactivation in a glucose calciumalginate gel was studied by measuring the residual enzyme activity after a time-heat treatment of the gelsystem in a closed cell at different moisture content-temperature combinations. In the following subsections, the design of the inactivation experiment, together with the enzyme assay for the determination of residual lipoxygenase activity are treated.

5.2.2 *Preparation of the gel.*

The gel was prepared by following a standard recipe, in order to obtain a moisture content of 0.75 on total basis. The general procedure for the preparation and further treatment of the gel is shown schematically in *fig. 5.1*, whereas the necessary amounts are given in *table 5.2*.
An aqueous solution of glucose and sodiumalginate (A) was prepared by mixing the sodiumalginate powder (Manucol DH, 1%-65cp, Alginate Industries Ltd. London) with D(+)-glucose monohydrate (nr. 8346, Merck, Darmstadt) and adding demineralized water in small portions under stirring and slightly heating. Final treatment with a high speed mixer (ultra turrax, Janke & Kunkel, IKA Werk) resulted in a clear viscous solution. Air bubbles were removed from this solution in a vacuum exsiccator

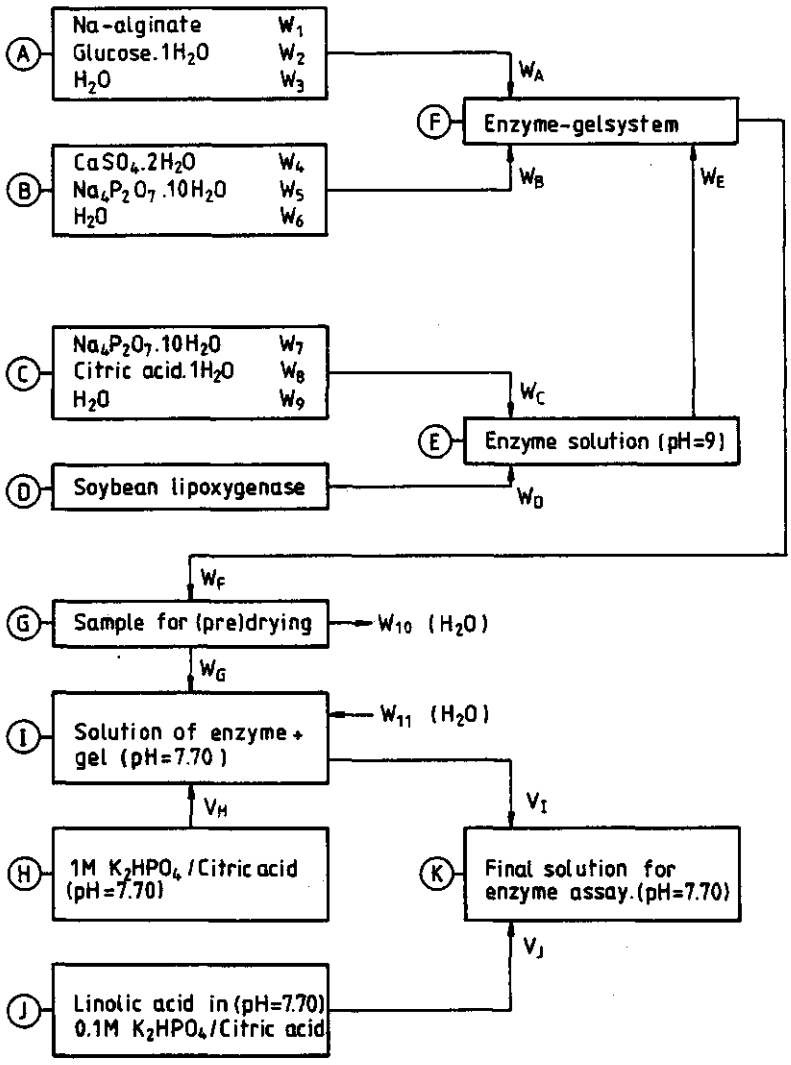

Fig. 5.1 General procedure for the preparation and further treatment of the enzyme/gel combination.

W_1= 2.4000g	W_6= 10.00g	W_A= 23.0000g	$\omega_{m,2}$= 9.0831×10^{-2}
W_2= 41.1600g	W_7= 1.00g	W_B= 1.0800g	$\omega_{m,4}$= 2.0910×10^{-1}
W_3= 94.4400g	W_8 (pH=9)	W_C= 5.0000g	$\omega_{m,5}$= 4.0353×10^{-1}
W_4= 1.2000g	W_9= 300.00g	W_D= 0.0200g	$\omega_{m,8}$= 8.5551×10^{-2}
W_5= 0.5500g		W_E= 3.0000g	d_m = 996 kg/m^3
		V_I= 0.2000ml	d_s = 1562 kg/m^3
		V_J= 3.000 ml	

Table 5.2 Standard amounts for the preparation of a gel with moisture content 0.75 on total basis and other data.

under low pressure, after which water was added in order to compensate for losses during the different treatments. The solution was allowed to stand overnight in a closed bottle at 4°C. Immediately before the preparation of the gel, calcium-sulphate (Nr. 31221 Riedel-de Haën AG, Seelze-Hannover) was suspended in a solution of sodiumpyrophosphate (Nr. 6591, Merck, Darmstadt), using the ultra turrax mixer. This suspension (B) was kept in melting ice, in order to diminish release of calcium ions. Next, a fresh enzyme solution (E) was prepared by dissolving lipoxygenase (Nr. 28021, Serva, Heidelberg) in a solution of sodiumpyrophosphate and citric acid (Nr. 244, Merck, Darmstadt) at pH=9 under slow magnetic stirring (Magnetic stirrer, Cenco Instrumenten Mij N.V. Breda, Holland). The enzyme solution (E) was carefully pipetted (Pipetman P5000, Gilson, France) into solution (A) under slow magnetic stirring, preventing inclusion of air bubbles. Finally an amount of the freshly prepared suspension (B) was added under slow magnetic stirring, after which crosslinking started.

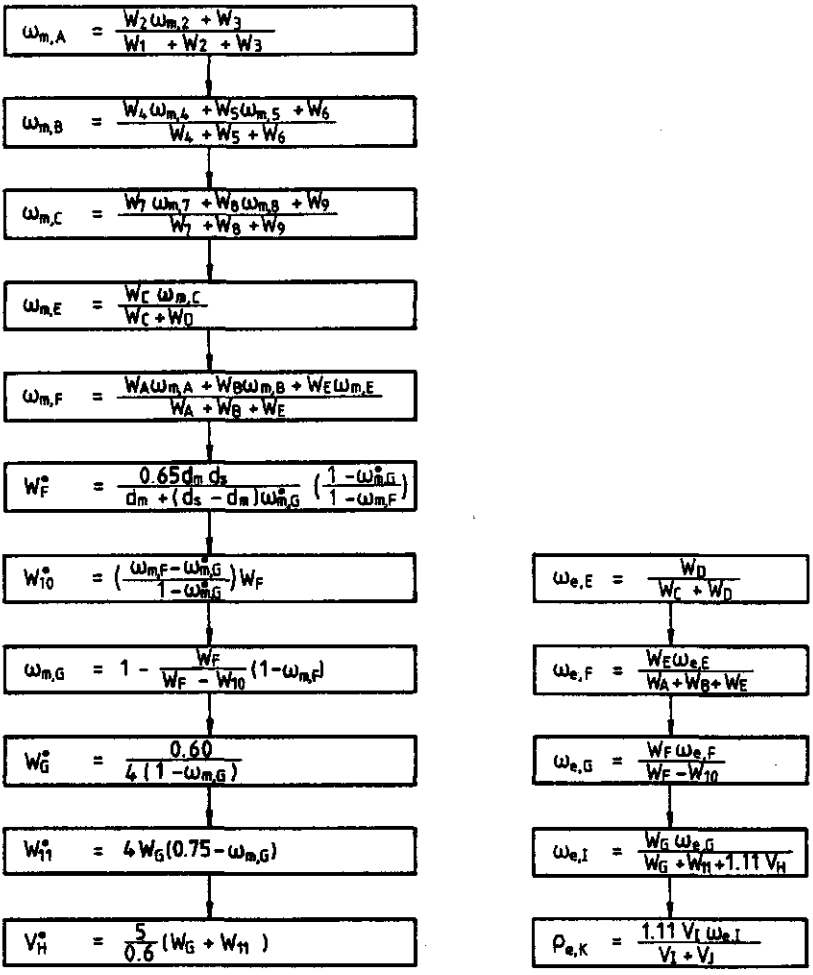

Fig. 5.2 Flow diagram for the calculation of moisture contents, necessary amounts for moisture adjustment and enzyme concentrations.

The gel remained in a liquid state for about 10 minutes and was injected in the bottom part of the inactivation cell, as shown in *fig. 5.4*. The necessary amount of gel (W^*_F) to be injected in order to obtain a final layer thickness of 0.9 mm was calculated according to the procedure as given in *fig. 5.2*. This diagram also gives the necessary formulas for the calculation of the moisture content of the gel $\omega_{m,F}$ and the amount of water W^*_{10} to be removed by drying, in order to adjust the moisture content of the gel to the desired value. Enzyme concentrations in the gel and in the final enzyme assay may be calculated according to the second sequence of this diagram.

5.2.3 The inactivation experiment.

The application of glassware capillaries [10] as inactivation cells poses some practical problems in case the gel has a low moisture content. Neither can a low moisture content gel be inserted easily in the capillary, nor is it possible to adjust moisture content in situ in an easy way. For these reasons, a stainless steel cell was designed, that could contain a circular gellayer of 0.9 mm thickness and 3 cm in diameter (*fig. 5.4*) and in which 99% temperature equalization could be achieved within 5 seconds.
The moisture content was adjusted by predrying the gel, for which purpose, a perspex cap was adapted to the bottom part of the cell as shown in *fig. 5.3*. Air of room temperature was passed through the cell, until the moisture content had reached the desired value, which was controlled by weighing the cell regularly on a high accuracy electronic balance (2001MP2,

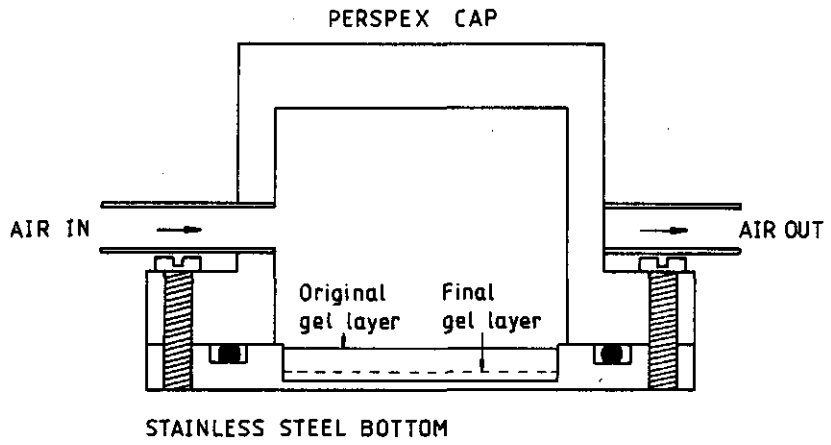

Fig. 5.3 Predrying of a gellayer in order to adjust moisture content.

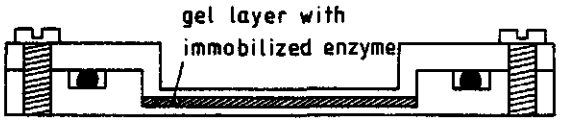

Fig. 5.4 Closed inactivation cell with gellayer.

± 0.1 mg, Sartorius). After adjustment of moisture content, the cell was closed and allowed to stand for several hours in order to achieve redistribution of moisture inside the gel-layer. For an inactivation experiment, 8 cells were used, of which 2 served as untreated reference samples, whereas the remaining 6 were immersed in a thermostatted waterbath (Tamson, Holland) during different times. Immediately after heat treatment, the cells were cooled in melting ice.

5.2.4 Determination of lipoxygenase activity.

An amount of W_G g of the gellayer after heat treatment was dissolved in V_H ml of a 1M solution of K_2HPO_4 (Nr. 5101, Merck, Darmstadt) and citric acid at pH=7.70 under slow magnetic stirring. Finally, W_{11} gram of demineralized water was added to the enzyme solution (I), which was kept in melting ice until use. The necessary amounts W_G^*, W_{11}^* and V_H^* were calculated according to the procedure as given in *fig. 5.2* in order to obtain a solution of standard composition, corresponding to a solution of 0.60 g gel, having a moisture content of 0.75 on total basis, in 5ml of solution (H). In this way, a similar composition of solution (I) was ensured for each experiment, which, in view of the comparability of the experimental results, was of course an absolute necessity. The residual activity of lipoxygenase was determined spectrophotometrically [51] by making use of the enzymatic oxidation of linolic acid. In this reaction, a change in UV light absorption occurs, due to the formation of optically active hydroperoxides. As linolic acid oxidation follows Michaelis-Menten kinetics, the rate is expressed by:

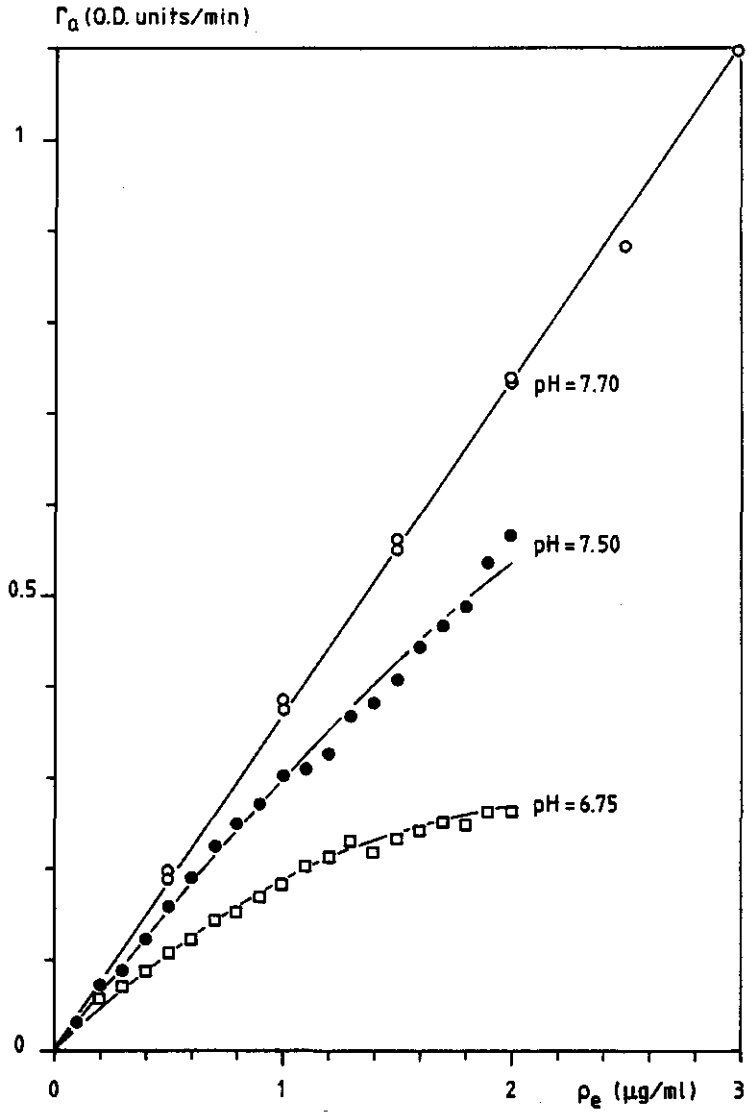

Fig. 5.5 Rate of increase of absorbance r_a as a function of enzyme concentration ρ_e at different pH values.

$$r_l = -k_r \frac{\rho_l}{K_m + \rho_l} \rho_e \qquad (5.1)$$

where k_r denotes the specific rate of linolic acid oxidation, K_m the Michaelis-Menten constant and ρ_e and ρ_l the mass concentrations of enzyme and linolic acid respectively. In case linolic acid is present in excess, eqn.(5.1) turns into:

$$r_l = -k_r \rho_e \qquad (5.2)$$

Because thermal inactivation of lipoxygenase follows first order kinetics [11], we may write according to eqn.(3.79) in case of a fixed moisture content-temperature combination:

$$\frac{\rho_e}{\rho_{e,o}} = exp(-k_e t) \qquad (5.3)$$

Under standard conditions (pH, ion strength, composition, temperature etc.) the specific rate of linolic acid oxidation k_r, is constant. From eqns.(5.2) and (5.3) then follows:

$$\frac{r_l}{r_{l,o}} = \frac{\rho_e}{\rho_{e,o}} \qquad (5.4)$$

indicating a linear relationship between oxidation rate and enzyme concentration. Following the procedure as given by Eriksson et al.[51], a significant deviation in linearity was however found at higher enzyme concentrations, despite the presence of an excess of linolic acid. A possible explanation for this phenomenon, may be a restricted availability of linolic acid, due to the low solubility at the pH prescribed by Svensson et al.(pH=6.75). An increase in pH resulted indeed in an increase of the oxidation rate, as is shown in *fig. 5.5.*

At a pH value of 7.70, the oxidation rate was almost linearly dependent on enzyme concentration. For this reason, the enzyme assays were carried out at a pH value of 7.70.

Preparation of the linolic acid solution (J).

In a 100 ml Erlenmeyer flask, 0.8 ml 1M K_2HPO_4, 0.1 ml Tween (Nr. 822184, Merck-Schuchardt, München) and 0.1 ml linolic acid (Nr. 5353, Merck, Darmstadt) were added under vigorous magnetic stirring, followed by addition of 4 portions of 0.8 ml 1M K_2HPO_4 and bringing the dispersion to a final volume of 40 ml by addition of 35.8 ml of demineralized water. With 1M KOH, the pH of the dispersion was brought to the value 9.50 (Knick-digital pH meter, type 634-1, Switzerland) at which a completely clear solution was obtained. Next, 1M HCl was added dropwise until the pH value of 7.70 was reached. Finally 10 ml of this solution was added to 70 ml of a 0.1M K_2HPO_4/citric acid solution, also at pH=7.70. This fresh linolic acid solution was used immediately for the enzyme assay.

Enzyme assay.

The activity of lipoxygenase was determined by UV light absorption at a wavelength of 234 nm with a CARY 118 spectrophotometer (Varian Instruments division) in thermostatted (25°C) 4 ml absorption cells (229.10s, Pye Unicam). Of the above mentioned linolic acid solution, 3 ml was pipetted in each of the absorption cells, of which one served as a reference cell. Next, 200 µl of the enzyme solution (I) was pipetted rapidly in the measuring cell. As under the prevailing conditions, the change of absorbance in time was linearly

dependent on enzyme concentration, the specific inactivation rate k_e was found by plotting the relative oxidation rate values logarithmically against the time of heat treatment, in accordance with eqn. (5.3).

5.2.5 *Results from inactivation experiments.*

The results from inactivation experiments at different moisture content-temperature combinations are given in *table 5.3*. From the Eyring plots (see chapter 2), presented in *fig. 5.6*, the changes in enthalpy ΔH and entropy ΔS were obtained by linear regression.

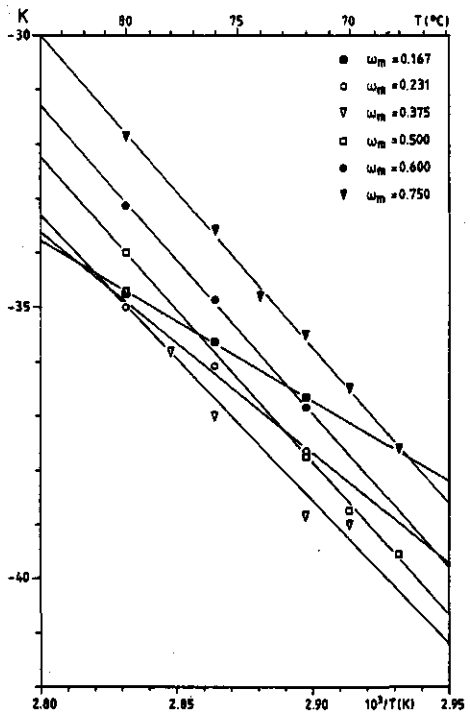

Fig. 5.6
Eyring plots for thermal inactivation of soy bean lipoxygenase at different moisture contents.

	$k_e (s^{-1})$					
T (°C) \ ω_m	0.167	0.231	0.375	0.500	0.600	0.750
68.0				4.85×10^{-5}		3.44×10^{-4}
70.0			7.96×10^{-5}	1.04×10^{-4}		1.03×10^{-3}
72.0	8.64×10^{-4}	3.16×10^{-4}	1.21×10^{-4}	2.88×10^{-4}	7.21×10^{-4}	2.71×10^{-3}
74.0						5.55×10^{-3}
76.0	2.44×10^{-3}	1.55×10^{-3}	6.25×10^{-4}		5.39×10^{-3}	1.95×10^{-2}
78.0			1.98×10^{-3}			
80.0	6.19×10^{-3}	4.65×10^{-3}	6.17×10^{-3}	1.25×10^{-2}	3.00×10^{-2}	1.08×10^{-1}
ΔH(kJ/Mole)	246.424	337.779	438.538	466.761	469.634	475.106
ΔS(kJ/Mole.K)	0.409	0.666	0.951	1.039	1.055	1.081

Table 5.3 The specific inactivation rate k_e for different combinations of moisture content ω_m and temperature T together with the resulting enthalpies ΔH and entropies ΔS.

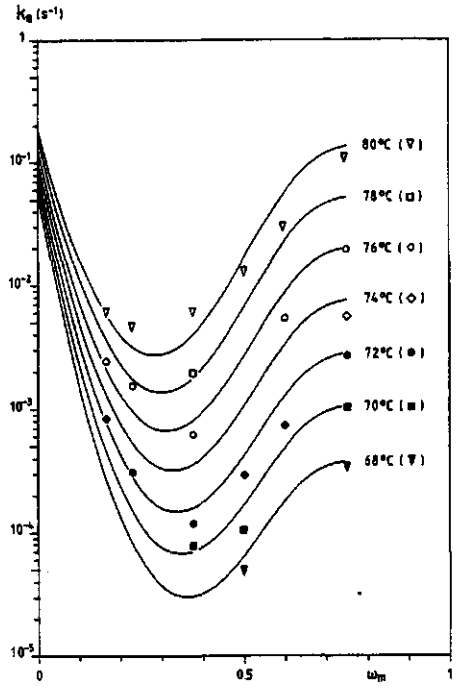

Fig. 5.7
Moisture dependence of the specific inactivation rate k_e of soy bean lipoxygenase at different temperatures. Experiment (dots) Eqn.(2.9) (lines).

p	q	ΔH_0	ΔH_1	ΔS_0	ΔS_1
		kJ/Mole	*kJ/Mole*	*kJ/Mole.K*	*kJ/Mole.K*
2.66	*2.45*	*92.0*	*484.0*	*0*	*1.108*

Table 5.4 Parameter values in eqn.(2.9).

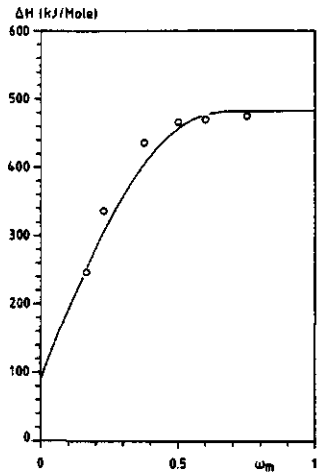

Fig. 5.8 Moisture dependence of the enthalpy ΔH for the thermal inactivation of soy bean lipoxygenase.
(o): experimental
(–): eqn.(2.7).

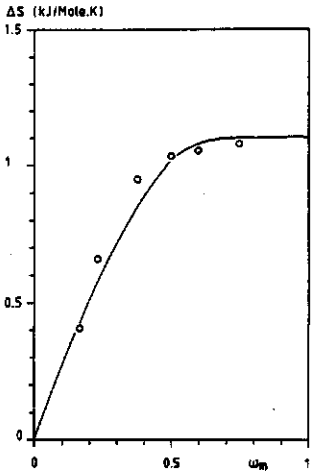

Fig. 5.9 Moisture dependence of the entropy ΔS for the thermal inactivation of soy bean lipoxygenase.
(o): experimental
(–): eqn.(2.8).

The moisture dependence of the specific inactivation rate k_e was determined by applying eqn.(2.9) for fitting of the complete data set. *Fig. 5.7* shows the specific inactivation rate as a function of moisture content on total basis, at different temperatures, where the drawn curves are calculated according to eqn.(2.9) together with the parameter values given in *table 5.4*. In addition, the experimentally determined values of enthalpy and entropy at different moisture contents are presented in *figs. 5.8* and *5.9* respectively, where the drawn curves are calculated according to eqns.(2.7) and (2.8) with the parameter values from *table 5.4*.

5.3 Drying experiments.

Enzyme inactivation during drying was realized in a thermostatted cylindrical drying cell, as drawn schematically in *fig. 5.10*. In this cell, either 8 hanging samples, attached to thermocouple wire or plastic strings, or 8 layers could be dried simultaneously. For the drying experiments, spherical samples were used, obtained by injecting liquid gel material in a perspex mould, consisting of two separable parts, each containing one half of the sphere volume (*fig. 5.11*). Attachment of the spheres to thermocouple wire or plastic string was achieved by inserting the wire or string in the mould before injecting the gel.
At different times during the drying experiment a sample was removed from the cell, weighed in order to determine its moisture content and finally dissolved in solution (H) for the determination of the residual enzyme activity, as described in section 5.2.4. The drying air was held at a constant flow rate and passed through a spiral-tube immersed in a thermostatted water bath at the desired temperature. The temperature of one of the samples and of the surrounding air was monitored continuously during the drying experiment by means of thermocouples. Uniform gas phase conditions were achieved by direct mixing in combination with a tangential/anti-tangential air inlet/outlet construction. The drying conditions for the test case examined here were: an initial moisture content of 0.75 on total basis and drying air (<1% RH) of 70°C. The results of this drying experiment will not be treated here, as they are discussed in chapter 6.

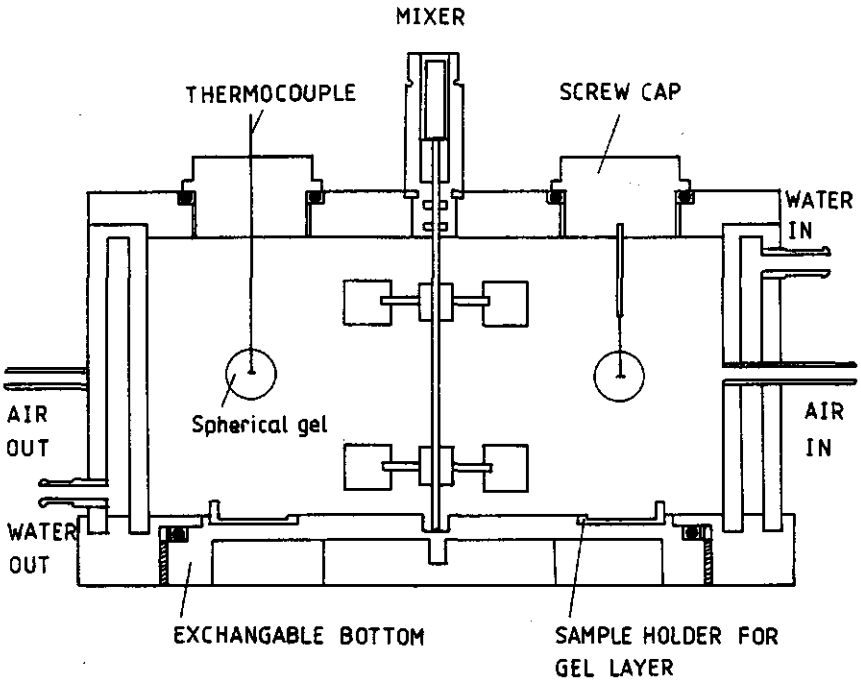

Fig. 5.10 Drying cell.

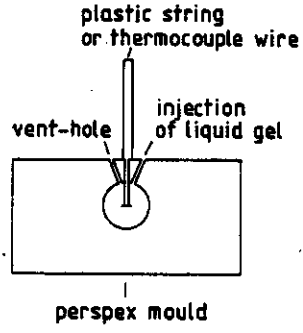

Fig. 5.11 Mould for the preparation of spherical gels.

5.4 *The diffusion coefficient of water in glucose-calcium-alginate.*

The moisture dependence of the diffusion coefficient was determined, according to the method, described by Luyben et al.[25]. Values of the diffusion coefficient at different moisture contents are given for the temperatures T=50°C and T=70°C in *table 5.5*.
In case the diffusion coefficient is described by a power function relation ($D_p = m^a$), eqn.(4.117) may be written as:

$$D = \frac{D_o \rho^2_{s,o}}{(\omega'_{m,o})^a} \left(\frac{1}{d_s} + \frac{\omega'_m}{d_m}\right)^2 (\omega'_m)^a \qquad (5.5)$$

By applying this relation for fitting the experimental values of the diffusion coefficient at T_{ref}=50°C, with d_s=1562 kg/m³ and d_m=1000 kg/m³, it appeared that the moisture dependence may be reasonably approximated by the power function relation, given above. This is shown in *fig. 5.12*, where the values of the diffusion coefficient are approximated by eqn.(5.5) with: $a = 0.5964$ and $D_o^{ref} = 3.69 \times 10^{-9}$ m²/s at $\omega'_{m,o}$=3 and T_{ref}=50°C.

As for the temperature dependence of the diffusion coefficient, eqn.(4.118) was applied, together with a moisture dependent activation energy, given by:

$$E_{a,d} = 80000\left(\frac{1}{1+10\omega'_m} + 0.147\right) \qquad (5.6)$$

which relation is in agreement with the moisture dependence, proposed by Van der Lijn [23] for glucose solutions.
In *table 5.6* the complete moisture and temperature dependence of the diffusion coefficient is given.

ω'_m	$D(m^2/s)$ 50°C	70°C
0.10	1.04×10^{-11}	5.17×10^{-11}
0.12	1.61×10^{-11}	6.40×10^{-11}
0.15	2.62×10^{-11}	7.86×10^{-11}
0.20	4.25×10^{-11}	9.90×10^{-11}
0.25	5.24×10^{-11}	1.27×10^{-10}
0.30	7.09×10^{-11}	1.43×10^{-10}
0.40	1.15×10^{-10}	1.86×10^{-10}
0.50	1.51×10^{-10}	2.24×10^{-10}
0.60	1.89×10^{-10}	2.80×10^{-10}
0.80	2.71×10^{-10}	4.24×10^{-10}
1.00	3.95×10^{-10}	5.77×10^{-10}
1.20	5.39×10^{-10}	7.86×10^{-10}
1.50	8.72×10^{-10}	

Table 5.5
Diffusion coefficient of water in glucose-calciumalginate.

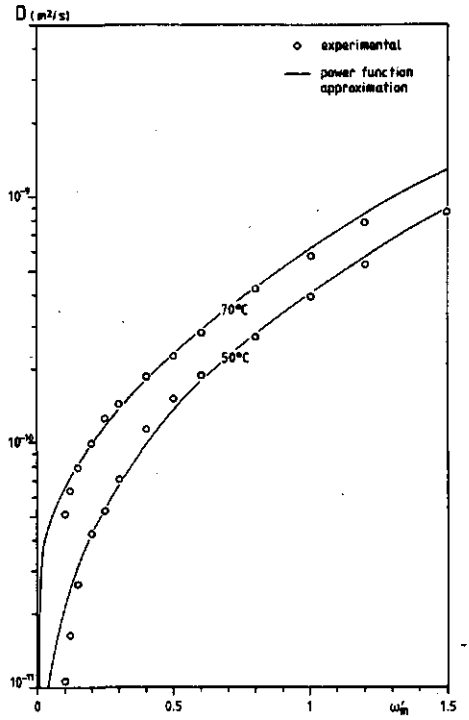

Fig. 5.12
Power function approximation for the diffusion coefficient of water in glucose-calciumalginate.

$$D = D_o^{ref} exp[-\frac{E_{a,d}}{R}(\frac{1}{T} - \frac{1}{T_{ref}})]\frac{\rho_{s,o}^2}{(\omega'_{m,o})^a}(\frac{1}{d_s}+\frac{\omega'_{m,o}}{d_m})^2(\omega'_m)^a \quad m^2/s$$

$$E_{a,d} = 80000(\frac{1}{1+10\omega'_m} + 0.147)\ ;\ \omega'_{m,o}=3\ ;\ \rho_{s,o}= 274.71\ kg/m^3\ ;$$

$$T_{ref} =323.15K;\ D_o^{ref}=3.69\times10^{-9}m^2/s;\ d_s=1562kg/m^3;\ d_m=1000kg/m^3$$

Table 5.6 Moisture and temperature dependence of the diffusion coefficient of water in glucose-calciumalginate.

C H A P T E R 6

Results and discussion.

6.1 Introduction.

In this final chapter, we will discuss the results from the inactivation experiments with soy bean lipoxygenase and compare the results obtained from the drying experiment, mentioned in chapter 5, with computer simulations of the experiment by applying the complete model of chapter 3 and the approximate model of chapter 4.
These computer simulations required the moisture and temperature dependence of the diffusion coefficient as well as the specific inactivation rate of lipoxygenase. For the moisture and temperature dependence of the diffusion coefficient of water in glucose-calciumalginate, the power function approximation, given in *table 5.6* was applied, whereas eqn.(2.9) together with the parameter values of *table 5.4* served for the evaluation of the specific inactivation rate.

6.2 Moisture and temperature dependence of enzyme inactivation.

From the experimental results on the thermal inactivation of soy bean lipoxygenase, it was found , that moisture content strongly influences thermal stablity of the enzyme. Moreover, it appeared that lipoxygenase exhibited the kind of behaviour as postulated in chapter 2. A comparison between *figs. 2.1* and *5.7* shows that lipoxygenase may be classified in the category $p>q$.

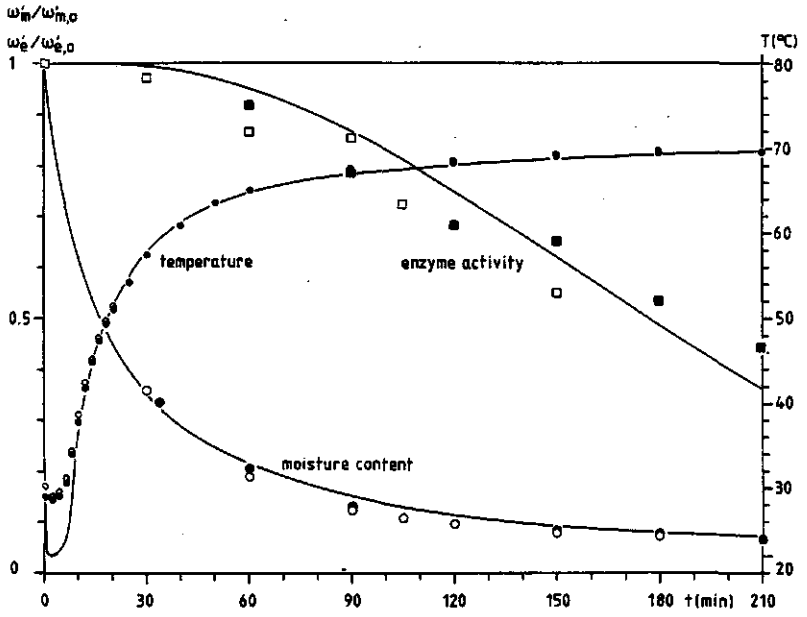

Fig. 6.1

Enzyme inactivation during drying of a spherical glucose-calciumalginate gel (R_o= 5 mm, $\omega'_{m,o}$= 3 kg/kg solids), containing soy bean lipoxygenase. Air temperature T_b= 70°C. Experimental (dots). Simulation with the complete model of chapter 3 (lines).

6.3.1 Computer simulation with the complete model (chapter 3)

In *fig. 6.1* the results from a drying experiment are shown together with a computer simulation of the experiment, applying the model of chapter 3. This figure presents the transient behaviour of the average moisture content, particle temperature and residual enzyme activity. The experiment was carried out in duplicate and the results are distinguished by open and black dots. As may be observed, hardly any differences occur between the two data sets, as far as moisture content and temperature are concerned. The values of residual enzyme activity are somewhat more scattered, but their differences remain within 10%. The parameter values, used in the computer simulation are tabulated in appendix B.
A comparison between experiment and computer simulation shows a good agreement. The predicted temperature exhibits a slight undershoot at the initial stage, which is probably caused by the occurrence of temperature profiles inside the material, as the time constant of temperature equalization (99% equalization in about 1s) is of the same order of magnitude as the length of the constant activity period (about 1s). Consequently, the temperature at the centre will be higher than the surface temperature, which is in agreement with the experiment. This phenomenon, however, has no serious consequences regarding enzyme inactivation, as the temperature is still at moderate values. The predicted behaviour of moisture content and residual enzyme activity show no remarkable differences with the experimental results.

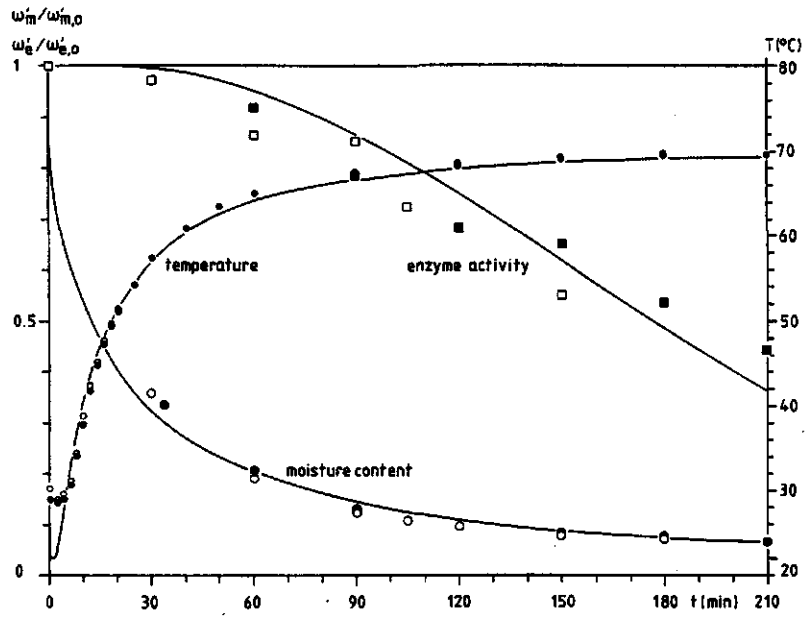

Fig. 6.2

Enzyme inactivation during drying of a spherical glucose-calciumalginate gel (R_o= 5 mm, $\omega'_{m,o}$= 3 kg/kg solids), containing soy bean lipoxygenase. Air temperature T_b= 70°C. Experimental (dots). Simulation with the approximate model of chapter 4 (lines).

6.3.2 *Computer simulation with the approximate model (chapter 4).*

Fig. 6.2 shows the same experimental results as *fig. 6.1*. The drawn curves represent a computer simulation of the experiment, generated with the approximate model of chapter 4. In this simulation, the intersection point of the fluxes belonging to the period of constant activity and the falling rate period was taken as the transition point between both periods. Furthermore, the moisture profile, corresponding to the Dirichlet boundary condition was assumed to be valid in the period of constant activity. We also examined the other extreme situation of a uniform moisture profile throughout the entire period of constant activity. However, the results for this case, regarding enzyme inactivation, showed hardly any differences with the former case. This may be explained by the fact, that the initial temperature is relatively low and consequently, differences in inactivation rate due to differences in moisture content are less pronounced.
It may be observed, that the moisture content decreases faster than in the simulation with the complete model. This is not very surprising, as the Neumann boundary condition overestimates the initial flux, due to the assumption of a saturated water vapour concentration at the interface. At larger times, however, the predicted behaviour of moisture content is in good agreement with the experiment.
The computed curve for the residual enzyme activity appears to be hardly distinguishable from the simulational results, obtained with the complete model. In view of the length of the drying experiment, the predicted curves are fairly accurate.

6.4 Conclusions.

1. The application of the power function approximation for the moisture dependence of the diffusion coefficient, as given in *table 5.6*, yields satisfactory results, regarding the prediction of the drying behaviour of a glucose-calciumalginate gel *(fig. 6.1 and 6.2)*.

2. The postulated relation for the moisture and temperature dependence of the specific inactivation rate, given by eqn.(2.9), applies to the enzyme soy bean lipoxygenase, immobilized in a glucose-calciumalginate gel *(fig. 5.7)*.

3. The application of the above-mentioned relation for the specific inactivation rate of soy bean lipoxygenase in a computer simulation of drying a glucose-calciumalginate gel with simultaneous enzyme inactivation, resulted in a satisfactory prediction of the transient behaviour of residual enzyme activity *(fig. 6.1)*.

4. The computational results, obtained by applying the approximate model for enzyme inactivation during drying (chapter 4) are in good agreement with the experimental results *(fig. 6.2)*.

S U M M A R Y

One of the main reasons for drying of foods is the wish to improve the keepability of the end product. Deterioration of foods during storage is caused to a large extent by enzymatic and/or microbial conversions, which lead to changes in taste, colour, texture and nutritional value. It is therefore of importance, to choose drying conditions in such a way, that undesired micro organisms and enzymes are destroyed during drying. At the same time, however, food quality has to be preserved, which requires careful process control. Similar problems, although of opposite character, are encountered in the production of enzyme granulates (marumes) for application in detergents, immobilized enzymes for biotechnological applications, enzyme powders for pharmaceutical purposes and dried micro organisms, of which spray dried yeast is a prominent example. Evidently, thermal destruction of enzymes or micro organisms is not wanted here and process conditions have to be adjusted corresponding to the requirement of minimizing losses of enzyme or microbial activity.

A prerequisite for optimum control is a fundamental knowledge of the process. In particular, a quantitative approach is indispensable in studying processes of high complexity. The application of mathematical models and simulation techniques facilitate the interpretation of process data and may lead to a better understanding of the process dynamics. However, the description of complex processes, often leads to mathematical models of equivalent complexity, cumbersome for practical applications. For this reason, simplified computational models are desirable.

This thesis comprises the design of such a simplified computational model for the simulation of enzyme inactivation during drying. As a starting point served the diffusion equation for a binary system, consisting of water as a diffusing component and a solid component, in order to describe moisture transport in the dispersed phase.

By means of an analysis of the results, obtained from a numerical solution of the diffusion equation with a concentration dependent diffusion coefficient (power dependence), correlations could be set up, which led to a simple approximate solution of the nonlinear diffusion equation, regarding the average moisture content as a function of time. These correlations apply to a diffusion process in both non-shrinking and shrinking systems of slab, cylindrical or spherical geometry, in case of an initially uniform moisture profile and a constant surface concentration. Moreover, these correlations also apply under non-isothermal conditions.

In addition to these correlations, an approximate solution was constructed in order to evaluate the moisture profiles inside the drying material.

For the thermal inactivation of enzymes, a model was postulated, which includes a possible moisture dependence of the inactivation rate. This model was applied to the description of the experimentally determined inactivation kinetics of soy bean lipoxygenase, immobilized in a glucose-calcium-alginate gel.

For this model material, also the moisture and temperature dependence of the diffusion coefficient was determined experimentally, according to the method, developed by Kerkhof [21], Schoeber [22] and Luyben [25], and described by

the above-mentioned power dependence.

With the model material, drying experiments were carried out, in which moisture content, temperature and residual lipoxygenase activity were determined as a function of the drying time. These experiments served for testing the complete computational model as well as the approximate model. Computer simulations with both models resulted in a correct description of the drying experiments.

By means of the simplified computational model, computing times could be reduced considerably (factor 1000), which makes the model pre-eminently suitable for incorporation in more complex descriptions, in which for instance particle size distribution and residence time distribution in dryers are involved; and for which the complete model would require excessive computing times. Moreover, if only drying times are of interest, a simple programmable pocket calculator will be sufficient, which makes the model more accessible to a larger audience in the process industry.

Finally, as far as the experimental part is concerned, it should be mentioned that the determination of the moisture and temperature dependence of the inactivation kinetics is simple, but rather laborious. The determination of the moisture and temperature dependence of the diffusion coefficient is automated to a large extent, but consequently requires much peripheral equipment.

S A M E N V A T T I N G

Eén van de belangrijkste redenen voor het drogen van levensmiddelen, is de wens, de houdbaarheid van het product te verhogen. Bederf van levensmiddelen tijdens opslag wordt voor een belangrijk deel veroorzaakt door enzymatische en/of microbiële omzettingen, welke leiden tot veranderingen in smaak, kleur, textuur en voedingswaarde. Het is daarom van belang, de droogcondities zodanig te kiezen, dat ongewenste micro-organismen en enzymen worden vernietigd tijdens het drogen. Tegelijkertijd, dient echter de kwaliteit van het levensmiddel behouden te blijven, wat een nauwkeurige procesbeheersing vereist. Soortgelijke problemen, hoewel van tegengestelde aard, komt men tegen in de productie van enzymgranulaten (marumes) voor waspoeders, geïmmobiliseerde enzymen voor biotechnologische toepassingen, enzympoeders voor pharmaceutische doeleinden en gedroogde micro-organismen, waarvan gesproeidroogde gist een prominent voorbeeld is. Thermische destructie van enzymen of micro-organismen is hier natuurlijk ongewenst en de procescondities dienen zodanig te worden geregeld, dat minimale verliezen aan enzymatische of microbiële activiteit optreden.

Een eerste vereiste voor een optimale procesregeling is een fundamentele kennis van het proces. In het bijzonder, is daarbij een kwantitatieve benadering onmisbaar voor het bestuderen van complexe processen. De toepassing van wiskundige modellen en simulatietechnieken vergemakkelijken de interpretatie van procesgegevens en kunnen leiden tot een verbeterde kennis van de procesdynamica. Vaak echter, leidt de beschrijving van complexe processen tot wiskundige modellen van ge-

lijkwaardige complexiteit, die onhandzaam zijn voor praktische toepassingen. Om deze reden zijn vereenvoudigde rekenmodellen wenselijk.

Dit proefschrift omvat het ontwerp van een dergelijk vereenvoudigd rekenmodel voor het simuleren van enzyminactivering tijdens drogen. Als uitgangspunt hiervoor diende de diffusievergelijking voor een binair systeem, bestaande uit water als diffunderende component en een vaste stofcomponent ter beschrijving van het watertransport in de disperse fase.

Via een analyse van de resultaten, verkregen uit een numerieke oplossing van de diffusievergelijking met een concentratie afhankelijke diffusiecoefficient (machtsafhankelijkheid), konden correlaties worden opgesteld, waarmee op eenvoudige wijze de oplossing van de niet lineaire diffusievergelijking, wat betreft het verloop van het gemiddeld vochtgehalte met de tijd, kon worden benaderd. Deze correlaties zijn van toepassing op een diffusieproces in zowel niet krimpende als krimpende systemen in de vorm van vlakke lagen, cylinders en bollen, uitgaande van een initieel uniform vochtprofiel en een constante oppervlakte concentratie. Verder gelden deze correlaties ook onder niet isotherme condities.

Naast deze correlaties werd een benaderende oplossing geconstrueerd ter bepaling van de vochtprofielen als functie van de tijd in het drogende materiaal.

Voor de thermische inactivering van enzymen werd een model gepostuleerd, dat voorziet in een mogelijke vochtafhankelijkheid van de inactiveringssnelheid, met behulp waarvan de experimenteel bepaalde inactiveringskinetiek van het enzym lipoxygenase uit sojabonen, geïmmobiliseerd in een glucose-calciumalginaat gel, werd beschreven.

Voor dit modelmateriaal werd tevens vocht-en temperatuur afhankelijkheid van de diffusiecoefficient experimenteel bepaald volgens de methode, ontwikkeld door Kerkhof [21], Schoeber [22] en Luyben [25], en beschreven met bovengenoemde machtsafhankelijkheid.

Met het modelmateriaal werden droogexperimenten uitgevoerd, waarbij vochtgehalte, temperatuur en resterende lipoxygenase activiteit werden bepaald als functie van de droogtijd. Deze experimenten dienden als toetsing van zowel het volledige rekenmodel als het vereenvoudigde rekenmodel. Computer simulaties met beide rekenmodellen resulteerden in een juiste beschrijving van de droogexperimenten.

Met behulp van het vereenvoudigde rekenmodel konden rekentijden aanzienlijk worden gereduceerd (factor 1000), wat het model bij uitstek geschikt maakt voor inpassing in meer complexe beschrijvingen, waarin bijvoorbeeld deeltjesgrootteverdeling en verblijftijdsspreiding in drogers zijn opgenomen; en waarvoor het volledige rekenmodel teveel rekentijd zou vergen. Indien alleen droogtijden van belang zijn, kan zelfs met een eevoudige, programmeerbare zakrekenmachine worden volstaan, wat de methode toegankelijker maakt voor een breder publiek in de procesindustrie.

Tenslotte, wat de experimentele kant betreft, dient gezegd te worden, dat de bepaling van de vocht-en temperatuurafhankelijkheid van de inactiveringskinetiek eenvoudig, maar nogal bewerkelijk is. De bepaling van de vocht-en temperatuurafhankelijkheid van de diffusiecoefficient is in belangrijke mate geautomatiseerd, maar vereist hierdoor veel randapparatuur [25].

A P P E N D I X A

A.1 The large time solution for a slab: derivation of the space dependent part.

The space dependent part of the diffusion equation for a slab is obtained by separation of variables, resulting in eqn.(4.8):

$$\frac{d}{d\phi}(g_r^a \frac{dg_r}{d}) = -P_{a,0} \cdot g_r \qquad (A.1)$$

subject to the boundary conditions:

$$g_r = 1, \frac{dg_r}{d\phi} = 0 \text{ at } \phi=0 \qquad (A.2)$$

$$g_r = 0 \text{ at } \phi=1 \qquad (A.3)$$

Multiplying both sides of eqn.(A.1) by $2g_r^a \cdot \frac{dg_r}{d\phi}$ and subsequent integration yields:

$$g_r^a \cdot \frac{dg_r}{d\phi} = (\frac{2P_{a,0}}{a+2})^{\frac{1}{2}} \cdot (1-g_r^{a+2})^{\frac{1}{2}} \qquad (A.4)$$

Substitution of $z=g_r^{a+2}$ in eqn.(A.4) and integrating once more results in:

$$[2(a+2)P_{a,0}]^{\frac{1}{2}}(1-\phi) = \int_o^z z^{\frac{-1}{a+2}}(1-z)^{-\frac{1}{2}}dz \qquad (A.5)$$

The right hand side of eqn.(A.5) is the integral representation of the incomplete beta function $B_z(\frac{a+1}{a+2},\frac{1}{2})$ [47]. Applying the boundary condition: $z=0$ at $\phi=0$, eqn.(A.5) yields:

$$[2(a+2)P_{a,0}]^{\frac{1}{2}} = B(\frac{a+1}{a+2},\frac{1}{2}) \qquad (A.6)$$

where B represents the beta function for $z=1$. From eqn.(A.6) follows:

$$P_{a,0} = \frac{B^2(\frac{a+1}{a+2},\frac{1}{2})}{2(a+2)} \qquad (A.7)$$

whereas eqn.(A.5) turns into:

$$B_z(\frac{a+1}{a+2},\frac{1}{2}) = B(\frac{a+1}{a+2},\frac{1}{2}).(1-\phi) \qquad (A.8)$$

which implicitly gives z as a function of ϕ. The beta functions may be evaluated from the infinite series representation:

$$B_z(\frac{a+1}{a+2},\frac{1}{2}) = (\frac{a+2}{a+1}) \sum_{n=0}^{\infty} \frac{(2n)!}{2^{2n}(n!)^2[n(\frac{a+2}{a+1})+1]}.z^{n+\frac{a+1}{a+2}} \qquad (A.9)$$

The average value of g_r follows from:

$$\bar{g}_r = \int_0^1 g_r d\phi \qquad (A.10)$$

with: $g_r=1$ at $\phi=0$ and $g_r=0$ at $\phi=1$.
Integration by parts of eqn.(A.10) then leads to:

$$\bar{g}_r = \int_0^1 \phi \, dg_r \qquad (A.11)$$

with, according to eqn.(A.8):

$$\phi = 1 - \frac{B_z(\frac{a+1}{a+2},\frac{1}{2})}{B(\frac{a+1}{a+2},\frac{1}{2})} \qquad (A.12)$$

Elaboration of the integral in eqn.(A.11) finally yields:

$$\bar{g}_r = \frac{2}{B(\frac{a+1}{a+2},\frac{1}{2})} \qquad (A.13)$$

A.2 Polynomial and rational approximations for the functions: $J_0(z)$, erfc(z), $K_{\frac{1}{3}}(z)$ [45,47].

The Besselfunction of order 0: $J_0(z)$ $(-3 \leq z \leq 3)$

$$J_0(z) = 1 - 2.2499997\left(\frac{z}{3}\right)^2 + 1.2656208\left(\frac{z}{3}\right)^4 - 0.3163866\left(\frac{z}{3}\right)^6 + 0.0444479\left(\frac{z}{3}\right)^8 - 0.0039444\left(\frac{z}{3}\right)^{10} - 0.0002100\left(\frac{z}{3}\right)^{12} + |\varepsilon|$$

with: $|\varepsilon| < 5\times10^{-8}$ (A.14)

The complementary errorfunction: erfc(z).

$$erfc(z) = (0.254829592x - 0.284496736x^2 + 1.421413741x^3 - 1.453152027x^4 + 1.061405429x^5)e^{-z} + |\varepsilon|$$

with:

$$x = \frac{1}{1 + 0.3275911z} \quad \text{and} \quad |\varepsilon| \leq 1.5\times10^{-7} \qquad \text{(A.15)}$$

The modified Besselfunction of order $\frac{1}{3}$: $K_{\frac{1}{3}}(z)$. Approximation for large values of argument z.

$$K_{\frac{1}{3}}(z) = \left(\frac{\pi}{2z}\right)^{\frac{1}{2}} \cdot e^{-z}\left[1 - \frac{0.75}{8z} + \frac{6.5625}{2(8z)^2} - \frac{162.421875}{6(8z)^3}\right] \qquad \text{(A.16)}$$

A P P E N D I X B

B.1 Physical constants.

Boltzmann's constant: $k = 1.38\times10^{-23}$ (J/Mole.K)
Planck's constant : $h = 6.62\times10^{-34}$ (J.s)
Gas law constant : $R = 8.314$ (J/Mole.K)

B.2 Conversion factors.

Pressure : $P(atm) = 1.01325\times10^{5}\ P(Pa)$
Temperature: $T(K) = 273.15 + T(°C)$

B.3 Physical properties of air, water and glucose.

Air:

Molecular weight	[55]:	$M_a = 28\times10^{-3}$	(kg/Mole)
Heat capacity	[57]:	$c_{p,a,g} = 1010$	(J/kg.K)
Thermal conductivity	[56]:	$\lambda_{a,g} = 4.5\times10^{-3}+7.26\times10^{-5}T$	(W/m.K)

Water:

Molecular weight	[55]:	$M_m = 18\times10^{-3}$	(kg/Mole)
Liquid density	[55]:	$d_m = 1000$	(kg/m^3)
Vapour heat capacity	[57]:	$c_{p,m,g} = 2000$	(J/kg.K)
Vapour diffusivity	[56]:	$D_g = 5.28\times10^{-9}T^{3/2}$	(m^2/s)
Heat of vaporization	[23]:	$\Delta H_{vap} = 2.5\times10^{6} - 2.25\times10^{3}(T-273.15)$	(J/kg)
Saturated water vapour concentration	[52]:	$\rho^{sat}_{m,g,i} = \frac{2.1936\times10^{-3}}{T} exp[\frac{-7246.5822}{T} + 77.641232 + 5.7447142\times10^{-3}T - 8.2470402\ lnT]$	(kg/m^3)

Glucose:

Density [55]: $d_s = 1562$ (kg/m^3)

The *heat capacity* of the system glucose/water was estimated by using the data of Norrish [54] for sucrose solutions, which were fitted with the following equation:

$$\bar{c}_{p,d} = 4184[(0.5983-1.7235\times10^{-3}(T-273.15))\bar{\omega}_m + 1.7757\ 10^{-3}(T-273.15) + 0.4009\ ] \quad (J/kg.K)$$

Sorption isotherm [5,53]:

$$a_w = \begin{cases} 0 \quad for\ \omega'_{m,i} = 0 \\ \dfrac{2 + (W/\omega'_{m,i}-1)C - [(2+(W/\omega'_{m,i})C)^2 - 4(1-C)]^{\frac{1}{2}}}{2K(1-C)} \\ \dfrac{\omega'_{m,i}}{K(W+\omega'_{m,i})} \quad for\ C = 1 \end{cases}$$

with:

$$C = 2.777778\ exp[\frac{50000}{R}(\frac{1}{313.15} - \frac{1}{T})]$$

$K = 1$

$W = 0.12$

B.4 Parameter values in computer simulations.

$\nu = 2$

$a = 0.5954$

$D_o^{ref} = 3.69 \times 10^{-9}$ (m^2/s)

$T_{ref} = 323.15$ (K)

$\omega'_{m,o} = 3$ $(kg/kg\ solids)$

$R_o = 5 \times 10^{-3}$ (m)

$T_{d,o} = 302.15$ (K)

$T_g = 343.15$ (K)

$k_g^{eff} = 0.50 - 0.60$ (m/s)

$p = 2.66$

$q = 2.45$

$\Delta H_0 = 92000$ $(J/Mole)$

$\Delta H_1 = 484000$ $(J/Mole)$

$\Delta S_0 = 0$ $(J/Mole.K)$

$\Delta S_1 = 1108$ $(J/MOle.K)$

R E F E R E N C E S .

[1] *Svensson, S.* Inactivation of enzymes during thermal processing. In: Physical, chemical and biological changes in food caused by thermal processing.
(Ed. T. Høyem & O. Kvåle) Applied Science Publishers Ltd. London (1977)202-217.

[2] *Liou, J.K., Bruin, S.* A model for watermigration in porous hygroscopic materials caused by temperature gradients.
Lebensm. Wiss. Technol., 14(1981)206-212.

[3] *Glasstone, S., Laidler, K.J., Eyring, H.*
The theory of rate processes.
McGraw-Hill. London (1941)442-447.

[4] *Saguy, I., Mizrahi, S., Villota, R., Karel, M.*
Accelerated method for determining the kinetic model of ascorbic acid loss during dehydration.
J. Food Sci., 43(1978)1861-1865.

[5] *Luyben, K.Ch.A.M., Liou, J.K., Bruin, S.*
Enzyme degradation during drying.
Biotechnol. Bioeng. To be published.

[6] *Daemen, A.L.H.* Neth. Milk Dairy J., to be published.

[7] *Rothe,M.* Eigenschaften und Reaktionsverhalten pflanzlicher Samenlipasen in natürlichen Milieu. II. Mitt. Einfluss der Feuchtigkeit auf das Temperaturverhalten.
Ernährungsforsch., 3(1958)41-51

[8] *Rothe, M.* Thermoresistenz von Weizenenzymen in Abhängigkeit von der Feuchtigkeit des Mediums.
Ernährungsforsch., 10(1965)29-36.

[9] *Rothe, M., Stöckel, J.* Thermisch bedingte Aktivitätsänderungen bei Enzymen. I. Mitt. Lipase, Acetylesterase, Peroxydase und Lipoxydase von Getreideprodukten.
Die Nahrung, 2(1967)741-749.

[10] *Farkas, D.F., Goldblith, S.* Studies on the kinetics of lipoxidase inactivation using thermal and ionizing energy.
J. Food Sci., 27(1962)262-276.

[11] *Svensson, S.G., Eriksson, C.E.* Thermal inactivation of lipoxygenase from peas (*Pisum sativum L.*)
III. Activation energy obtained from single heat treatment experiments.
Lebensm. Wiss. Technol., 7(1974)142-144.

[12] *Tumerman, L.* Thermal inactivation of enzymes.
In: Encyclopedia of food technology (Ed. A.H. Johnson & M.S. Peterson).
Avi publishing company, Westport (1974)292-306.

[13] *Verhey, J.G.P.* Vacuole formation in spray powder particles. 3. Atomization and droplet drying.
Neth. Milk Dairy J., 27(1973)3-18.

[14] *Hillier, R.M., Lyster, R.L.J., Cheeseman, G.C.*
Thermal denaturation of α-lactalbumin and β-lactoglobulin in cheese whey: effect of total solids concentration and pH.
J. Dairy Research, 46(1979)103-111.

[15] *Roozen, J.P., Pilnik, W.* Uber die Stabilität adsorbierter Enzyme in wasserarmen Systemen. I. Die stabilität von Peroxydase bei 25°C.
Lebensm. Wiss. Technol., 3(1970)37-40.

[16] *Kulys, J.J., Kurtinatiene, B.S., Akulova, V.F.* Stabilization of glucose oxidase from *Penicillium vitale* entrapped in high concentration gels.
J. Solid Phase Biochem., 3(1978)95-105.

[17] *Fortes, M., Okos, M.R.* A non-equilibrium thermodynamics approach to transport phenomena in capillary porous media.
Trans. ASAE, (1981)756-760.

[18] *Fortes, M., Okos, M.R.* Non-equilibrium thermodynamics approach to heat and mass transfer in corn kernels.
Trans. ASAE, (1981)761-769.

[19] *Whitaker, S.* Simultaneous heat, mass and momentum transfer in porous media. A theory of drying.
In: Advances in heat transfer, 13(1977)119-203.

[20] *Lehmer, F.K.* On the validity of Fick's law for transient diffusion through a porous medium.
Chem. Eng. Sci., 34(1979)821-825.

[21] *Kerkhof, P.J.A.M.* A quantitative study on the effect of process variables on the retention of volatile trace components in drying.
Ph. D. Thesis, Technical University Eindhoven, The Netherlands (1975).

[22] *Schoeber, W.J.A.H.* Regular regimes in sorption processes.
Ph. D. Thesis, Technical University Eindhoven, The Netherlands (1976).

[23] *Lijn, J. van der.* Simulation of heat and mass transfer in spray drying.
Ph. D. Thesis, Agricultural University Wageningen, The Netherlands (1976).

[24] *Kerkhof, P.J.A.M., Thijssen, H.A.C.*
Quantitative study of the effects of process variables on aroma retention during the drying of liquid foods.
A.I.Ch.E. Meeting on dehydration and concentration of foods. November, 16-25, 1975, Los Angeles, California, U.S.A.

[25] *Luyben, K.Ch.A.M., Olieman, J., Bruin, S.*
Concentration dependent diffusion coefficients derived from experimental drying curves.
Proc. 2nd Int. Symp. Drying. July, 6-9, 1980, Montreal, Canada.

[26] *Kerkhof, P.J.A.M., Schoeber, W.J.A.H.*
Theoretical modelling on the drying behaviour of droplets in spray driers.
In: Advances in preconcentration and dehydration of foods. (Ed. A. Spicer) Appl. Sci. Publ., London, (1974)349-397.

[27] *Wijlhuizen, A.E., Kerkhof, P.J.A.M., Bruin, S.*
Theoretical study of the inactivation of phosphatase during spray-drying of skim-milk.
Chem. Eng. Sci., 34(1979)651-660.

[28] *Bird, R.B., Stewart, W.E., Lightfoot, E.N.*
Transport phenomena. Wiley, New York (1960).

[29] *Beek, W.J., Muttzall, K.M.K.*
Transport phenomena. John Wiley & Sons Ltd. Chichester, (1975).

[30] *Geankoplis, C.J.*
Transport processes and unit operations.
Allyn and Bacon, Inc., Boston (1978).

[31] *Peletier, L.A.* Asymptotic behaviour of temperature profiles of a class of nonlinear heat conduction problems. Quart. J. Mech. Appl., 23(1970)441-447.

[32] *Peletier, L.A.* Asymptotic behaviour of solutions of the porous media equation. SIAM J. Appl. Math., 21(1971)542-551.

[33] *Atkinson, F.V., Peletier, L.A.* Similarity profiles of flows through porous media. Archs. ration. Mech. Analysis, 42(1971)369-379.

[34] *Duyn, C.J. van, Peletier, L.A.* A class of similarity solutions of the nonlinear diffusion equation. Nonlinear Analysis, Theory, Methods and applications, 1(1977)223-233.

[35] *Shampine, L.F.* Concentration dependent diffusion I, Q. appl. Math., 31(1973)441-452.

[36] *Shampine, L.F.* Concentration dependent diffusion II, Q. appl. Math., 31(1973)287-293.

[37] *Shampine, L.F.* Concentration dependent diffusion III, Q. appl. Math., 33((1976)429-431.

[38] *Crank, J.* The mathematics of diffusion. 2nd ed., Clarendon Press Oxford, 1975.

[39] *Suzuki, M., Maeda, S.* An approximation of transient change of moisture distribution within porous materials being dried. Proc. First Int. Symp. Drying, Montreal, Canada, (1978)42-47.

[40] *Steff, J.F., Singh, R.P.* Liquid diffusivity of rough rice components. Trans. ASAE, (1980)767-774.

[41] *Misra, R.M., Young, J.H.* Numerical solution of simultaneous moisture diffusion and shrinkage during soy bean drying.
Trans. ASAE, (1980)1277-1282.

[42] *Schoeber, W.J.A.H., Thijssen, H.A.C.* Paper presented at the A.I.Ch.E. Meeting on dehydration and concentration of foods. Los Angeles, 1975.

[43] *Fowler, R.H.* The solution of Emdens's and similar differential equations.
Mon. Not. R. astr. Soc., 91(1920)63-91.

[44] *Aris, R.* The mathematical theory of diffusion and reaction in permeable catalysts.
Clarendon Press, Oxford, vol 1(1975)109, 144.

[45] *Luikov, A.*
Analytical heat diffusion theory.
Academic Press, London, (1969)97-147, 495.

[46] *Villadsen, J., Michelsen, M.L.*
Solution of differential equation models by polynomial approximation.
Prentice Hall, Englewood Cliffs, N.J. (1978)212, 432.

[47] *Abramowitz, M., Stegun, I.*
Handbook of mathematical functions.
Dover, New York (1970).

[48] *Friedmann, N.E.* Quasilinear heat flow.
Trans. ASME, 80(1958)635-645.

[49] *Pelaez, C., Karel, M.* Improved method for preparation of fruit-simulating alginate gels.
J. Food Proc. and Preserv. 5(1981)63-81.

[50] *Axelrod, B.* Lipoxygenasen. In: Food related enzymes. (Ed. J.R. Whitaker). Adv. in Chem. Series (1974)324-328.

[51] *Eriksson, C.E., Svensson, S.G.* Activation energy of reaction catalyzed by alcohol dehydrogenase, lipoxygenase, denaturated peroxidase and hematin.
Lebensm. Wiss. Technol., 7(1974)38-41.

[52] *Wexler, A., Greenspan, L.* Vapor pressure equation for water in the range 0-100.
J. Res. Natn. Bur. Stand., 75A(1971)213-

[53] *Berg, C. van den, Leniger, H.A.* The wateractivity of foods. In: Miscellaneous papers, Agricultural University Wageningen, 15(1978).

[54] *Norrish, R.S.* Selected tables of physical properties of sugar solutions.
The British food manufacturing industries research assoc. Scientific and technical surveys, 51(1967)96

[55] *Weast, R.C. (Ed.)*
Handbook of chemistry and physics.
53rd edition. CRC Press, Cleveland, Ohio (1972).

[56] *Mason, A.E., Monchick, L.* Survey of the equations of state and transport properties of moist gases.
In: Humidity and moisture. (Ed. A. Wexler), chapter 4.
New York, 1965.

[57] National Research Council. Int. Crit. Tables.
(Ed. E.W. Washburn) McGraw-Hill, New York, 1926.